Review

Aerogels Part 1. A Focus on the Most Patented Ultralight, Highly Porous Inorganic Networks and the Plethora of Their Advanced Applications

Silvana Alfei *

Posted Date: 1 August 2025

doi: 10.20944/preprints202508.0009.v1

Keywords: aerogels (AGs); sol-gel method; inorganic-based AGs; silica oxide AGs; metal oxide AGs; alumina oxide Ads; zirconia oxide AGs; titania oxide AGs

 doi:10.20944/preprints202508.0009.v1

Review

Aerogels Part 1. A Focus on the Most Patented Ultralight, Highly Porous Inorganic Networks and the Plethora of Their Advanced Applications

Silvana Alfei

Department of Pharmacy (DIFAR), University of Genoa, Viale Cembrano, 4, 16148 Genoa, Italy; alfei@difar.unige.it; Tel.: +39 010 355 2296

Abstract

Aerogels (AGs) are highly porous, low-density, disordered, ultralight macroscopic materials having immense surface areas. Traditionally synthesized using aqueous sol–gel chemistry, starting by molecular precursors, the nanoparticles (NPs) dispersions gelation method is nowadays the most used procedure to obtain AGs with improved crystallinity and broader structural, morphological and compositional complexity. Sol-gel process consists of preparing a solution by hydrolysis of different precursors, followed by gelation, ageing and a drying phase, via supercritical, freeze-drying or ambient evaporation. AGs can be classified based on various factors, such as appearance, synthetic methods, chemical origin, drying methods, microstructure, etc. Due to their nonpareil characteristics, AGs are completely different from common NPs, thus covering different and more extensive applications. AGs can be applied in supercapacitors, acoustic devices, drug delivery, thermal insulation, catalysis, electrocatalysis, gas absorption, gas separation, organic and inorganic xenobiotics removal from water and air and radionucleotides management. This review provides first an analysis on AGs according to data found in CAS Content Collection. Then, an AGs' classification based on the chemical origin of their precursors, as well as the different methods existing to prepare AGs and the current optimization strategies have been discussed. Following, focusing on AGs of inorganic origin, silica and metal oxide-based AGs were reviewed, deeply discussing their properties, specific synthesis and possible uses. These classes were chosen based on the evidence that they are the most experimented, patented and marketed AGs. Several related case studies have been reported some of which have been presented in reader-friendly tables and discussed.

Keywords: aerogels (AGs); sol-gel method; inorganic-based AGs; silica oxide AGs; metal oxide AGs; alumina oxide Ads; zirconia oxide AGs; titania oxide AGs

1. Introduction

Aerogels (AGs) are porous, ultra-lightweight, nanostructured materials, commonly obtained from a variety of hydrogels by substituting the liquid component with a gas, using different drying techniques. The first AG was synthesized starting from silica precursors by Kistler in 1931[1]. By the 1990s, NASA used AGs for thermal insulation in spacecraft, space suits, and blankets. Over the years, AGs have been adopted for insulation in subsea systems, oil refineries, industrial pipelines, buildings, refrigerators, and clothing like jackets and shoe inserts [2]. The synthetic methods mostly used to prepare AGs provide first hydrogels which need drying methods to become AGs. Concerning this, the most adopted techniques used to transform hydrogels into AGs strongly contribute to the physical characteristics of resulting materials [3]. The use of advanced drying procedures, such as the supercritical CO_2 method, can lead to the formation of a robust, ultra-lightweight, dendritic microstructure consisting of pores smaller than 100 nm and 90 to 99.8% of empty space [4]. So tiny pores are too small for air to travel through, thus making AGs highly efficient as insulation materials

 doi:10.20944/preprints202508.0009.v1

[2]. AGs display high specific surface area (SSA), a low mean free path for diffusion, low thermal conductivity, low acoustic velocity, low refractive index, low dielectric constant, and extremely low density, ranging from 0.0011 to ~0.5 g/cm³ [5]. A large variety of AGs have been produced, which demonstrated to be promising candidates for other applications different from insulation, which include their use as catalysts [6,7], supports for catalysts [8], sensors [9], filters [10], cosmic dust collectors [11,12], detectors in particle physics [13,14], thermal insulators [15], interlayer dielectrics, optical applications [9], and many others [9,16–19]. Additionally, as conductive matrices, AGs could be potentially applied in battery materials, capacitors and components in fuel- or solar cells [20]. Anyway, despite their huge application potential, the sol–gel process, which is the most popular method to synthesized AGs, is not completely controllable and requires costly precursors [21], thus limiting their widely translation in daily practice. Moreover, hydrogels obtained via the sol–gel route are for the most part amorphous and need calcination at high temperatures for crystallization, which can lead to the loss of many properties typical for AGs. In fact, particle growth and coalescence lower the specific surface area (SSA) and the porosity of AGs leading to the collapse of the structure and destruction of the monolithic body. Recent advancements have allowed scientists to prepare more durable materials, with enhanced structural integrity and thermal properties. Several types of AGs are known, including inorganic, organic and composite AGs. Among inorganic AGs, those deriving by metal oxides precursor, especially when they are mixed oxides, are hard to be synthesized in gel form, since it is difficult to adjust and control the hydrolysis of the molecular precursors and condensation rates, which are the first steps of the sol-gel method [22]. However, versatile sol–gel routes, including dispersed inorganic sol–gel (DIS) method and epoxide addition (EA) process, which use inorganic salt solutions, as reagents, polyacrylic acid (PAA), as template and propylene oxide (PO), have expanded the range of available materials [23]. By such approaches, several monolithic AGs have been achieved, but the optimal crystallinity has not yet been reached [23]. Furthermore, pure metallic AGs are generally not directly synthesized via molecular routes and need thermal treatments in reducing atmospheres [24]. Anyway, the recent use of preformed nanoparticles (NPs) as building blocks to be assembled for achieving AGs, represents an elegant and likewise powerful method to overcome the abovementioned issues [25]. Nevertheless, the use of templates is needed to control the assembly behaviour of NPs into a 3D percolating network, which could be stable enough to allow further processing.

1.1. An Analysis of AGs According to the CAS Content Collection

As abovementioned, based on the chemical composition of their precursors, AGs can be classified in inorganic, organic and composites AGs, whose subclasses have been disserted in detail later in this review [26]. An analysis of the CAS Content Collection has provided evidence of the extensive growth in publications, in terms of journal and patents, relating to AGs over the last two decades. Mainly from 2013, the number of patents has risen consistently, even more than journals in some years, indicating a significant commercial interest in this field (Figure 1).

 doi:10.20944/preprints202508.0009.v1

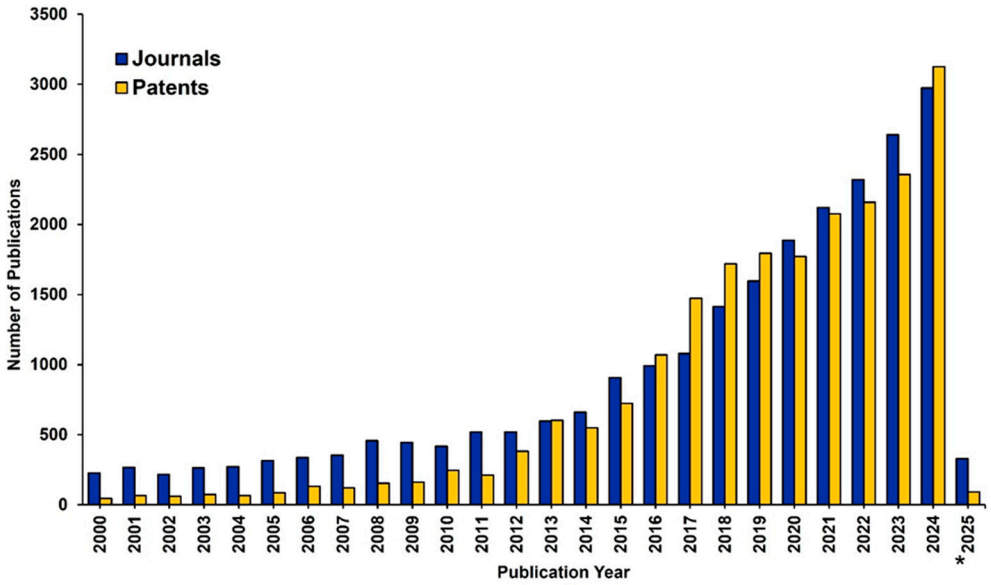

Figure 1. Publication trend in the field of AGs. Data include journal and patent publications for the period 2000-2025. Data for 2025 is partial and includes only January. Source: CAS Content Collection which is an open free platform, and no permission is required for images reproduction [2].

Patents have even exceeded journals, both for inorganic AGs, that have been in the market for many years, and for the newer synthetic polymer-based AGs, as evidenced in Figure 2.

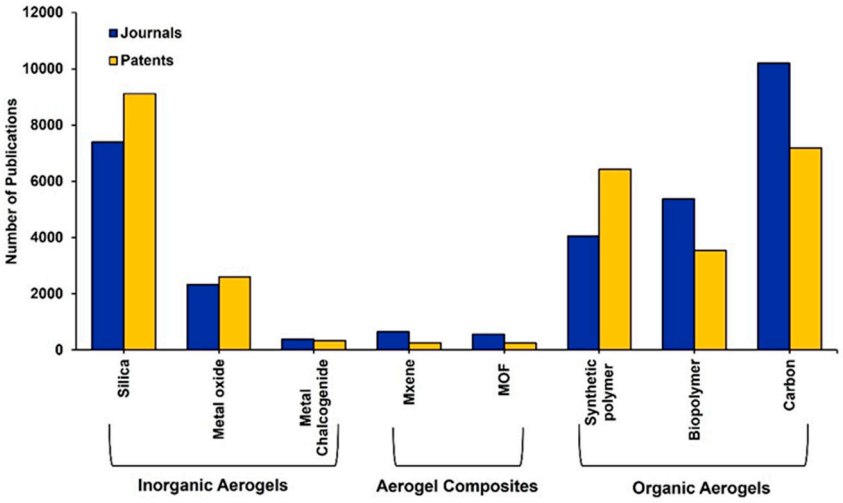

Figure 2. Number of journals and patents for the different types of AGs. Source: CAS Content Collection which is an open free platform, and no permission is required for images reproduction [2].

Conversely, the very recent composites AGs have understandably fewer related publications, and journals are slightly outpacing patent publications, to this moment. In the following Figure 3, the compounds most used as precursors to achieve particular classes of AGs, have been reported, according to the CAS Content Collection™.

 doi:10.20944/preprints202508.0009.v1

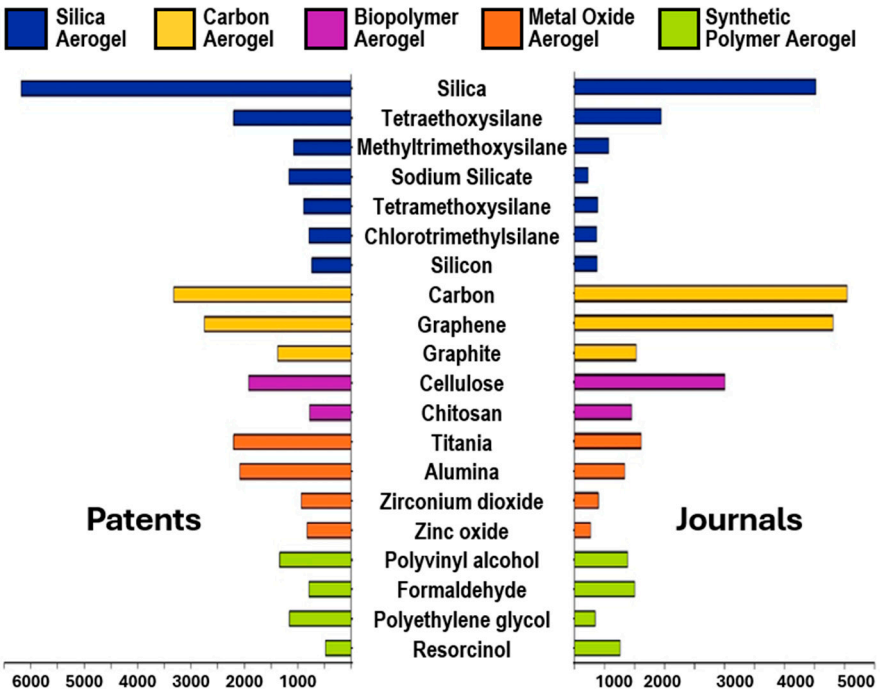

Figure 3. Top 20 substances from the CAS content collection in the field of AGs. CAS Content Collection which is an open free platform, and no permission is required for images reproduction [2].

Despite the AGs market is still in its infancy, due to the survival of certain challenges not yet fully solved, the future for these materials is bright, and their marketplace is expected to experience an annual growth rate (AGR) of approximately 17% over the future period of 2025-2035. This is because AGs are showing considerable promise in energy storage, catalysis, and various biomedical applications, as well as cosmetics and acoustics (soundproofing) industries, as confirmed by the several patent publications [2]. In fact, patents surpassed publications on journals, thus establishing their translation from academic and laboratory setting to the industrial one, thus highlighting the high commercialization of AGs in the abovementioned fields (Figure 4).

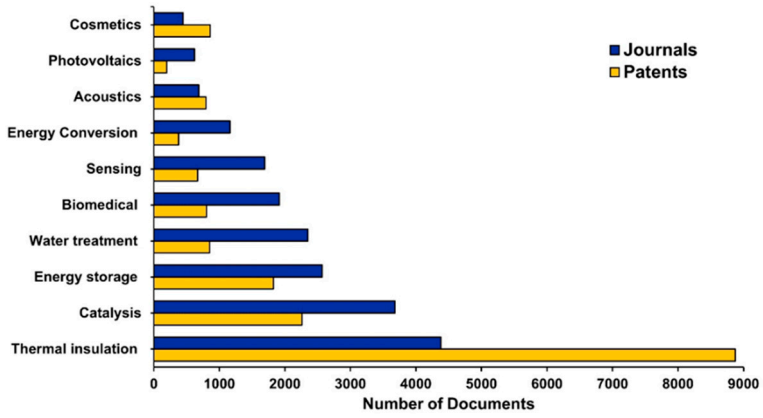

Figure 4. Number of journal publications and patents for the few emerging aerogel applications. CAS Content Collection which is an open free platform, and no permission is required for images reproduction [2].

Due to their ability to diminish the speed and amplitude of sound waves, AGs can be used as acoustic insulation materials, while in cosmetics, AGs can act as anti-shine agents in creams. Composite titanium and silica oxide AGs are being added to sunscreen because of their

 doi:10.20944/preprints202508.0009.v1

photoprotective properties, which can increase the sun protection factor (SPF) over that of conventional formulations.

On this promising scenario about AGs, the main purpose of this paper was to give an updated view on the current state of art of AGs both in academia and industry. The following sections provide first an AGs' classification based on the chemical origin of their precursors. Then, the different methods which exist to prepare AGs, with related optimization strategies, have been discussed. Specifically, the traditional sol-gel and not sol-gel chemical routes involving molecular precursors, up to the sol-gel methods using NPs as building blocks, were discussed. Following, focusing on AGs of inorganic origin, silica and metal oxide-based AGs were reviewed, deeply discussing their properties, specific synthesis and possible uses. These classes were chosen based on the evidence that they are the most experimented, patented and marketed AGs. Several related case studies have been reported and discussed, some of which have been presented in reader-friendly tables.

2. Classification of Aerogels According to Their Chemical Origin

A detailed classification of AGs based on the chemical origin of their precursors has been reported in Table 1.

Table 1. Classification of AGs according to their chemical origin.

AGs	Types	Description/ Subtypes	Refs
Inorganic AGs	Silica-based	N.R.	[9,27]
	Chalcogenides	Sulphide chalcogenide aerogels	[9,28]
	Oxide-based	Sn, W, Zr, Ti, Al, Mg, Co/Ni oxide	[29–32]
	Carbide-based	Silicon carbide, carbide-derived carbons, Mo carbide	[33–35]
	Nitride-based	Carbon nitride, Al nitride, B nitride	[36–39]
	Metal/Noble Metal	Fe, Au, Ag nanofoams	[40]
Organic AGs	Polysaccharide	Alginate, cellulose, pectin, starch, chitosan, carrageenan, mucilage *	[41,42]
	Phenolic	N.R.	[43–45]
	Polyol	Polyurea aerogels	[46,47]
	Protein	Whey, albumin, collagen, gluten, silk fibroin *	[48–50]
	Carbon	carbon nanotube, graphene, polymeric	[51–53]
Composite AGs		MXOAGs, MOFAGs, MXEAGs, CIOAGs	[2]

* Polysaccharides used to generate aerogels; Sn = tin, W = tungsten; Zr = zirconium; Ti = titanium; Al = aluminium; Mg = magnesium, Co = cobalt; Ni = nickel; Mo = molybdenum; B = boron; Fe = iron, Au = gold; Ag = silver; N.R. = not reported; MOFAGs = metal organic framework aerogels; MXOAGs = mixed-oxide aerogels; MXEAGs = Mxene aerogels; CIOAGs =combined inorganic-organic aerogels.

Inorganic aerogels (IAGs) comprehend silica AGs, chalcogenides, oxide-based, carbide-based, nitride-based, and metal/noble metal AGs [2]. IAGs are typically synthesized from inorganic precursor materials, like metal alkoxides or metal salts. In this class, silica aerogels (SAGs) possess a variety of nonpareil properties, such as low density (0.003–0.5 g/cm^3), large porosity (80–99.8 %), low thermal conductivity, allowed by their small mesopores (0.005–0.1 W/(mK)), ultra-low dielectric constant (k = 1.0–2.0), and a low refractive index (1.05)[54]. SAGs have technological applications, mainly based on their low thermal conductivity. In fact, the market for SAGs thermal super insulators is growing quickly worldwide. Anyway, it is possible to think to apply SAGs also as gas filters and dielectric materials, and/or for acoustic insulation and catalysis, even if they have not yet had a substantial impact on the market in these terms [55].

Chalcogenide-based AGs (CAGs) or metal chalcogenide AGs (MCAGs) are made from chalcogenides[28], which include sulfides, selenides, tellurides, and polonides. MCAGs are preferentially applied to absorb heavy metals [56], such as mercury, lead and cadmium from water[56], while MCAGs of non-platinum metals are very good for desulfurization[57].

 doi:10.20944/preprints202508.0009.v1

Additionally, high surface areas MCAGs are promising for gas separation [58,59] and for capturing radionuclides from nuclear waste such as ^{99}Tc, and ^{238}U, and especially ^{129}I [60]. Oxide-based aerogels (OAGs) are the most extensively used AGs. Various metal oxide AGs, including stannic oxide and tungstic oxide AGs were prepared by Kistler et al. for the first time [32], but other the years, zirconia, titania, alumina, magnesium oxide, and cobalt-nickel oxide AGs have been extensively experimented [29–31]. In addition to the OAGs reported here and in Table 1, which are among the most studied ones, there are also examples, for which the literature is much more limited [9]. They include Fe–Cr–Al mixed oxides, gold–iron oxides, $Li_2O{\cdot}B_2O_2$, GeO_2, ZnO and V doped ZnO, Sn–Al oxides, Nb_2O_5, Pd doped CeO_2, MnO_2, Ta_2O_5 and more complex compositions like $MgFe_2O_4$, $BaTiO_3$, $SrTiO_3$, $PbTiO_3$, $Li_4Ti_5O_{12}$, $VOHPO_4{\cdot}0.5H_2O$, $La_2Mo_2O_9$ and $CuO–Zr_xCe_{1-x}O_y$ [9].

Carbide-based AGs (CRAGs) include silicon carbide, carbide-derived carbons and molybdenum carbide AGs. Such materials have been extensively applied as catalysts for hydrogen production, electrodes in supercapacitors, gas turbine components, heat dissipation substrates and heat exchangers [33–35].

Nitride based AGs (NAGs) comprise carbon nitride, aluminium nitride [36,37] and boron nitride AGs. The latter is mostly applied as photocatalyst and to construct phase change materials from smart devices or used for pollutant degradation or removal [38,39].

Metal aerogels (MAGs) and noble metal aerogels (NMAGs) represent a singular class of inorganic AGs, which possess the properties of both metals and AGs and are widely applied in detection-based sectors [40,61]. MAGs and NMAGs are obtained from networks of metal NPs, that have been super critically dried to produce nanofoams mainly of iron, gold and silver [40].

Organic aerogels (OAGs) include polysaccharide-based, phenolic-based, polyol-based, protein-based, and carbon-based materials. OAGs were researched because of the non-biocompatibility of the most part of IAGs. Polysaccharide-based aerogels (PAGs) are obtained using natural saccharide polymers, like alginate, cellulose, pectin, starch, chitosan, carrageenan, mucilage, etc., which represent renewable resources. Methods to prepare PAGs involve dissolving polysaccharides in organic solvents or using cross linking reactions or ionic liquids, followed by drying to remove liquid [41]. PAGs are currently applied for drug delivery, catalysis, environmental remediation or as thickeners [42].

Phenolic-based aerogels (PHAGs) were for the first time developed by Pekala et al. by a condensation reaction between resorcinol with formaldehyde [45]. Nowadays, PHAGs are prepared via the same reaction using basic and acidic activators, where gelation occurs by phenolic furfural cross-linking [44]. PHAGs are mainly applied as reinforcement materials, for thermal and sound insulators [43].

Polyol based aerogels (POAGs), including polyurea AGs, are organic materials containing multiple hydroxyl groups, which are obtained via a polycondensation reaction between multifunctional isocyanates and amines, water, or mineral acids. Due to their optical transparency, POAGs can be used in sensors and the glaring system of insulating windows [46,47].

Protein-based aerogels (PRAGs) are manufactured starting from proteins isolated from plants and animal sources like whey, albumin, collagen, gluten, silk fibroin, etc. PRAGs are biodegradable and biocompatible and are mainly finalized to tissue engineering as scaffold materials or are used in food industry for encapsulating bioactive food constituents or for enhancing food properties like texture, taste, and nutritional values [48–50].

Carbon-based aerogels (CBAGs) could belong to the class of IAGs, due to their carbonaceous nature. Anyway, they are classified as organic-based materials, due to the origin of biological sources, which are pyrolyzed or combusted to produce them. Moreover, they are considered organic materials since some of them are produced using organic precursor materials like phenol formaldehyde resin. CBAGs mainly include carbon nanotube, graphene and polymeric AGs [2]. CBAGs are mainly exploited as adsorbents, as well as electrodes in electrical devices [51–53].

 doi:10.20944/preprints202508.0009.v1

Finally, composite aerogels (COAGs) include mixed-oxide AGs, aerogel-metal organic framework (MOF) composites, aerogel-Mxene composites, and aerogels synthesized by combining inorganic and organic precursors[2].

3. Synthetic Methods to Achieve Aerogels

3.1. Molecular Routes to Aerogels (AGs) by Wet Sol-Gel Processes

The traditional methods to prepare AGs start from molecular precursors of different types and use aqueous sol-gel chemistry, which is a useful technique for altering substrate surfaces and producing large surface areas and stable surfaces [62]. Sol-gel process basically involves the hydrolysis of precursors in acidic or basic solutions, followed by polycondensation of the hydrolysed products [63]. Ionic liquids are special solvents, which are considered better solvents for numerous chemical processes, including AGs preparation, due to their low vapor pressure and wide range of characteristics, [63]. Scheme 1 simplify such chemical sequence in case the precursors would be metal alkoxides to provide metal oxide AGs (MOAGs) [62].

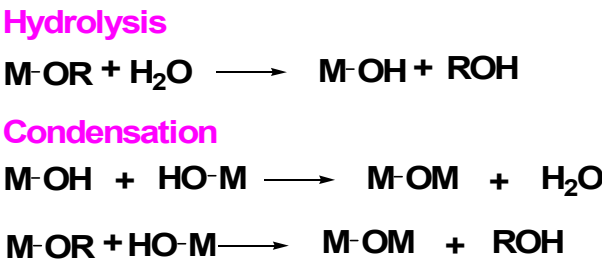

Scheme 1. Main reactions of the sol–gel process using metal alkoxides (represented by M–OR) in aqueous solutions: hydrolysis and condensation involving both oxolation (elimination of water) and alkoxolation (elimination of an alcohol ROH).

Through nucleation and growth processes, the hydrolysis and condensation reactions produce an amorphous colloidal dispersion [9]. Additional condensation and crosslinking reactions beyond the so-called sol-to-gel transition drives to an open-porous network (gel), including still a continuous liquid phase [64]. The major problem associated to the sol-gel synthesis consists of the high rapidity of the hydrolysis and condensation rates, which are hard to control, thus making difficult to adjust the gelling behaviour and to tune the final porosity. Several strategies have been implemented to influence the reaction kinetics of the sol–gel process and to control morphology and particle size [64], including the use of precursors with bulky inert side chains, precursors concentrations, addition of surfactants, variation of solvents, regulation of pH and many more [65]. Anyway, the kinetic control remains a major challenge in the production of AGs. Non optimal hydrolytic conditions could have detrimental effects on gelling behaviour [66], which is the second substantial step towards the AG formation [32]. Moreover, once the gel network is formed, several unreacted groups can still survive in the gel backbone and further structural changes within the gels are needed to obtain a mechanically more stable scaffold. Enough time is necessary for the gel network to be strengthened by managing the overlaying solution's pH, concentration, and water content. To this end, once formed, gels are often aged and ripened before supercritical, spry-, freeze- or ambient temperature drying [67]. During ageing gel structure can change, due to various factors, including the dissolution of microscopic particles into bigger ones. Upon aging, the solvents evaporate, producing gel shrinkage before a stable sol–gel network forms. Controlling the aging duration is crucial in the AGs synthesis. In fact, too long aging disposes to lower pore volume, while too little aging time promote gel network instability, which can translate in gel network collapse during solvent extraction, by drying methods. In this regard, the use of ionic liquids can extend aging timing, since their low vapor pressure inhibits solvent evaporation, while strong ionic strength accelerates aggregation. To eliminate any leftover water from the pores, the gel should be cleaned with ethanol and heptane once it has aged [68]. The

 doi:10.20944/preprints202508.0009.v1

final step of the sol-gel procedure for engineering AGs consists of a drying procedure, which may occur by ambient pressure drying, supercritical drying and freeze drying. Supercritical CO_2 drying of gels is considered as the most important step of AGs production, since it enables preservation of the three-dimensional pore structure which lead to unique material properties such as high porosity, low density, and large surface area [69]. Supercritical CO_2 drying of aged gels can be performed at high or low temperature and in autoclave at a critical level of heating or at the atmospheric pressure. It prevents the occurrence of surface tension in the gel pores and constant compression, thus avoiding the production of concave menisci and preventing pore and gel body collapse [63]. Methanol is usually used as supercritical drying solvent for AGs. High-temperature supercritical CO_2 drying causes less shrinking of the gel. Figure 5 shows a typical flow diagram of a continuous supercritical CO_2 drying process [69].

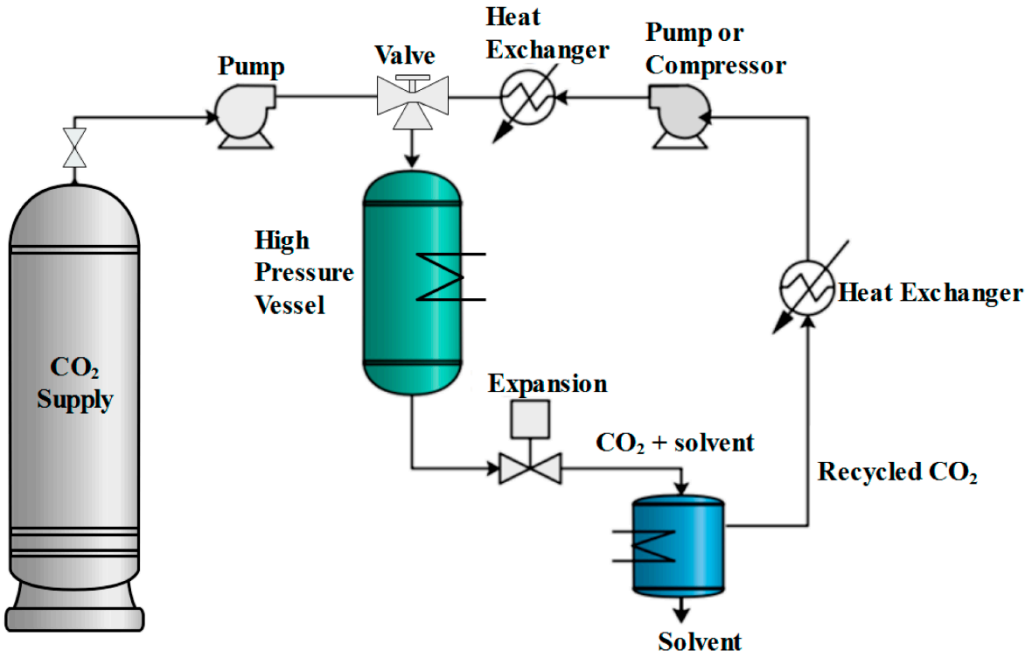

Figure 5. Flowsheet of a supercritical CO_2 drying cycle [69]. The image has been reproduced by an open access article published under a Creative Commons CC BY 4.0 license (accessed on 27 May 2025), which permit the free download, distribution, and reuse, provided that the author and preprint are cited in any reuse.

Estok et al. produced an AE in a kerbed mould inside a 24-ton hydraulic hot press, provided by Tetrahedron associates, completing the synthetic progression, with a quick supercritical extraction process [70]. A stainless-steel mould with 16 wells with diameter 1.9 cm depth 1.9 cm and dimensions of 11 × 11 × 1.9 cm was constructed and sealed prior to processing with gasket material. A nonstick spray was applied to the mould. Similarly, Anderson et al. used a hydraulic hot press and a bespoke steel two-part mould, which was sandwiched between Kapton and a high-temperature gasket material, to achieve rapid supercritical extraction [71]. At the beginning, the mould was heated at 38 °C and stabilized by adjusting the hot press limiting strength to 94 kN for 2 to 7 h. Yoda and Ohshima modified methanol supercritical drying by adding water, nitric acid and ammonia, during preparation of SAGs from tetra-methoxy-silane, heated the autoclave to 553 °C at a rate of 40 °C per hour, while the temperature remained constant for further 3 hours[72]. By comparing the obtained results with those observed using normal supercritical drying processes, the authors evidenced that gel-component extraction decreased, especially when water was added. The constituting particle and pore sizes increased when water or a base were added, while the use of acids increased the specific surface area (SSA) [72]. Quignard et al. prepared polysaccharide AGs by drying the obtained the polysaccharidic microspheres first by immersion in a series of sequential ethanol–water baths with increasing alcohol concentrations (10%, 30%, 50%, 70%, 90%, and 100%) for 15 min each [73] and then

 doi:10.20944/preprints202508.0009.v1

in Polaron 3100 equipment under supercritical CO_2 circumstances (74 bar, 31.5 °C). Although supercritical CO_2 drying process have several advantages, high costs, process continuity, and safety, strongly limit its extensive utilization. To overcome these issues, a commercially available ambient pressure drying (APD) technology was devised and proposed by Brinker et al. to produce SAGs, involving ambient pressure evaporation as the last step. APD is the most used method for preparing low-costs AGs [74]. Cai and Shan performed a two-steps acid-base sol-gel synthesis of SAGs using methanol (MeOH) as solvent and oxalic acid and ammonia (NH_3H_2O) as catalysts, followed by ambient pressure drying [75]. Feng et al. produced SAGs with a large surface area by means of sol–gel technique using water glass made from rice husks as precursor, whose modulus strongly affected the characteristics of AGs. Also in this case, ambient pressure drying was used in the final step [76]. Also, Yun et al. prepared SAGs and dried them at ambient pressure in a furnace at 80 °C for 24 h and finally at 120 °C for 12 h [77]. Avoiding acid corrosion on the equipment during the drying process, Zhao et al. evaporated liquid in AGs, at ambient pressure, without the silica skeleton structure collapsing [78]. Wu et al. found that highly porous AGs, with unprecedented hydrophobic characteristics, can be achieved using fly ash and trona ore as raw ingredients and drying the wet product at ambient pressure [79]. AGs can be dried also using the freeze-drying techniques by which, the liquid of the long-time aged wet gel is frozen and subsequently vaporized under reduced pressure [63]. The long-time aging is necessary to achieve a full solidification of gel network, while a solvent with a lower thermal expansion and a higher sublimation pressure should be used [63]. This approach was used by Pan et al., who employed various molar ratios (5.1–0) of MTMS/water-glass co-precursor, to create hybrid AGs of silica and carbon with low thermal conductivity and great thermal stability [80]. Experimental findings showed that the MTMS/water-glass molar ratio greatly influenced the hybrid AGs' characteristics. After 8 h of drying at −80 °C in a laboratory freeze drier, the AGs were vacuum-dried for roughly 48 h. Additionally, glass fibre-reinforced SAGs were produced by Zhou et al [81].

3.1.1. Improved Sol-Gel Procedure by Epoxide Addition Methods

By the sol-gel approach above described, a robust assortment of metal oxide, chalcogenide and other classes of AGs has been developed. Anyway, for example in the case of MOAGs preparation, even under ideal conditions, the hydrolysis and condensation of the precursors, frequently provides dense hydroxide or oxide sediments, due to the fast reaction kinetics of this process. Consequently, porosity of the products results significantly limited and not controllable. In this regard, it is necessary to slow down the hydrolysis and condensation rates for achieving material with high porosity [67]. A modified sol-gel method was used by Tilloston et al. to prepare mixed lanthanide-silicate and pure lanthanide AGs from erbium, praseodymium, and neodymium chlorides, using different catalysts [82]. Particularly, to prepare mixed AGs, authors used a two-step sol-gel method using a sub-stoichiometric amount of water in the first step, thus achieving a partially condensed silica-lanthanide precursor. Conversely, the pure lanthanide AGs were obtained directly from the chlorides using propylene oxide (PO) to neutralize the hydrochloric acid evolved during reaction, thus slowing down hydrolysis kinetics [82]. On the example of the procedure previously described by Tilloston et al. [82], Gash et al. proposed the epoxide addition (EA) method using PO associated with the sol-gel alkoxide chemistry, to prepare Fe_2O_3 [83]and Cr_2O_3 [84]. Specifically, AGs were prepared by sol-gel procedure, using of inorganic salts as precursors, acidic hydrolysis and epoxides to induce gelation. Lower-rate kinetics were achieved avoiding the formation of gelatinous precipitates commonly obtained by traditional sol-gel method, thus allowing the formation of monolithic semi-transparent AGs. Various types of epoxides were experimented to investigate the effects of different epoxydic structures on the microstructural properties of iron oxides (Figure 6) [85].

 doi:10.20944/preprints202508.0009.v1

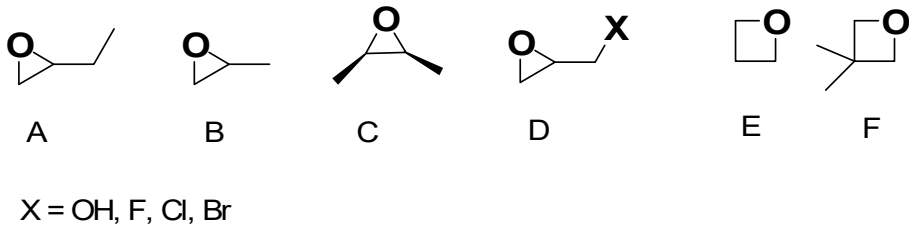

Figure 6. Main types of epoxydic compounds experimented in EA methods for the formation of AGs. (a) 1,2-Epoxybutane, (b) propylene oxide, (c) *cis*-2,3-epoxybutane, (d) glycidol (X = OH) and epihalohydrines (X = F, Cl, Br), (e) trimethylene oxide, and (f) 3,3-dimethyloxetane.

Inspired by studies of Gash et al., many different unprecedented materials were prepared by EA methods, thus significantly escalating the range of possible monolithic AGs materials. The most reported EA approaches involved the use of propylene oxide (PO) for gel formation by the following mechanism. In the first step (Figure 7a), the PO oxygen becomes protonated by the H^+ of HA catalyst necessary for sol-gel process, while in the second one (Figure 7b), the anion A^- makes a basic attack on the less substituted carbon atom of PO, leading to a ring opening reaction. By this mode, acidic proton atoms, are captured, thus slowly raising the pH value. Such pH change brings to hydrolysis and condensation of the inorganic salts and slows down the condensation rate.

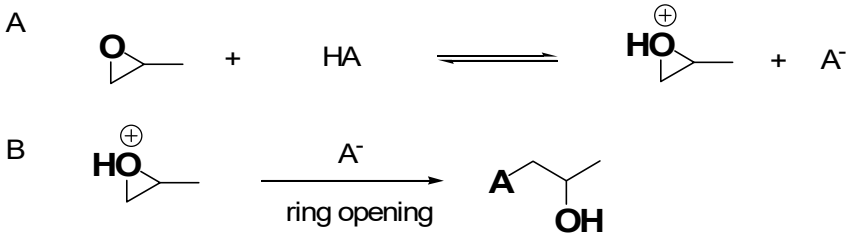

Figure 7. (a) Protonation of PO by HA; (b) ring opening reaction via nucleophilic attack.

These early studies of Gash et al. on Fe_2O_3 [83] were then gradually extended to Fe_3O_4 [86,87], β-FeOOH [85], Fe_3C [88], Pd and K [89,90] doped iron oxide and iron–chromium mixed oxides [91]. The EA method was utilized by Hu et al. to obtain nickel cobaltite ($NiCo_2O_4$) AGs, which in fact were synthesized by a chloride-based epoxide-driven sol–gel process [92]. The as obtained AGs were crystallized already at a calcination temperature of 200 °C and were tested as capacitor materials. They exhibited ultrahigh specific capacitances (1400 F g^{-1}), excellent reversibility, and outstanding cycle stability, at a relatively high mass loading of 0.4 mg cm^{-2} [92]. Al_2O_3–based AGs with tuneable pore size were possible adding to the reaction mixture PO [93–95]. Heterogeneous AGs based on Al_2O_3 associated with CuO and ZnO were obtained by Epple et al. by methanol synthesis [96], while Hope-Weeks et al. co-gelled aluminium and nickel nitrate salts [97]. The EA method was combined also with non-alkoxide chemistry, thus allowing to synthesize yttria (Y) stabilized zirconia (Zr)-based AGs [98]. The influence of various factors on surface area and morphology of such materials were investigated thoroughly by different authors [99,100], as well as alternative synthesis using different salts and alkoxides [101], including the nitric acid-assisted EA synthesis, was utilized by Zhong to prepare monolithic Zr AGs [102]. They were prepared using zirconium oxychloride ($ZrOCl_2$) as the precursor in the presence of PO in both ethanol and mixed ethanol–water solutions, respectively, followed by calcination at 750 °C for 2 h [102]. High surface area AGs based on SnO_2 [103] and ZnO [104–106], as well as their AG composite (ZnO–SnO_2 AG), which demonstrated efficiency in degrading rhodamine B (RhB)[107], were synthesized by different scholars. Indium-doped tin oxide AGs were obtained by Davis et al. through the EA method, utilizing a non-alkoxide procedure with glycidol, thus achieving stable frameworks with a regular pore structure and considerable electrical conductivity [107]. These AGs may meet the increasing demand for porous conducting networks to

 doi:10.20944/preprints202508.0009.v1

be used in battery materials [108] and fuel cells [109] and for transparent electrodes for LCD, LED and solar cells [110–112]. Similarly, Agrios et al. fabricated transparent conducting AGs via EA doping tin oxide with antimony, which may be utilized as electron scavenger in dye sensitized solar cells [113,114]. Already before the year 2020, several materials had been used for preparing AGs via EA which have been reported in Table 2.

Table 2. Materials experimented to prepare AGs via EA.

Formula	Chemical name	Applications	Refs
TiO_2	Titanium oxide	N.R.	[115]
V_2O_5	Vanadium oxide		[116]
Co_3O_4	Cobalt oxide	Supercapacitors	[117]
UO_3	Uranium trioxide		[118]
Gd_2O_3	Gadolinium oxide		[119]
La_2O_3	Lanthanide oxides		[120]
ZnO_2/TiO_2, SiO_2/TiO_2	Zinc/titanium oxide, silica/titanium oxide	N.R.	[121]
Ta_2O_5	Tantalum oxide		[122]
Mn_3O_4	Manganese oxide		[123]
Y_2O_3	Yttrium oxide		[124]
Eu doped Y_2O_3	Europium-doped yttrium oxide	Luminescence	[125]
Eu doped ThO_2	Europium-doped oxide	N.R.	[126]
NiO/Al_2O_3	Nickel oxide/alumina oxides	Hydrogen production	[127]
$ZnFe_2O_4$	Zinc-ferrite oxides	N.R.	[128,129]
VFe_2O_x	Vanadium-ferrite oxides	Electrochemical charge storage	[130]
$La_{0.85}Sr_{0.15}MnO_3$	Lanthanum-strontium-manganese oxides	Electronic conductivity	[131]
$MnFe_2O_4$	Manganese-ferrite-oxide	Magnetism	[132]
$NiFe_2O_4$	Nikel-ferrite oxide	Magnetic sector	[133]
$Zn_5(OH)_8Cl_2{\cdot}H_2O$	Simonkolleite	Photoluminescence	[134]

N.R. = Not reported. La = lanthanum; Sr = strontium; Mg = manganese.

EA method provided significantly improved AGs, but crack-free monolithic materials from bivalent metal ions (Cu^{2+}, Ni^{2+}, Zn^{2+}, etc.) were still not easily reachable. Gash et al. were the first, who synthesized a divalent metal oxide-based AG by EA [135]. However, it was the discovery of the dispersed inorganic method (DIS), which made easy the achievement of AGs containing divalent metals. DIS consists of a modification of the EA procedure developed by Du et al., which implicates the addition of polyacrylic acid (PAA) and PO to inorganic salt solutions [136]. In the reaction mixture, PAA serves as both dispersant by its steric hindrance and as nucleation site for gel formation. By using DID method, bivalent metal containing AGs with less shrinkage and stronger scaffold were achieved and three-dimensional crosslinking was easily possible [23,136]

3.1.2. Sol-Gel Methods to Prepare Noble Metal Aerogels (NMAGs)

Sol–gel method is the most used method for preparing NMAGs under mild conditions. Two-steps and one-step sol–gel methods terminated with supercritical CO_2 drying were reported to obtain noble metal monolithic AGs, which represent a unique class of materials having high specific surface areas and large open pores, thus being very promising in various applications such as in heterogeneous gas-phase catalysis, electrocatalysis, and sensors [137]. The only difference between the two methods is whether a separated NP colloidal solution is required [138]. The two-step method involves the reduction of metal ions to metal nanoparticles (MNPs) followed by gelation, while the second proceeds via an in situ spontaneous gelation process of metal ions [137,139]. Specifically, in the two-step strategy, citrate-capped monometallic NPs with size 3-6 nm are first synthesized via reduction of the metal precursor ($HAuCl_4$, $AgNO_3$, H_2PtCl_6, or $PdCl_2$) with $NaBH_4$ using trisodium

 doi:10.20944/preprints202508.0009.v1

citrate as a stabilizer [140,141]. Also, hollow preformed bimetallic nano-shell particles can be prepared via galvanic displacement reaction between citrate-stabilized AgNPs and metal precursors such as $HAuCl_4$, K_2PdCl_4, and K_2PtCl_4, while thiolate-coated Ag nano-shell particles can be obtained via fast chemical reduction of preformed Ag_2O NPs [142,143]. The following step involving gelation of the preformed metal NP solutions or their mixtures is induced by deliberate destabilization via typical sub-steps including solution concentration by a factor of 10–50 with polystyrene centrifuge filters or a rotary evaporator with water washings to minimize residual stabilizer and impurities. Then the gelation occurs by settling of the concentrated NP solutions at room or increased temperature (323–348 K) or via addition of destabilizers such as ethanol, H_2O_2, etc. By such destabilization, the hydrogels formed in about 1–4 weeks, which greatly limits their applications [138]. Anyway, the gelation time can be shortened and gel kinetics accelerated by various novel destabilization methods developed, such as changing the synthetic parameters (e.g., temperature and disturbance) [23,141,144–147], adding extra initiators (e.g., dopamine (DA), salts, tetranitromethane ($C(NO_2)_4$), $NaBH_4$, and hydrazine monohydrate ($N_2H_4{\cdot}H_2O$) [138]. A wide range of monometallic hydrogels, including Au, Ag, Pt, and Pd, and multi-metallic hydrogels, including Au–Ag, Au–Pd, Pt–Ag, Pd–Ag, Pt–Pd, Au–Ag–Pt, Au–Pt–Pd, Ag–Pt–Pd, and Au–Ag–Pt–Pd, have been prepared using this strategy which were transformed in aerogels by drying [138,140,141].

In the second strategy, hydrogels form spontaneously via in situ reduction of metal precursors with $NaBH_4$ in a single step, without the preformation of adequately stabilized NPs [138]. α,β,γ-cyclodextrin (CD)-protected Pd ($Pd_{\alpha,\beta,\gamma}$-CD) hydrogels [148], pure Pd and Pt hydrogels, and bimetallic Pt_nPd_{100-n} hydrogels were prepared by this strategy [148,149]. However, due to a too long gelation time (3–10 days) and the large amounts of organic residuals (44 wt %) in the final product, great difficulties were encountered in investigating the intrinsic activity of NMAGs. To address this issue, in situ kinetically controlled reduction and synthesis of M–Cu (M = Pd, Pt, and Au) hydrogels within 6 h via increasing the reaction temperature was pioneered by Zhu et al. [150]. Furthermore, Shi et al employed a similar way, thus fabricating for the first time fabricated $AuPt_x$ bimetallic hydrogels at 60 °C in 2–4 h [151].Supercritical CO_2 drying has demonstrated to be the most appropriate way to retain the internal structure of the hydrogel also in the dry state of AGs, minimizing the factors which may lead to the collapse of the fragile pores inside the structure, thus allowing the gel to be dried with very little shrinkage. AGs with higher surface area, an intact pore shape, and a larger pore volume than those porous structures obtained using conventional drying methods are allowed by CO_2 supercritical drying. Before supercritical drying, the water in the pores of the hydrogels is replaced by acetone and further with liquid CO_2.

Additionally, methods such as non-sol–gel synthesis techniques of dealloying, combustion, and templating approaches, thus achieving bio-templated metal AGs composites and salt-templated structures, have been reported [139].

3.1.3. Non-Sol-Gel Methods to Prepare Metallic Aerogels

Dealloying and combustion synthesis is a non-sol-gel method to achieve metal nanofoams and aerogels, addressing the challenges of synthesis time and shape control of the one- and two-step aerogel synthesis above reported. Additionally, bio-templating strategy has allowed a strict control over nanostructure length and diameter, as well as overall monolith shape. Also, salt templating.is an emerging synthesis method for high-surface area, porous, and scalable metal-based AGs [139].

Dealloying and Combustion

Dealloying is a general term for a corrosive process that selectively removes one or more components from an alloy, leaving the remaining to evolve spontaneously into a porous structure and was the first method employed to synthesize porous noble metal foams [139]. Subsequently, this method has been employed to prepare films, foams, and porous nanoparticles [152–157]. Alloys based on the association of Ag and Au were exploited for selective dealloying, since silver is easily dissolved, while Au atoms tend to aggregate thus forming relatively homogeneous 3D porous

 doi:10.20944/preprints202508.0009.v1

structure. Among the disadvantages of this techniques, the small number of alloy combinations available and the impossibility to scale well beyond 1 mm are comprised[158], while sizes range down to approximately 10 nm resulted in specific surface areas lower than 10 m^2/g. Collectively, despite this technique may be promising when in combination with another synthetic strategies, limitations for scale-up and practical device implantation make it low attractive. Combustion synthesis has also been used to prepare gold and palladium aerogels through the ignition of metal complexes with highly energetic ligands [158,159]. Specific surface areas for Au and Pd monoliths prepared via combustion synthesis are reported to be 10.9 m^2 /g and 36.5 m^2/g, respectively, suggesting a similar challenge as dealloying in attaining small-scale feature sizes.

Bio-Templating

Bio-templating is an approach which allow to achieve materials with biological morphology and having different compositions and shapes, utilizing material chemistry. Specifically, bio-templating exploits biological molecular structures, such microorganisms, viruses, and biomolecules such as DNA, cellulose, and proteins as shape templates to synthesize nanostructures via binding preformed nanoparticles, vapor deposition, or electroless depositing metals onto the template surface [160,161]. By this technique several nanomaterials and porous film have been prepared but its use to achieve noble metal aerogels is still in its infancy.

Salt Templating

Dealloying and gravity-driven gelation approaches can provide noble metal foams and NMAGs as thin films with characteristics which make them suitable as electrodes [153,162]. Easy scaling-up, short time, and low costs are the main advantages to prepare thin films, due to the shorter diffusion path to remove synthesis by-products and conduct solvent exchanges. Burpo et al. used insoluble salt needles as templates for porous macro-tubes and macro-beams that may be assembled into arbitrary shapes, such as thin films, and with tuneable densities [163–166]. The reduction of salts formed with varied concentrations of $[PtCl_4]^{2-}$ and $[Pt(NH_3)_4]^{2+}$ ions, namely Magnus' salts [139], used as insoluble precursor salt needles, yielded hierarchically highly porous macro-tubes with square cross sections and contour lengths consistent with the salt templates (SEM). SEM images showed porous sidewalls comprised of Pt nanoparticles (NPs) (~100 nm in diameter), in turn comprised of textured nanofibrils with an average diameter of 4.9 ± 0.7 nm. Reduction was carried out with 0.1 M $NaBH_4$ at 1:50 (v/v) salt needle. It has been reported that two $[Pt(NH_3)_4]^{2+}$ are necessary in solution to maintain a charge balance for each $[PtCl_4]^{2-}$ ion reduced. X-ray photoelectron spectroscopy and X-ray diffractometry analyses indicated the presence of platinum structures with no oxide content, while electrochemical impedance spectroscopy (EIS) demonstrated a specific capacitance of 18.5 F/g and an electrochemically active surface area (ECSA) of 61.7 m^2/g. Cyclic voltammetry (CV) showed characteristic hydrogen adsorption and desorption and platinum oxidation-reduction peaks [166]. By combining different square planar noble metal salts to form Magnus' salt derivative needles as salt template allowed the achievement of bimetallic and alloy noble metal-based materials. In this regard, Burpo et al. studied the salt-template reduction-dissolution mechanism for the formation of platinum-palladium hierarchical metal nanostructures [164] Particularly, the addition of $[Pt(NH_3)_4]^{2+}$ ion solutions with varied concentrations of $[PtCl_4]^{2-}$ and $[PdCl_4]^{2-}$ anions provided bimetallic salt templates with lengths between 15 and 300 μm, which, upon chemical reduction with $NaBH_4$ formed porous Pt-Pd macro-beams with square cross sections that were in compliance with the length of the initial salt template. Porous sidewalls and internal structure comprised of primary Pt and Pd NPs of 8–16 nm in diameter, or fibrils 4–7 nm in diameter, depending on the ratio of platinum to palladium ions in the salt template were observed for macro-beams, each beam representing an AG structure. ECSA values were in the range 23.2- 26.7 m^2/g. Despite these values are almost half the BET determined specific surface area values of Pt-Pd bimetallic aerogels synthesized by Bigall et al. using the two-step gelation approach [140], in the salt template method the formation of the salt template is instantaneous and their electrochemical reduction, very rapid.

 doi:10.20944/preprints202508.0009.v1

3.2. Nanoparticle-Based Routes to Aerogels (AGs) by Wet Sol-Gel Processes

Upon years of studies in nanotechnology, a robust arsenal of NPs owing different sizes and shapes is nowadays available, which can be used as versatile building blocks with distinct properties and functionalities to achieve AGs. Various types of NPs can be assembled as LEGO bricks in a bottom-up process [167], to form AGs monoliths conserving the NPs properties in a nanostructured macroscopic bulk material. Despite the as prepared AGs do not possess high porosity, high surface area and low density, they encompass new nonpareil functionalities, such as super-paramagnets [168], ferroelectricity[169], luminescence[170], (photo)catalytic activity[171,172] or electrical conductivity[20,173], which were proper of their NPs precursors, thus being very interesting as batteries[174], fuel[175] or solar cells[113]. Following, a general overview of the different steps of assembling preformed NPs into AGs has been available. The gelation of preformed nanocrystal building blocks dispersed in high concentration in solvents to form three-dimensional macroscopic AG monoliths, usually occurs by controlled destabilization. In most systems this phenomenon leads to the assembly of the NPs in gels at random crystallographic orientation (it is the case of chalcogenides add metals AGs) or by an oriented attachment mechanism (it is the case of TiO_2 and SnO_2 AGs). Finally, the dispersions of anisotropic NPs building blocks can often be destabilized through mild centrifugation (it is the case of WO_x, and Y_2O_3 AGs). Collectively, the entire procedure requires the synthesis of the nanosized building blocks by wet chemical processes thus having good control over particle size, size distribution and shape, as well as over the surface chemistry, thus preventing or minimizing agglomeration for good re-dispersibility in the next step. Available wet synthetic methods encompass aqueous [176] and nonaqueous sol–gel processes [175,177], polyol route [178], hot-injection [179], heating-up method [180], hydro- and solvothermal processing [181] etc. Once synthesize the building blocks need to be immersed in solvents to provide dispersions concentrated enough to reach a percolation threshold during gelling, but not excessively high to avoid aggregation. For stabilizing the dispersion, scientists recover to the use of brushes, surfactants or electronic charges to avoid spontaneous aggregation. Up to date, generally applicable protocol to prepare ideally concentrated colloidal NPs dispersions is still missing and intensively researched. For any specific system, there is a unique combination of stabilizing strategies and solvents to be used, as well as a peculiar balance of attractive and repulsive forces between particles which decide if the particles form a stable dispersion or undergo coagulation [182–184]. The third step towards AG formation is the controlled and efficient destabilization of the dispersions. The most adopted strategies for destabilization encompass photochemical treatment [185], temperature change [173], sonication [169], adding chemicals [170] or additional solvents [173] for the removal of stabilizing ligands from the surface of the NPs [172] or neutralizing surface charges by changing the ionic strength [142] or pH [186] of the media. The impairment of the balance between attractive and repulsive forces leads the attractive interactions to prevail [187]. Upon this, NPs loss their hard sphere-like behaviour becoming more “sticky” and colliding/fusing together [188]. In this phase, it is of paramount importance to control the rate of the destabilization process [189,190], to avoid flocculation and sedimentation in place of AGs formation via a percolating network formation throughout the entire volume of the sample [187]. In most systems, the NPs fuse upon contact at random orientations and atom diffusion can occur, while TiO_2 and SnO_2 are systems undergoing oriented attachment upon controlled. In the last step, the wet gel is super critically dried to obtain the NP-based AGs. The assembly of building blocks of just a few nanometres in size to centimetre sized macroscopic structures looks particularly impressive, if we consider that such a process bridges seven orders of magnitude in length scale.

4. More in Deep into the Most Patented Classes of Inorganic Aerogels

In this section we have deeply studied the two most experimented and patented classes of inorganic AGs, such as silica and metal oxide AGs, in terms of main properties and applications.

 doi:10.20944/preprints202508.0009.v1

4.1. Silica-Based Aerogels (SAGs)

Silica-based aerogels (SAGs) present a distinct nanoporous networks, made of interconnected silica nanoparticles (SiNPs) and a high-volume nanosized pores, which have attracted the interest of many researchers. Silica was the first material produced in form of AG, and it became the most extensively studied system in the community, and nowadays, most publications on inorganic AGs are dedicated to silica-based AGs. The most used precursor material to prepare SAGs is silica, followed in the order by $Si(OCH_2CH_3)_4$ (tetra-ethoxy-silane), $CH_3Si(OCH_3)_3$ (methyl tri-methoxy-silane), sodium silicate, $Si(OCH_3)_4$ (tetra-methoxy-silane), $Cl\text{-}Si(CH_3)_3$ (chlor-trimethyl silane), $SiO_n(OC_2H_5)_4$ (poly-ethoxy di-siloxane) and silicon [2]. AGs from tetra-methoxy-silane and poly-ethoxy di-siloxane have much lower thermal conductivity than those from tetra-ethoxy-silane precursors [191]. Tetra-ethoxy-silane precursor is the best option to achieve high-quality clear aerogels. They are achieved via the "sol-gel" process, which, as above reported, is a popular and effective method for making the various types of aerogels [192]. Chemistry and kinetics of sol-gel reactions to prepare SAGs are well known and controllable and silica offers extensive potential for surface functionalization [67,171]. The steps in the sol-gel process include precursors preparation and formation of colloidal solutions (sol) by their acidic or basic hydrolysis followed by gelation, through stable covalent cross-linking or weaker intermolecular interactions, which can undergo reversible sol-gel and gel-sol transitions under external conditions [193] and aging. During aging, the just formed gel network is allowed to expand with the help of managing factors like pH level, temperature, and time. Aging parameters, such as Ostwald ripening, coarsening, sintering, and syneresis, have a significant impact on the physical features of the product, particularly in terms of fortifying the fragile structure of the gel which is formed by improving siloxane bonds between particles before drying [194]. Finally, a drying procedure like supercritical CO_2, freeze, or ambient pressure drying and densification conclude the process [192]. SAGs hydrophobicity or hydrophilicity mainly depend on the synthesis process or on the surface silanol groups [195]. SAGs on the market find applications in high-tech engineering such thermal insulation, separation, coatings, sensing, and catalysis due to their unique features [195]. Additionally, they find application in biomedical sectors for drug delivery, tissue engineering and regenerative medicine [67,196–198]. Recently SAGs have been applied for environment remediation, air purification, CO_2 capture and VOC removal, as well as in water treatment, to remove oil and toxic organic compounds and heavy metal ions [195]. Table 3 collects fundamental physical properties of SAGs while some of the important SAGs along with their mechanical properties in terms of Young's modulus, bulk density and/or compressive stress are listed in Table 4.

Table 3. Fundamental physical properties of SAGs.

Property	Value	Ref.
AD	0.003–0.35 g/cm³	[199]
ISA	600–1000 m²/g	
MPD	20 nm	
CTE	2.0–4.0 × 10^{-6} / °C	
SV	100 m/s	

AP = Apparent density; ISA = internal surface area; MPD = mean pore diameter; CTE = coefficient of thermal expansion; SV = sound velocity.

 doi:10.20944/preprints202508.0009.v1

Table 4. A summary of mechanical properties of various SAG composites.

SAG materials	Preparation method	Mechanical properties	Ref.
SAGs/glass fibre composite		YM (MPa) = 0.6342, BD (g.cm $^{-3}$) = 0.142	[200]
SAGs /sepiolite fibre composite	Sol-gel via SD	BD (g.cm $^{-3}$) = 0.21	[201]
SAGs /ceramic fibre composite		YM (MPa) = 106, BD (g.cm $^{-3}$) = 0.45	[202]
Amine-modified SAGs	Traditional cross-linking	YM (MPa) = 108.12	[203]
CNT/SAG composite	Sol-gel	YM (MPa) = 14, BD (g.cm $^{-3}$) = 75.3	[204]
Sodium-silicate-based composite	Ambient pressure drying	YM (MPa) = 13.5, CS (MPa) = 11	[205]
Aramid fibre/SAG composite	Sol-gel	YM (MPa) = 972, BD (Kg.cm $^{-3}$) = 150	[206]
TiO_2-opacifier/fibre/ALAGs	Freeze drying	YM (MPa) = 3.58	[207]
Cellulose- SAGs	SD	YM (MPa) = 11.5, BD (g.cm $^{-3}$) = 0.225	[208]

SAG = Silica aerogel; ALAG = alumina aerogel; SD = supercritical CO_2 drying; YM = Young's modulus; CS = compressive stress; BD = bulk density.

The interested reader can refer to other publications and reviews covering the recent advances in SAG research [13,67,209–211].

4.1.1. Main Properties of SAGs

SAGs are endowed with unprecedented properties which confer them broad utility in various high-performance applications. SAGs own a typical microstructure characterized by particle with size of 2-5 nm and ultra-fine pores, sized in the range of 50-100 nm, depending on the specific synthesis conditions, tailored during their production. Unfortunately, despite SAGs are praised for their excellent thermal insulation, deriving from their high porosity, they often exhibit poor mechanical strength. Changes in density can influence their brittleness or ductility, with higher densities typically leading to increased fragility, which strongly limit their industrial utilization [212,213]. This vulnerability essentially depends on their delicate "pearl-necklace" microstructure, particularly susceptible to the interparticle neck regions, which compromises structural integrity under mechanical stress [214]. Integrating polyethylene glycol (PEG) into the aerogel matrix is a typical approach for enhancing mechanical properties of SAGs, by modifying the pore sizes, thus enhancing they overall durability, and making them less prone to mechanical failure under stress [215,216]. Also, studies have shown that a lower pH and a longer aging time can lead to smaller pores and a denser particle network, which subsequently enhance the mechanical properties and increase the thermal resistance of the aerogels [217,218]. Moreover, the introduction of carbon-based materials into SAGs network leads to improved mechanical strength and elasticity, higher resistance to compressive and tensile stresses without significantly compromising the SAGs lightweight characteristics [219]. Toughness and durability of SAGs can be improved also by combining them with polymers and ceramics, which can support the AG structure, thus achieving materials more suitable for applications in construction and industrial practices, where endure capability in fluctuating environmental conditions and mechanical loads are required [220]. Supercritical CO_2 drying methods that reserve AGs microstructure avoiding pores collapse, can greatly contribute to

 doi:10.20944/preprints202508.0009.v1

enhance their mechanical profiles [221]. The hybridization of SAGs with more robust materials through co-gelation processes including organic materials, such as fibres and polymers, has led to reinforced monolithic structures, with improved mechanical properties suitable for large-scale industrial applications, as extensively discussed in the notable review by Xue et al. [222]. Patil experimented that the integration of just 2 % double-walled carbon nanotubes (DWCNTs) into DWCNTs meaningfully augmented their mechanical properties, tripled their elastic modulus and markedly enhanced tensile strength [223]. The reinforcement of SAGs with polyacrylonitrile fibres enhanced their durability, reusability and Young's modulus, thus making them exceptionally effective in oil adsorption. Conversely, the introduction of polyaniline nanofibers has increased SAGs flexural strength while maintaining their essential electrical properties, thus providing materials with more potentials in electrical applications, including the development of chemo-resistor sensors [224]. Polymer-reinforced SAGs that exhibited increased elastic recovery were synthesized. Pettignano et al. explored alginate, as reinforcing material for SAGs, finding enhanced [225]. Cao et al. studied the integration of SAGs with polyurethane foams creating composites that maintain high porosity while showing improved deformability and mechanical resistance. Such materials are suitable for a wide range of applications, extending from construction to aerospace sectors, where both lightness and durability are critical [226]. Advanced manufacturing techniques like direct ink writing allowed the obtainment of objects with customized mechanical properties and low thermal conductivity, proper for high-performance thermal insulation applications [227]. SAGs possess also significant optical, acoustic and low thermal conductivity properties. SAGs inherent transparency, which can be effectively controlled through adjustments in synthesis parameters, such as pH levels, aging durations, and the types of precursors used for synthesizing SAGs[228], renders them particularly attractive for use in optical fibres and solar collectors, where precise light manipulation is necessary, and to improve the efficiency and performance of photonic devices, which are pivotal in telecommunications and information processing technologies[229–231]. Their low refractive index is ideal for optical fibres, which trust on minimal light loss to maintain signal integrity over long distances, thus making SAGs excellent candidates for inclusion in optical devices such as lenses and light guides [232,233]. Also, SAGs are capable of controlled light scattering, thus being suitable for architectural applications and for modern, energy-efficient building designs. They are promising in the development of translucent insulating windows that allow for natural light diffusion while preserving energy efficiency and thermal comfort [234,235]. Additionally, the combination of SAGs low density and high porosity facilitates their use in high-precision imaging and sensing devices, for both terrestrial and aerospace applications [236,237]. Optical components have been developed for outdoor applications, which can withstand environmental variables such as temperature fluctuations and mechanical stress, without compromising their optical integrity [238]. Conversely, SAGs acoustic properties are due to their lightweight, porous structure and larger particle sizes, which effectively absorbs sound, by reducing sound velocity. For this, SAGs could be ideal for soundproofing applications in various settings, from recording studios to automotive manufacturing, where controlling environmental noise is critical [239,240]. Acoustic properties of SAGs are particularly attracting for uses in environments where controlling noise pollution is crucial, such as recording studios, industrial settings, vehicles cabins, engines and aerodynamic components [241–244], thus improving workers quality of life and aligning with environmental sustainability goals by aiding in the creation of quieter, more energy-efficient vehicles [245]. Also, SAGs are exceptional materials for the construction of partition walls or ceiling tiles, where they can provide also thermal insulation, while reducing buildings structural load [246,247]. As in the previous case, the combination of SAGs with polymers and fibres has afforded hybrid materials superior in sound absorption, while maintaining structural integrity have been developed [248]. Particularly, the combination of SAGs with shape-memory polymers and phase-change materials, smart acoustic systems capable to adapt their noise insulation properties in response to environmental changes, such as temperature and pressure fluctuations have been engineered, particularly impactful in dynamic industrial environments where ambient conditions vary significantly [249]. SAGs capability to disrupt sound

 doi:10.20944/preprints202508.0009.v1

wave propagation is particularly advantageous in environments where precision in sound control is paramount, such as in acoustic laboratories or high-fidelity audio production settings [250]. SAGs low density and high porosity may allow a better transmission and reception of ultrasonic waves, making them appealing for ultrasonic applications, thus revolutionizing medical imaging techniques, such as ultrasonography [251]. The low thermal conductivity of SAGs, typically around 15 mW/mK, is mainly due to the sparse conduction paths in their mostly air-filled pores and the intricate structural network that impedes heat transfer through both convection and radiation. For this, SAGs are precious in sectors that demand high-performance insulation solutions, including the construction and aerospace industries [252,253]. SAGs are used in the construction of insulating clothing for extreme environments and in the creation of energy-efficient windows that reduce heat loss without sacrificing transparency. They are capable to provide critical thermal protection for spacecraft and satellites, ensuring that instruments and crew are shielded from the intense thermal variations encountered in outer space [254,255]. The incorporation into SAAGs scaffolds of materials with complementary thermal and mechanical properties, such as graphene and carbon fibres provided composite AGs with maintained low thermal conductivity and improved strength and durability [256]. Such enhanced SAGs can find applications in the building industry, for the development of aerogel-infused plaster, as well as in the field of personal protective equipment [257]. The ability of SAGs to insulate against heat, while being lightweight and thin may allow to realize compact electronic assemblies, where managing heat is crucial for device performance and longevity [258]. Together, these diverse properties highlight the versatility and potential of silica aerogels, positioning them as critical materials in the advancement of various technological and industrial applications. These attributes are not only pivotal for their current uses but also for the innovation and development of future applications that leverage their unique characteristics. Wu et al. [259] and additional studies [260,261] have experimented that pore size, density and insulating properties of SAGs can be modified adjusting the tetramethyl-orto-silicates (TMOS) precursor, thus achieved SAGs tailored for specific uses, extending from energy-efficient building materials to components in electronic devices. Similarly, Mandal et al. demonstrated that altering the TMOS content significantly influenced the light transmittance of the SAGs [262]. In fact, by tuning TMOS concentration, the authors optimized the optical transparency achieving AGs suitable for applications in specialized environments, requiring high-levels light transmission [263,264]. Bi et al. have documented that SAGs can achieve sound velocities between 100 and 300 m/s, a significant reduction compared to the sound velocity in air, which is approximately 343 m/s [265]. Malfait et al. [266]and Gu and Ling have shown that, despite slightly less insulating, due to decreased porosity, denser aerogels can offer enhanced structural integrity [267]. This skill between thermal insulation and mechanical strength is pivotal for designing AGs for specific applications where both properties are important [268]. Additionally, progresses in bio-templating technique to prepare SAGs have allowed to synthesize AGs with biomimetic scaffolds which imitate natural structural systems, such as the fibrous conformations of plant stems and/or the complex lattice structures of bones. As obtained materials can boast enhanced mechanical resilience and flexibility, thus being exploitable in more dynamic environments where traditional AGs would fail [269].

Case Studies

Based on the above discussed properties, SAGs can have various applications, including science-based and engineering-based uses. In this section the main applications of SAGs have been reported and discussed following the scheme reported in Table 5. Table 5 highlights the direct correlation between the SAGs physical attributes and their application in fields that benefit from their unique properties such as thermal insulation, acoustic damping, and optical transparency reported in the previous section [5,270].

 doi:10.20944/preprints202508.0009.v1

Table 5. Possible applications of SAGs based on their functional properties.

FP	Functional properties	Applications
TI	Ability to resist heat transfer	Space shuttles, building insulation, appliance insulation
LD	Lightweight relative to volume	Filters for pollutants, oil adsorption, sensors, fuel storage
OT	Allows light to pass through with minimal scattering	Cherenkov detectors, lightweight optics
AD	Absorbs sound, reducing noise transmission	Soundproofing in buildings and vehicles
EI	High resistance to electrical flow	Used as dielectrics in electronic components

FP = Functional properties; TI = thermal insulation; LD = low density; OT = optical transparency; AD = acoustic damping; electrical insulation.

As reported in Table 5 (first row), SAGs known for their unprecedented thermal insulation features, are increasingly being integrated into numerous engineering sectors, including building construction and aerospace sector, where they have been utilized for thermal shielding in spacecraft. NASA used SAGs to insulate and protect the delicate instrumentation of Mars Rover during its mission on the Martian surface [271]. Another notable example of using SAGs to insulate buildings for energy saving is the Alaska Building in Manchester, UK, in which SAGs plaster application resulted in a reduction of energy consumption by over 35 % [272]. According to several authors, SAGs could revolutionize glazing industry, thus significantly reduce energy consumption, while maintain light transmittance. In the relevant review on SAGs by Firoozi et al, it has been reported that filling double-glazing systems with SAGs lows by over 50% the use of energy to heat and cool, with respect to traditional glazing, while maintaining indoor comfort [199], thus underscoring the potential of SAGs in green building practices. Aerogel-based glazing systems are recognized for their superior performance over conventional glazing due to their exceptionally low thermal conductivities. Innovations in this domain include both monolithic and granular aerogel-based systems. For instance, Li et al. developed a glazing system comprising two 6 mm glass panels with aerogel powder sandwiched in between and sealed with aluminum brackets [273]. Their studies demonstrated that this aerogel glazing system not only ensured a comfortable indoor visual environment but also achieved significant energy savings by reducing air conditioning requirements and enhancing indoor thermal comfort compared to traditional single-glazed systems. Liu et al. engineered a glazing system encompassing two 16 mm sheets of transparent plastic with a granular SAG filling, which showed a solar energy transmittance of 35 % and a heat transfer coefficient of 0.5 W/mK [274]. Later, the same authors studied the relationships between the size of SAGs granules and the efficiency of SAGs glazing units in reducing heat loss and decreasing heat transmittance, finding that larger granule could reduce them by 58 % and 38 %, respectively [275]. Belloni et al. developed a SAGs solar collector with a solar transmittance of 17-35 % and a low thermal conductivity coefficient of0.4 W/m^{2}K, thus showcasing substantial improvements in energy efficiency [276]. To study the energy performances of glazing systems filled with different SAGs, Liu et al. calculated their solar extinction coefficient by Mie scattering and Monte Carlo method, discussed the influences of porosity and nanoparticle's size, calculated their solar heat gain coefficients versus incidence angle and simulated their energy performances, by a dynamic heat transfer model [275]. The results indicated that more porosity of monolithic SAGs than diameter influences the solar extinction coefficient and that the reciprocal effect between the porosity and the diameter is negligible [275]. Additionally, it was assumed the SAGs having small nanoparticles and low porosity will lead to a better energy conservation performance in cooling dominated region. Also, it has been reported that creating an airtight seal by

 doi:10.20944/preprints202508.0009.v1

evacuating the air from double glazing units by using vacuum insulation glazing (VIG) technology, improve their thermal performance and insulation effect, while reducing thermal loss, representing nearly 40% of a building's heat dissipation [277]. In this context, due to the superior thermal performance of SAGs, many researchers have embedded them into double-glazing windows, thus developing hollow silica-based double-glazing windows [278–280], which were subsequently subjected to air vacuum process. Schultz et al. applicated a VIG to monolithic SAGs between two glass panes, whose vacuum was 1,000-10,000 times less intense than in standard VIG, achieving glazing systems with superior insulation, regardless of the low vacuum [281]. Neugebaurer et al. conducted a study and developed a technique to compact the bed of granular SAGs having thermal conductivity of 24 mW/(m K) (when uncompacted) to reduce it at 13 mW/(m K) (after compaction) [282]. The authors found that there is an optimum level of compaction to minimize the thermal conductivity, above which the contact area between the granules increases and the granules densify, increasing conduction through the solid [283]. Despite these unequivocal advantages, challenges such as high-cost production and mechanical fragility strongly hinder their broader application in civil engineering fields. Anyway, Karim et al. successfully developed SAGs-incorporated mortars (namely AIMs in the study) achieving amphibious materials, with improved binding properties, thus effectively addressing these limitations. Like Karim, Jia et al. developed AIMs containing from 50% to 70% SAGs by volume, with decreased compressive strength (from 20 MPa to 4 MPa) [284]. In addition to the glazing industry, SAGs have been used to develop AGs-based plasters, renders, roof panels, insulation blankets and vacuum-insulating panels, mainly motivated by the global demand for energy-efficient building solutions to cut costs and mitigate environmental [285–288]. In this context, United States spend 19% of total energy use to heating and cooling buildings, while regions like Romania miss modern insulation, thus urgently demanding for more efficient insulating materials, possessing mechanical strength, longevity, cost-effectiveness, and environmental sustainability [289,290]. Song et al. successfully incorporated 10 % SAGs by volume, into geopolymer foam AGs renders, achieving ultralight materials with superior thermal and acoustic insulation capacities [291]. Fantucci et al. have developed plaster coatings encompassing 90% of SAGs pellets, which demonstrated a thermal conductivity 10 times lower than that of conventional plasters. (0.05 W/mK vs. 0.5 W/mK) [292]. Similarly, Zhu et al. used SAGs cement mortar for coating concrete tunnels, successfully augmenting protection against fire and preventing humidity-induced explosive spalling [293]. Conversely, Wang et al. developed phosphorus-doped molybdenum disulfide/epoxy SAGs, demonstrating enhanced fire resistance, thus being notable materials in critical applications such as battery enclosures, where preventing thermal runaway is a critical safety concern in the energy sector [294]. Ganobjak et al. successfully replaced traditional silica sands with SAGs masses to generate lightweight and thermally insulative cement renders with significantly lower thermal conductivities of 0.085W/mK and densities of 0.41 g/cm^3 than conventional cement renders [295]. Also, Rostami et al. investigated the Incorporation of SAGs particles into concrete matrices, finding that they can partially or fully replace conventional aggregates, while enhancing the thermal insulation efficiency of traditional concrete products [296]. Zhang et al. have recently reported a real use of SAGs render, which was applied as a 6 mm thick filler to a building constructed in 1989, designed to be waterproof externally while allowing internal moisture to escape [297]. This application effectively reduced the wall's thermal conductivity from 1.0 W/mK to 0.3 W/mK, demonstrating the practical benefits of aerogel in real-world applications. Row two in Table 5 evidence that SAGs find application also for environment remediation, because of their superior absorption capabilities, mainly due to their hydrophobic nature of their inner scaffold and high porosity [298–300]. On the other hand, SAGs possess hydrophilic surfaces, due to the presence of hydroxyl groups, which, despite facilitating the attraction and retainment of water molecules from the air, facilitating adsorption, pose risks of structural collapse due to capillary stresses. Çok et al. and Renjith et al. developed methods to chemically modify SAGs, making them more hydrophobic and effective for adsorbing non-polar substances such as oils and organic solvents [301,302]. These modified SAGs have shown strong efficiency in the adsorption of oil spills in marine environments,

 doi:10.20944/preprints202508.0009.v1

thus limiting the devastating impact that oil spills can have on aquatic ecosystems. As absorbent materials, SAGs are highly effective in absorbing pollutants without saturating quickly and, particularly, in oil spill cleanups. Notably, SAGs were used to absorb oil efficiently, during the cleanup efforts in the Gulf of Mexico, significantly mitigating environmental damage [303]. Saharan et al. synthesized SAGs starting from MTMS as precursor, under acidic conditions, achieving absorbent materials with superior oil adsorption capacities, underscoring the influence of synthesis conditions on AGs efficiency [304]. SAGs have showed efficiency in carbon dioxide, argon, nitrogen, and oxygen adsorption, from the air, mainly if modified with amine groups. Amine-modified SAGs have been shown to adsorb considerable amounts of CO_2, thus being valuable in air purification and greenhouse gas reduction [305]. According to the third row in Table 5, due to their unique optical properties, SAGs can find application in Cherenkov counters to detect high-speed particles and for the precise measurement of the Cherenkov effect, essential in high-energy physics experiments. Yan et al used SAG samples of different densities and thicknesses to develop a Cherenkov radiator for the measurement of the time spectrum of high-energy pulsed electron sources [306]. In his relevant review, Kharzheev discussed Cherenkov counters based on SAGs, reporting cases showing that they notably enhance particle identification in accelerator experiments [307]. Cherenkov counters that employ SAGs as radiators and photodetectors are often used to identify subatomic charged particles, including electrons, protons, and ions, to measure particle velocities in accelerator-based particle- and nuclear-physics experiments and in space- and balloon-borne experiments in the field of cosmic-ray physics [308]. In the past, Tabata et al. developed hydrophobic SAGs tiles with large-area (18 cm × 18 cm × 2 cm), uniform density and high refractive index ($n \sim 1.05$) which were installed in a Cherenkov detector for the next-generation accelerator-based particle physics experiment Belle II [309]. By optimizing the supercritical CO_2 drying, the initially observed cracking has been eliminated from the prototype materials [309]. More recently, the same authors engineered a SAGs ring-imaging Cherenkov detector to be used in the spectrometer of a planned balloon-borne cosmic-ray observation program, HELIX (High Energy Light Isotope Experiment) [310]. In the last-step production, a pin-drying technique, which led to fabricate 40 out of the 48 tiles with no tile cracking [310] was used, while a water-jet cutting device was employed to fit the aerogel tiles into a radiator support structure [310]. In this field, particle identification power of SAGs RICH detectors strongly depends on optical properties of radiators. Barnyakov et al. demonstrated that among the several procedures of polishing of SAGs tested to improve their optical properties, the best performing was that used natural silk tissue, allowing the production of radiators for the Focusing Aerogel RICH detectors [301]. Furthermore, as reported by García-González et al., aerogels are making substantial contributions to nanomedicine, as drug delivery systems, due to their highly porous structure, which allows fast drug loading and controlled release [311]. According to Esquivel-Castro et al., the intimate structure of SAGs promotes both rapid drug loading and targeted release, addressing critical challenges in the delivery of therapeutics, such as low drug absorption and early degradation by stomach enzymes [312]. Moreover, chitosan (CH)-containing SAGs have been applied in regenerative medicine, where their biocompatibility and tunability facilitated enhanced drug delivery mechanisms, bioimaging and biosensors [21,63,313,314]. Additionally, the utilization of SAGs for wound healing application has been extensively reported, due to their high porosity and specific surface area that allows gas exchange and rapid absorption of a large amount of exudate as well as loading bioactive molecules [315,316]. Chen et al. developed a multifunctional SAGs (CG@DA@VEGF) by a simple and eco-friendly freeze-drying process combined with harmless EDC/NHS, which were used as crosslinking agents, while CH and dopamine-grafted gelatine were the raw materials [316]. *In vitro* experiments showed the notable antibacterial and antioxidant effects of CG@DA@EGF, as well as supreme cytocompatibility. *In vivo* experiments demonstrated the capability CG@DA@VEGF of improving angiogenesis and re-epithelialization, while promoting collagen deposition, thus accelerating wound healing with excellent biosafety[316]. In this field, algae-deriving alginate was used to develop SAGs wound dressings, which were biodegradable and non-adherent to wound tissues, as well as demonstrated inflammatory effects, which accelerate

 doi:10.20944/preprints202508.0009.v1

significantly the healing process. The additional capacity of SAGs to incorporate bioactive substances further improves their effectiveness in complex wound management scenarios [199]. López-Iglesias et al. processed chitosan (CH) in the form of aerogels, thus gifting CH with enhanced water sorption capacity and air permeability. Subsequently, vancomycin was entrapped in its scaffold observing high drug loading capacity and a fast drug release, that permitted to efficiently achieve local therapeutic levels. In vitro studies using fibroblasts and antimicrobial tests against *S. aureus* showed that the vancomycin-loaded AGs possessed good cytocompatibility and were effective in preventing high bacterial loads at the wound site [315]. Afrashi et al. engineered CH SAGs loaded with vancomycin, observing the same outcomes observed by López-Iglesias et al. [317]. Batista et al. carried out an in vitro study, which evidenced that, when the poor soluble ketoprofen was administered by SAGs, it exhibited release rates improved with respect to its crystalline form, further underling the potential of SAGs to enhance the efficacy of hydrophobic drugs [318]. Collectively, due to the good mucoadhesive properties of CH and its composites, they have appeared as promising matrices to incorporate active pharmaceutical ingredients (API) and other bioactive compounds and preparing CH-SAGs [319]. They have demonstrated to possess optimal drug loading capacity and in vitro release efficiency for various antibiotics [320–322], antifungals [323], anti-inflammatory [324–327], anticancer [328,329], and corticosteroid drugs [330], as well as insulin [331–333], enzymes [334], proteins [335,336], and nucleic acids [337]. Table 6 collects some relevant examples of CH SAGs which have been used to engineer various DDSs.

Table 6. CH-containing SAGs and freeze-dried gels for drug delivery.

Materials	Loaded API	Efficiency %[a]	Drying	Shape	Method	Ref.
CHI, glycerol, mannitol	Bovine serum albumin	91.6–94	FD	Monolith	Co-gelation	[336]
CHI, PPG, AA	5-Fluorouracil	>60				[328]
CHI	–	–	sc-SD	µ-Beads	Post-gelation	[338]
CHI	Alendronate	–	APD		Co-gelation	[339]
CHI	Insulin	>70				[332]
CHI	Doxycycline hyclate	>80		Monolith	Post-processing	[320]
CHI	Dexamethasone	90	FD		Post-gelation	[330]
CHI, GRDE, ethanol	Triamcinolone acetonide	>90			Co-gelation	[340]
CHI, ethanol	Camptothecin, griseofulvin	100	SCD	Sheet	syn-SCD	[323]
CHI, ethanol	Ibuprofen	60	sc-SD	µ-Beads	Co-gelation	[325]
CHI, acetone	–	–		powder		[341]
CHI, KOH	Curcumin	>80	SD-FD	Beads	Post-gelation	[342]
CHI chloride, STPP	Insulin	70	FD			[331]
CHI, STPP	Rifampicin	100		µ-Beads	Co-gelation	[343]
CHI, STPP	β-Lactoglobulin	40	SCD			[335]
CHI, STPP	Salbutamol	>80				[344]
CHI, STPP, EGDGE	Indomethacin	–		Beads	Post-gelation	[324]
CHI, carrageenan, CMC	Curcumin	50	FD	Monolith		[345]
CHI, collagen	Ibuprofen	–			Syn-SCD	[323]
CHI, CD, starch	Berberine	–			Co-gelation	[346]
CHI, HEC	Metronidazole	80		Sheet		[322]

 doi:10.20944/preprints202508.0009.v1

CHI, PEG	Amoxicillin, metronidazole	65	FD, APD	Monolith		[321]
CHI, PMMA, PAA	Lysozyme	>70			Post-gelation	[334]
CHI, PGA	Insulin	>60	FD			[333]
CHI, polyNIPA	Bemiparin	–		μ-Beads	Cc-gelation	[347]
CHI	RNA	–	SCD	Powder		[337]
CHI, alginate, CPP	Tetracycline hydrochloride	40/80		μ-Spheres		[348]
CHI, cellulose, ZnO	Curcumin	65	FD		Post-processing	[349]
CHI, clinoptilolite	Diclofenac sodium, indomethacin	>70		Monolith		[327]
CHI, CMC, GO	5-Fluorouracil	98			Post-gelation	[329]

[a] Release efficiency (bioavailability) reported here is the maximum/final release, the values depend on pH, loading concentration, crystallinity of the drug, and release periods. STTP = sodium tripolyphosphate; FD = freeze-drying; SCD = supercritical drying; APD = ambient pressure drying; SD = spray drying; CHI = chitosan; HEC = hydroxy ethyl cellulose; CMC = carboxymethyl cellulose; GO = graphene oxide; CPP = calcium polyphosphate; PEG = polyethylene glycol; PGA = polyglutamic acid; PAA = polyacrylamide; PPG = propylene glycol; AA = aspartic acid ; GRDE = glutaraldehyde; EGDGE = ethylene glycol di-glycidyl ether; CD = cyclodextrin; - = missing data.

Moreover, other materials were employed to prepare DDSs based on SAGs. Athamneh et al. prepared SAG microspheres using alginate and hyaluronic acid as ingredients for the drug delivery of pulmonary drug delivery by an emulsion gelation process, followed by supercritical CO_2 drying. The measured properties by various techniques of the alginate- hyaluronic acid microspheres suggested that they could be suitable as drug carrier for pulmonary delivery [350]. Later, the same authors used AGs technology to develop products like those previously reported loaded with sodium naproxen as pulmonary DDSs [351]. This case authors carried out also biological essays missing in the previous study. I*n vitro* drug release investigations showed a non-Fickian drug release mechanism, with no significant difference between the release profiles of alginate and alginate–hyaluronic acid microspheres [351]. In addition to the great contribute that SAGs can provide in drug delivery and wound care, it is expected that the ongoing research in the biomedical application of SAGs will revolutionize traditional therapeutic strategies thus ameliorationg patients' conditions suffering from various diseases.

4.2. Metal Oxide-Based Aerogels (MOAGs)

OAGs or better metal oxide aerogels (MOAGs) can be prepared using almost all transition metal elements of the fourth and fifth groups in the periodic table [352]. Among them, alumina, zirconia and titania are ionic crystals with high ionic bond energy and high melting points, which impart these materials excellent thermal and chemical stability at high temperatures, thus being suitable for high-temperature applications. Collectively, there are two synthesis methods for the preparation of single-component MOAGs depending on different precursors, which include the metal alkoxide sol-gel method for metal alkoxides and the epoxide addition method for inorganic salts, previously described. After the formation of a gel via hydrolysis and condensation, a specific drying process is required to avoid the collapse of the gel structure. As described in detail in previous sections, the three available drying methods include supercritical fluid (usually ethanol or CO_2) drying (SCD), ambient pressure drying (APD), and vacuum freezing drying (VFD). In this context, alumina (ALAGs), zirconia (ZRAGs) and titania (TIAGs) AGs can be easily fabricated by these routes, due to their ready availability and controllable precursors. Specific information concerning ALAGs, ZRAGs

 doi:10.20944/preprints202508.0009.v1

and TIAGs has been included in Tables 7 and 8, while Figure 6 schematize the sol-gel process leading to MOAGs [353].

Table 7. Main precursors for the preparation of Al_2O_3, ZrO_2, and TiO_2 AGs.

Precursors	Al_2O_3	ZrO_2	TiO_2
Metal alkoxides	ASB, AIP	ZPO, ZBO	TIP, TBO
Inorganic salts	$Al(NO_3)_3{\cdot}9H_2O$, $AlCl_3{\cdot}6H_2O$	$ZrOCl_2{\cdot}8H_2O$, $ZrO(NO_3)_2{\cdot}2H_2O$	$TiCl_4$

ASB = Aluminium-tri-sec-butoxide; AIP = aluminium isopropoxide; $Al(NO_3)_3{\cdot}9H_2O$ = aluminium nitrate; $AlCl_3{\cdot}6H_2O$ = aluminium chloride; ZPO = zirconium n-propoxide; ZBO = zirconium butoxide; $ZrOCl_2{\cdot}8H_2O$ = zirconium oxychloride; $ZrOCl_2{\cdot}8H_2O$ = zirconium oxynitrate; TIP = titanium isopropoxide; TBO = titanium n-butoxide; $TiCl_4$ = titanium tetrachloride.

Table 8. Different drying methods.

DM	T(°C)	MPa	Main process	Advantages	Disadvantages
EtOH SCD	>243	>6.3	EtOH heated ↑critical point, ↓↓↓	↓↓↓SST, BP	↑ EC ↑ risk process
CO_2 SCD	>31	>7.3	CO_2 heated ↑critical point, ↓↓↓	Safer, BPs	LP, LC
APD	~25	~0.1	SM by methylation, SR with ↓SST	Safe, ↓cost	SST not completely ↓↓↓, LP
VFD	<0	vacuum	SS under FP and VC	Safe, ↓cost	Water as solvent, ↑↑ PS

SST = solvent surface tension; BPs = better/best properties; DM = drying method; ↓↓↓ completely eliminated; LP = long process; LC = low crystallinity; PS = pore structure; ↑↑ larger; ↑ high, enhanced, improved; EC = energy consumption; SM = surface modification; SR = solvent replacement; SS = solvent sublimation; FP = freezing point; VC = vacuum conditions.

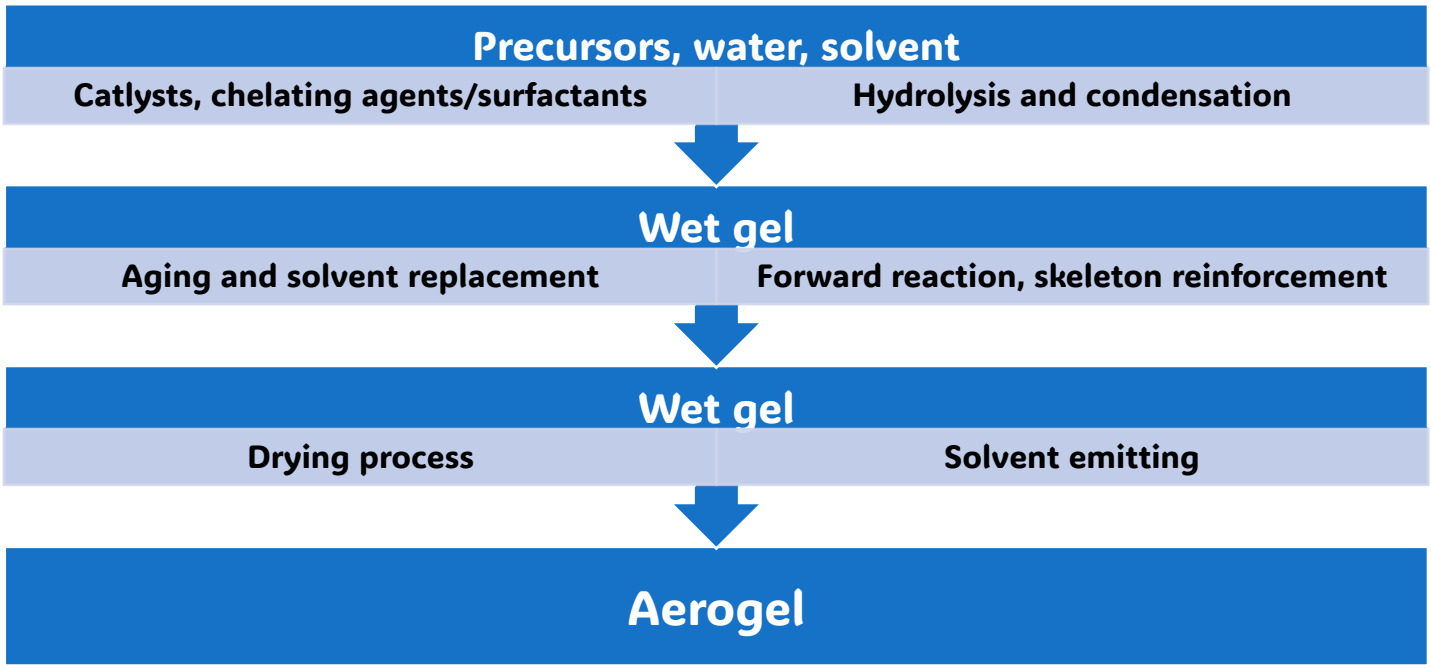

Figure 6. Sol-gel process to fabricate MOAGs.

 doi:10.20944/preprints202508.0009.v1

Since it is necessary reducing the reactions speed to obtain an intact gel rather than a precipitate, chelating agents such as acetylacetone (ACAC), ethyl acetoacetate (ETAC), acetic acid and long-chain carboxylic acids were the most used compounds to control the hydrolysis and condensation reaction rates [354].

4.2.1. Alumina Aerogels (ALAGs)

Alumina (Al_2O_3) is an ionic crystal with a high ionic bond energy and high melting point (2054 °C), mainly used as a high-temperature refractory material, for fabricating firebricks, crucibles, porcelain, and artificial stones. Alumina is available as α-Al_2O_3 also indicated as the most thermodynamically stable corundum form or as many metastable η, γ, δ, and θ Al_2O_3 forms. Face-centred cubic structures (FCCs) and hexagonal close-packed structures (HCPs) are the most common configuration of alumina according to the arrangement of oxygen ions. As reported by Wu et al. [353], Yoldas and his groups were the first who prepared ALAGs in 1975 using AIP and ASB alumina alkoxides as precursors and chelating agents or complex solvent mixtures to control the hydrolysis and condensation reaction. Unfortunately, the pore structure of alumina aerogels collapses after calcination at high temperature, due to the rapid dehydration and condensation of surface hydroxyl groups and phase transition.

Case Studies

Yoldas was the first, who reported the preparation of alumina oxide (Al_2O_3)-based AGs (ALAGs) from alkoxides. The product was not completely in compliance with the porosity requirements for be defined AGs, but they were the first example of highly porous non-siliceous scaffolds [355,356]. The ALAGs were heat treated at 1000 °C, thus achieving transparent discs or rectangles with 4.8 mm thickness. Transparency was improved by impregnating specimen with benzyl alcohol. Several experimentations were therefore finalized to study the intermediate species [357] to improve the mechanical properties [358] and to ameliorate thermal stability [359]. ALAGs are mainly applied as catalysts and catalysts supports [360–363], for the removal of mustard gas [9] and for capturing cometary fragments, in place of using silica-based compounds [364]. Horiuchi et al. used AIP and ultra-pure water to produce a boehmite sol and upon addition of nitric acid, ethanol replacement, and supercritical drying ALAGs were reached, which were analysed to assess their SSA, crystalline phase, particle size with the change of pH, bulk densities, and their relationship with thermal treatment temperature [365]. The sample with a lower bulk density (0.06 g/cm^3) had a higher θ-α phase transition temperature (1300 °C) and higher SSA (12 m^2/g at 1300 °C). Pierre et al. synthesized ALAGs in organic solvent using ASB as precursor, and ethyl acetoacetate (ETAC) as chelating agent for slowing down the hydrolysis rate of ASB, whose carbon side groups remained in the structure of ALAG, thus reducing drastically its thermal stability [366]. Transparency was achieved after heat treatment at 900 °C. Kim et al. fabricated alumina aerogel/xerogel via solvothermal reaction methods using AIP precursors and five different alcoholic solvents followed by calcination from 500 to 1200 °C [367]. The authors found that the ALAGs derived from EtOH showed a stable θ-Al_2O_3 phase and highest SSA of 66 m^2/g at 1200 °C. Other authors used inorganic salts in place of alumina oxides to prepare ALAGs via a PO addition method, as a capture agent of H^+, which is simple, low cost and environmentally friendly method, widely used in the synthesis of other types of metal oxide aerogels. Tokudome et al. prepared alumina aerogel from $AlCl_3{\cdot}6H_2O$ by PO addition method using PO as a gelation initiator and polyethylene oxide (PEO) as a phase separation inducer, to control the sol-gel reaction [368]. By proper analytical techniques, authors concluded that the ALAGs had a hierarchical porous structure, and the size of the primary particles and secondary particles were greatly influenced by the drying process and sol-gel parameters. Bao et al. engineered ALAGs using oil shale ash, and several metal oxides, including 26% aluminium oxide, which was leached by sulfuric acid, sodium hydroxide, and filtration [369]. The alumina gel formed upon addition of hydrochloric acid and PO. The obtained alumina aerogels after dehydration demonstrated a mesoporous structure with a maximum pore size around 20 nm and flaky morphology. By the incorporation of inorganic ceramic

 doi:10.20944/preprints202508.0009.v1

fibres, Yang et al. improved the mechanical properties of ALAGs, achieving a nanocomposite with superior creep resistance, thermal stability, and heat insulation properties at 800 °C [370]. Wu et al. fabricated aerogel-like alumina materials using the epoxide addition method replacing the solvent with isopropanol and concluding the synthesis with APD method [371]. The as prepared material demonstrated bulk density (0.133 g/cm^3) and SSA (505.6 m^2/g) very close to the values of traditional ALAGs resulting from the SCD method. Collectively, researchers follow mainly two procedures to achieve ALAGs. The first is the alkoxide method completed with SCD, and the second is the inorganic salt method accomplished with APD. Despite, the alkoxide method requires complex chemical reactions to be controlled and risky drying processes, whereas the resultant ALAGs possess better heat resistance up to 1200 °C, due to a better crystallinity and skeleton strength. Conversely, the inorganic salt process, despite simpler, safer and appropriate for large-scale production, provides ALAGs with larger shrinkage, worse crystallinity and thermal stability. Anyway, when compared with other metal oxide aerogels, ALAGs possess the best heat resistance and lowest density and are particularly suitable for high-temperature thermal insulation applications.

4.2.2. Zirconia Aerogels (ZRAGs)

Zirconia is an ionic crystal, with ionic bond energy larger than that of alumina and a higher melting point of 2680 °C, thus having great potential application in high-temperature fields. Zirconia presents three crystal structures, including a monoclinic phase (m-ZrO_2), tetragonal phase (t-ZrO_2), and cubic phase (c-ZrO_2) [372]. Specifically, ZRAGs are produced in the t-ZrO_2 phase at temperature close to 500 °C and present a surface energy of t-ZrO_2 lower than that of m-ZrO_2, a skeleton in the amorphous state, and particle size of about 10 nm. ZRAGs transform partially or completely into m-ZrO_2 phase when temperature increases to 500 °C, which presents crystals of 30 nm in size [373]. Teichner et al. was the first, who prepared ZRAGs in 1976 starting from a zirconium alkoxide as the precursor and completing the synthesis by the SCD method, thus obtaining materials with high SSA, low thermal conductivity, and stable chemical properties [374]. The as prepared ZRAGs could be excellent candidates for engineering thermal insulators, as well as to develop catalysts and catalyst supports. Unfortunately, ZRAGs tend to drastic structure collapse and high shrinkage after heat treatments higher than 600 °C, which are attributable to the phase transition and dehydration condensation of hydroxyls, with consequent decreasing of SSA, significantly lower than that of ALAGs. This is the main problem in the field, which limit the ZRAGs high-temperature applications.

Case Studies

By various traditional sol–gel approaches using alkoxides or salts as starting materials followed by calcination several types of ZRAGs have been produced [11,375–380]. Baiker et al. studied the effect of acids and solvents on the structural properties of ZRAGs, while Zeng et al. their short-range order and the fractal properties by X-ray diffraction (XRD) and small angle X-ray scattering (SAXS) techniques [381–384]. ZRAGs are usually applied as catalysts [385–387], whose activity was improved by their impregnation with sulphur [388–395], for the phospho-peptide enrichment [396] and thermal insulation [397]. Also, ZRAGs stabilized with Y_2O_3 [398,399], doped with Rh398, Ni [392,394], Fe [400], Cu [401]and Co [393], and mixed oxides with Al_2O_3[402], TiO_2[403] or WO_x[388] were prepared. Jung et al. engineered ZRAGs using different surfactants, such as Brij S10 ($C_{18}H_{37}(OCH_2CH_2)_{10}OH$), triblock copolymer Pluronic P-123 ($EO_{20}PO_{70}EO_{20}$), and hexadecyltrimethylammonium bromide (CTAB), while N-propanol (n-PrOH) and glacial acetic acid (HAc) were employed as solvent and catalyst, respectively [404]. The authors observed that the different molecular weight and electrostatic attractive force of surfactants affected the pore size, SSA, and crystal growth of ZRAGs, being the cationic CTAB the best enhancer one. By using APD as desiccation method, Brij-76 ($C_{58}H_{118}O_{21}$) as surfactant, acetic acid as a catalyst and hexamethyldisilane (HMDZ) as silylating agent, Bangi et al. manufactured ZRAGs powders, starting from ZPO as precursors [405]. The presence of Brij-76 decreased the SSA of ZRAGs from 203 to 178 m^2/g at room temperature (RT) and increased their SSA (27 vs 45 m^2/g) at 500 °C. Two years later, the same authors used a simpler method to fabricate

 doi:10.20944/preprints202508.0009.v1

zirconia aerogel powders via ZPO as precursors and sulfuric acid (H_2SO_4) as a chelating agent, avoiding the use of surfactants via an APD process[9]. Although the authors asserted that a minimal concentration of H_2SO_4 provided ZRAGs with high SSA (328 m^2/g at RT), they omitted to mention their high-temperature properties. Monolithic ZRAGs were achieved by Zhong et al. starting from $ZrOCl_2$ as precursor and following a nitric acid-assisted PO addition method [102], fine-tuning the microstructure and SSA of zirconia aerogels by regulating the molar ratio of $HNO_3/ZrOCl_2$ and $H_2O/ZrOCl_2$. The as prepared ZRAGs exhibited SSA of 454 m^2/g at RT, a c-ZrO_2 and t-ZrO_2 mixed phases before 750 °C, which transformed into m-ZrO_2 phase after heat treatment at 850 °C. Also, monolithic ZRAGs were engineered by Wang et al. following an organic acid-assisted method in place of the PO addition method [406]. The authors experimented that smaller organic acids, such as acetic acid promoted condensation reactions through covalent or hydrogen bonds, providing monolithic ZRAGs with high SSA of 315 m^2/g at RT and t-m mixed ZrO_2 phase at 600 °C. Hydrous ZRAGs (ZrO_xH_y) were developed by Jeffrey et al. starting from anhydrous $ZrCl_4$ via PO addition, followed by CO_2 SCD process, achieving materials with amorphous structure and abundant hydroxyl[407]. Anyway, increasing calcination temperatures up to 450 °C gave ZrO_xH_y aerogels which crystallized to ZrO_2 (46% cubic phase and 54% monoclinic phase), while 12% cubic phase and 88% monoclinic phase were observed at 600 °C. Due to the BET SSA was 30 m^2/g, such materials demonstrated good efficiency in the adsorption and degradation of dimethyl methyl phosphonate. Like ALAGs, we can also find ZRAGs deriving from both alkoxides or inorganic salts, associated to APD or SCD methods, which were extensively investigated to assess their influence on crystal phases and SSAs at low temperatures.

4.2.3. Titania Aerogels (TIAGs)

Titania (TiO_2) is an ionic crystal possessing a melting point of 1870 °C, which is lower than that of alumina (2054 °C) and zirconia (2680 °C). TiO_2 may survive in 3 polymorph crystallographic phases, including the stable rutile (r-TiO_2) and the two metastable anatase (a-TiO_2) and brookite (b-TiO_2) phases. The latter is relatively sporadic, therefore the phase transition from anatase (610 °C) to rutile (915 °C) is the most observed one. TIAGs have high porosity and SSA and is widely used as a photocatalyst for water splitting and photodegradation of organic pollutants, mainly due to their translucency or transparency to visible light and chemical stability. Additionally, titania powders are functional as opacifiers to reduce the radiative heat transport at high temperatures, due to their lower thermal conductivity at high temperatures.

Case Studies

Like for ALAGs and ARAGs, TIAGs were prepared for the first time by Teichner et al. in 1976 [408], and nowadays they are usually produced using titanium alkoxide (TIP or TBO) or titanium inorganic salts ($TiCl_4$). TIAGs possess poorer mechanical strength and poorer thermal stability than ALAGS, thus tending to a large decline in SSA for heat treatments above 500 °C, which strongly hamper their thermal insulation and photocatalyst applications. In this context, TIAGs attracted the attention of several researchers [11,409], who usually synthesized 0them, by dispersing the corresponding titanium ethoxide [410], isopropoxide [411–416] or butoxide [417,418] in aqueous alcohol or ketone mixtures, via sol-gel methods followed by calcination. TIAGs are mainly used as catalysts [409,412,414], dye-sensitized solar cells [415] and as filling materials for chromatography columns [413]. To modify the porosity of TIAGs, co-gelling approaches with SiO_2 were attempted [419–423]. Conversely, doping with Eu [424], Fe [425] and Pt, enhanced the photocatalytic activity [426]. Materials with electron scavenging properties were achieved by introducing gold nanoparticles AuNPs as guests during gelling of TIAGs which acted as host [427]. TIAGs composites with CeO_2 [428], RuO_2 [429], MnO_x/V_2O_5 [430] and ZrO_2 [431] with TiO_2 were prepared to tune the photocatalytic activity. Lermontov et al. synthesized TIAGs using isopropanol, 2-methoxyethanol, and 2-ethoxyethanol as solvents, observing that the material resulting from 2-ethoxyethanol was amorphous with a high SSA of 560 m^2/g, while that was provided by isopropanol showed a-TiO_2

 doi:10.20944/preprints202508.0009.v1

phase and SSA of 150 m^2/g at RT [408]. Conversely, the effect of water on the structural properties of TIAGs achieved using TIP as precursor and HNO_3 as catalyst was studied by Sadrieyeh et al. [432]. The authors found that lower hydrolysis levels (around 3.75) did not give stable wet gel, while hydrolysis levels of about 7.35 provided the most suitable structural properties with an amorphous phase, SSA of 639 m^2/g at RT, while an anatase phase with SAA of 157 m^2/g was observed upon calcination at 450 °C for 2 h. Zhang et al. developed monolithic TIAGs in the form of 3D reticulate TiO_2 nanofibers displaying an anatase crystalline structure, using an economical and green method, which used bacterial cellulose as a template and preceramic polymer as a precursor, followed by freeze-drying process and calcination at 450 °C [433]. By proper analytical techniques, a low bulk density of 0.04 g/cm^3, moderate mechanical strength, and SSA of 152 m^2/g were observed for the achieved materials. Due to the worse thermal stability of TIAGs, than ALAGs and ZRAGs, researchers studied at major extent their photocatalytic properties, experimenting that usually the anatase phase exhibits better photocatalytic activity than other titania crystal phases, undergoing a phase transition to rutile ones upon heat treatment exceeding 600 °C. Finding methos to keep the anatase phase and high SSA of TIAGs at high temperature is a key challenge for their photocatalytic applications.

4.2.4. Other Metal Oxide Aerogels (OMOAGs)

Iron oxide (Fe_2O_3) [434–438], copper oxide (CuO) [136,439,440], vanadium oxide (V_2O_5)[353,441–443], chromium oxide (Cr_2O_3) [91,444], zinc oxide (ZnO)[445,446], manganese oxide (MnO_2) [447–450] etc. represent other varieties of MOAGs (OMOAGs). OMOAGs are always prepared via inorganic salts following the PO addition method and exhibit a nanostructure experimenting significant collapse upon calcination at 500 °C, which limits their high-temperature applications.

Case Studies

Yoo et al. achieved Fe_2O_3 aerogel (FEAGs) powders using a sol-gel method, starting from $Fe(NO_3)_3{\cdot}9H_2O$ as precursor and completing the preparation with the APD method [438]. The authors found that powders possessed amorphous nanoporous structure, high SSA of 421 m^2/g at RT, which transformed magnetite phase upon calcination at 300 °C, and to mixed phases of magnetite and hematite when temperature reached 500 °C, with significant structural collapse and decrease of SSA to 26 m^2/g after heat treatment at 500 °C. Du et al. engineered monolithic copper oxide aerogel (CUAGs) using cupric chloride ($CuCl_2$) as precursor via a dispersed inorganic sol-gel method and polyacrylic acid (PAA) to govern the nucleation and growth in the sol[136]. The as prepared CUAGs showed SSA of 267 mg/cm^3, uniform microstructure and monoclinic phase after calcination at 500 °C. Vanadium oxide (V_2O_5) is a talented material to act as cathode in lithium (Li) batteries, thanks to its capability to intercalate Li ions. In this regard, several scholars investigated the electrochemical properties of V_2O_5-AGs (VAAGs) for energy storage [443,451–463]. In addition to Li^+, other AGs hosting ions, such as Na^+, K^+, Mg^{2+}, Ba^{2+}, Al^{3+} and Zn^{2+} were experimented [464,465]. The electrochemical properties of VAAGs were modified by including along with V_2O_5 precursor, copper (Cu) or zinc (Zn) [466], by manufacturing nanocomposites with RuO_2[467] or with polypyrrole [468], as well as by hosting $Ba_{0.25}V_2O_4$ whiskers, as 1D electron conducting additives [469]. Nitridation of V_2O_5provided vanadium oxynitrides, which were tested in sensor devices [470]. The association of TiO_2 and V_2O_5 provided AGs endowed with excellent photocatalytic activity [430,471–478]. It has been reported by Wu et al., that VAAGs were developed by Cui et al. fabricated employing H_2O_2 and V_2O_5 powders as raw materials, achieving materials having SSA high to 395 m^2/g after heat treatment at 100 °C and SSA of 313 m^2/g after heat treatment at 350 °C [353]. Also, iron-chromium oxide aerogel (FCRAGs), exhibiting SSA (110 m^2/g) higher than that of pure Cr_2O_3 (27 m^2/g) or Fe_2O_3 (13 m^2/g), due to the high thermal stability of the Fe-Cr-O_x bond, were manufactured by Khaleel et al. utilizing $Cr(NO_3)_3{\cdot}9H_2O$ and $Fe(NO_3)_3{\cdot}9H_2O$ as precursors via a PO addition method[91]. Moreover, Hasanpour et al. reported on the efficient photocatalytic degradation activity of cellulose/ZnO aerogels (C-ZNAGs), vs methyl orange dye, upon five cycles of reuse [445]. C-ZNAGs demonstrated

 doi:10.20944/preprints202508.0009.v1

high stability, hemispherical, cone-like, rice grain-like, and flower-like morphologies and SSA from 44 to 353 m^2/g, based on the composition [445]. The following Table 9 collects details on these relevant case studies.

Table 9. Relevant case studies concerning OMOAGs.

Refs	Precursor/solvent/catalyst	DM	Special preparation	PTT	SSA (m^2/g) (°C)
[438]	$Fe(NO_3)_3$*/H_2O/NH_3	APD	N-butanol solvent exchange	Magnetite and hematite (500 °C)	421(RT), 26(500)
[479]	$CuCl_2$/EtOH, H_2O/HNO_3	CO_2 SCD	PO and PAA addition	Monoclinic CuO (420 °C)	N.R.
[480]	V_2O_5powder/EtOH/	APD	H_2O_2 addition and acetone solvent exchange	N.R.	395(100), 313 (350)
[481]	$Cr(NO_3)_3$*, $Fe(NO_3)_3$*/i-PrOH	CO_2 SCD/APD	PO addition	Cr_2O_3 and α-F_2O_3 (500 °C)	342(120), 110 (500)
[445]	CE, $Zn(NO_3)_2$**/H_2O/NaOH	VFD	Hydrothermal process at 120 °C for 6 h	Wurtzite ZnO (RT)	353 (RT)

* Nona-hydrated; ** exa-hydrated; CE = cellulose; EtOH = ethanol; i-PrOH = 2-propanol; DM = drying method; PTT = phase transforming temperature; RT = room temperature.

Furthermore, Gash et al. proposed a PO addition method to promote gelation by catching H^+, which demonstrated to be very useful to fabricate high valence state (≥3) metal oxide aerogels like Al_2O_3, ZrO_2, Fe_2O_3, and TiO_2 aerogels [135,362]. Precipitates are usually obtained instead of an opaque gel for low valence state (≤2) metal salts like CoO, ZnO, and CuO. The group of Klabunde et al. synthesized and investigated the formation of magnesium-based AGs (MGAGs) [482–485], other researchers experimented their gelation by adding glycerol and acetic acid, thus producing large and crack-free MGAGs [486], while recently, Hüsing et al. studied the influence of structure directing agents, such as Pluronic 123 [487]. The possible uses for MGAGs include catalysis or toxic gases remediation [488]. It has been reported that the catalytic activity of MGAGs can be improved by an AuNPs cargo onto the surface [489], by co-gelling with VO_x[490,491] or by producing MGZR mixed oxides [492]. Skapin et al. investigated the effects of organic materials components on the properties of chromium AGs (CRAGs) [493]. Effects of fluorination on CRAGs were later studied [494], and fluorination was then also applied to ALAGs [495–497]. While partially fluorination on the surface was possible, deep bulk fluorination led to the complete loss of the AG structure [498]. Also, CRAGs were synthesized by Landau [499,500] and co-workers including α-Cr_2O_3, α-CrOOH and other compounds as catalysts supports [501]. Younes et al. finally combined Cr_2O_3 with Al_2O_3 to catalyse the nitroxidation of toluene to benzonitrile [502]. Much more limited literature was found concerning Fe–Cr–Al mixed oxides [503,504], gold–iron oxides [505], MoO_3 [506–508], WO_3 [509,510], $Li_2O{\cdot}B_2O_2$[511], GeO_2[512], ZnO [513] and V doped ZnO[442,514–516], SnO_2[517–519], Sn–Al oxides[520], Nb_2O_5[521], Pd doped CeO_2[522], MnO_2[523,524], Ta_2O_5[525] and more complex compositions like $MgFe_2O_4$[526], $BaTiO_3$[527–529], $SrTiO_3$[529], $PbTiO_3$[530], $Li_4Ti_5O_{12}$[531], $VOHPO_4{\cdot}0.5H_2O$[532], $La_2Mo_2O_9$[533] and CuO–$Zr_xCe_{1-x}O_y$.[534]. Oxide-based AGs from inorganic salts containing chromium and copper ions (II) were also prepared [23,136,535], while Zhang et al. using DIS prepared amorphous nickel oxide-based AGs with enhanced firmness [440].

5. Opportunities, Challenges or Both?

The market of AGs, accounting for a current valuation of approximately $300 million, is expected to significantly growth in the next years. This phenomenon is made possible by the unprecedented advantage which could derive from their extensive application as insulative materials and by their versatile features which make them suitable for a variety of applications. When compared to

 doi:10.20944/preprints202508.0009.v1

traditional insulative materials, such as fiberglass, foam, or polystyrene, AGs offer very low thermal conductivities of about 15 mW/mK versus that of 40 mW/mK and 30–40 mW/mK of fiberglass and foam insulation, respectively [536,537]. For this characteristic mainly due to their high porosity close to 99%, AGs offer an invaluable contribute to critical sectors like aerospace and in high efficiency building projects, where they prevent undesirable heat transfer and slash energy costs significantly [538]. Nevertheless, the route to their widespread utilization is still challenging, due to AGs' inherent fragility, difficult scaling-up, high costs of production, and environmental alarms related to their manufacturing processes. AGs' inherent brittleness, makes them susceptible to damage under mechanical stress, limiting their practicality in scenarios requiring robust handling [539]. The inherent brittleness of AGs represents a considerable obstacle to their more extensive use, due to their tendency to break under mechanical tension. This breakability hampers their employment in sectors where robustness is mandatory. Anyway, several reinforcing agents, including various polymers are under study to develop composite AGs, where the low-density and high porosity typical of traditional AGs are maintained, while mechanical strength is improved. By this approach, AGs are developed with acquired sturdiness and capable to withstand dynamic stress, thus making them suitable for industries such as construction, automotive, and aerospace [540]. The still not solved problems of high costs production, due to sophisticated manufacturing processes and expensive chemical precursors, as well as the energy demand of supercritical CO_2 drying methods, necessary to maintain the porous structure in AGs, hamper their scaling up production and extensive utilization. Innovative drying techniques, such as ambient pressure drying, could improve production costs and reduce energy consumption, thus supporting larger-scale production and increased market accessibility [541]. Additionally, alternative, less expensive precursors, such as rice husk ash, silica-rich by-products, such as glasses and other agricultural waste, is a strategic measure being explored to reduce costs. The eco-friendly materials are not only cheaper but also readily available as by-products from other industrial activities, could be of great benefit in decreasing production costs and broadening aerogels' applicability across various industries [542]. So, the integration of AGs production with industries generating such waste materials, can streamline the supply chain and drastically cut material expenses by repurposing waste streams directly into AGs production, nurturing a circular economy where waste is transformed into new value, thereby diminishing environmental impact [543]. This strategy can contribute to waste reduction, enhance environmental sustainability and provide a use for otherwise discarded resources [544]. The research for less hazardous solvents or solvent-free processes can also dismissing the environmental impact, reduce the emission of volatile organic compounds (VOCs), which contribute to air pollution and potential health risks. This approach can support the global sustainability, increase the commercial and industrial viability of AGs and facilitate their transition from academic experimentation or niche markets to more conventional applications [545]. Efforts to reduce harmful emissions and enhancing the eco-friendliness of AGs production, involve also strategies to capture and recycle solvents or to eliminate harmful solvents entirely are continuously undergone, including the use of supercritical carbon dioxide as a greener alternative to traditional organic solvents [546]. The completely solvent-free synthesis routes, not only restrain VOC emissions but also eliminate the need for high-energy drying processes, thereby further decreasing the energy consumption in AGs production, aligning with broader environmental sustainability goals [547]. Also, 3D printing technologies are under study for AGs synthesis, and are promising for manufacturing complex AGs structures with high precision, possessing properties specifically tailored to diverse industrial applications, thus broadening their commercial appeal and utility [548]. Collectively, multidisciplinary research is urgently needed to develop strategies that could join advancements in materials science, for improving their mechanical robustness and scalability, while limiting manufacturing expenses [549,550]. Additionally, further research is expected to make possible the extension of the most common applications of AGs, such as thermal insulation, to other innovative fields like biomedicine and energy storage, thus confirming the versatile potential of AGs to transfigure diverse industries, and aligning with global goals for environmental sustainability [551,552]. This is particularly

 doi:10.20944/preprints202508.0009.v1

impactful in cost-sensitive markets like residential construction, where the high price point of AGs can deter their adoption. The complex and energy-intensive production processes, such as supercritical drying, not only inflate the cost but also restrict large-scale manufacturing capabilities [553]. These strategic innovations pave the way for expanding the AGs' roles beyond traditional insulation, toward other applications such as filtration, sensors, and energy storage systems [554]. It is noteworthy that AGs application in buildings and vehicles, reduce drastically energy consumption, by their insulating capacities. When incorporated in buildings as insulating materials, AGs can minimize heating and cooling demands, thus reducing both the carbon footprint and operational energy costs. Inserting AGs in vehicle for their insulation, enhance fuel efficiency, minimize heating and cooling calls, thereby lowering greenhouse gas emissions [555]. Application of AGs in thermal management systems as solar panels and wind turbines improves the performance and longevity of these devices [556].

Funding: This research received no external funding.

Institutional Review Board Statement: Not applicable.

Informed Consent Statement: Not applicable.

Data Availability Statement: No new data were created here.

Conflicts of Interest: The authors declare no conflicts of interest.

References

1. Vadanagekar, A.; Lapcik, L.; Kvitek, L.; Lapcikova, B. Silica Aerogels as a Promising Vehicle for Effective Water Splitting for Hydrogen Production. *Molecules* 2025, *30*, 1212, doi:10.3390/molecules30061212.
2. Hina Goyal Beyond Insulation: New Applications for Aerogels Available online: https://www.cas.org/resources/cas-insights/aerogel-applications#:~:text=Inorganic%20aerogels%20not%20only%20encompass%20silica%20aerogels%20but,precursor%20materials%20like%20metal%20alkoxides%20or%20metal%20salts (accessed on 26 June 2025).
3. Wu, Y.; Liu, T.; Shi, Y.; Wang, H. Dramatically Enhancing Mechanical Properties of Hydrogels by Drying Reactive Polymers at Elevated Temperatures to Introduce Strong Physical and Chemical Crosslinks. *Polymer (Guildf)* 2022, *249*, 124842, doi:10.1016/J.POLYMER.2022.124842.
4. Shafi, S.; Rasheed, T.; Naz, R.; Majeed, S.; Bilal, M. Supercritical CO2 Drying of Pure Silica Aerogels: Effect of Drying Time on Textural Properties of Nanoporous Silica Aerogels. *J Solgel Sci Technol* 2021, *98*, doi:10.1007/s10971-021-05530-0.
5. Montes, S.; Maleki, H. Aerogels and Their Applications. *Colloidal Metal Oxide Nanoparticles* 2020, 337–399, doi:10.1016/B978-0-12-813357-6.00015-2.
6. Pajonk, G.M. Catalytic Aerogels. *Catal Today* 1997, *35*, 319–337, doi:10.1016/S0920-5861(96)00163-0.
7. Schneider, M.; Baiker, A. Aerogels in Catalysis. *Catalysis Reviews* 1995, *37*, doi:10.1080/01614949508006450.
8. Vallribera, A.; Molins, E. Aerogel Supported Nanoparticles in Catalysis. In *Nanoparticles and Catalysis*; 2008.
9. Rechberger, F.; Niederberger, M. Synthesis of Aerogels: From Molecular Routes to 3-Dimensional Nanoparticle Assembly. *Nanoscale Horiz* 2017, *2*.
10. Hosticka, B.; Norris, P.M.; Brenizer, J.S.; Daitch, C.E. Gas Flow through Aerogels. *J Non Cryst Solids* 1998, *225*, 293–297, doi:10.1016/S0022-3093(98)00130-6.
11. *Aerogels Handbook*; Aegerter, M.A., Leventis, N., Koebel, M.M., Eds.; Springer New York: New York, NY, 2011; ISBN 978-1-4419-7477-8.
12. Burchell, M.J.; Graham, G.; Kearsley, A. Cosmic Dust Collection in Aerogel. *Annu Rev Earth Planet Sci* 2006, *34*, doi:10.1146/annurev.earth.34.031405.124939.
13. Gurav, J.L.; Jung, I.-K.; Park, H.-H.; Kang, E.S.; Nadargi, D.Y. Silica Aerogel: Synthesis and Applications. *J Nanomater* 2010, *2010*, doi:10.1155/2010/409310.
14. Hrubesh, L.W. Aerogel Applications. *J Non Cryst Solids* 1998, *225*, 335–342, doi:10.1016/S0022-3093(98)00135-5.

 doi:10.20944/preprints202508.0009.v1

15. Thapliyal, P.C.; Singh, K. Aerogels as Promising Thermal Insulating Materials: An Overview. *J Mater* 2014, *2014*, doi:10.1155/2014/127049.
16. Ayen, R.J.; Iacobucci, P.A. Metal Oxide Aerogel Preparation by Supercritical Extraction. *Reviews in Chemical Engineering* 1988, *5*, doi:10.1515/REVCE.1988.5.1-4.157.
17. Gesser, H.D.; Goswami, P.C. Aerogels and Related Porous Materials. *Chem Rev* 1989, *89*, doi:10.1021/cr00094a003.
18. Fricke, J.; Tillotson, T. Aerogels: Production, Characterization, and Applications. *Thin Solid Films* 1997, *297*, 212–223, doi:10.1016/S0040-6090(96)09441-2.
19. Akimov, Y.K. Fields of Application of Aerogels (Review). *Instruments and Experimental Techniques* 2003, *46*.
20. Rolison, D.R.; Dunn, B. Electrically Conductive Oxide Aerogels: New Materials in Electrochemistry. *J Mater Chem* 2001, *11*, doi:10.1039/b007591o.
21. Bokov, D.; Turki Jalil, A.; Chupradit, S.; Suksatan, W.; Javed Ansari, M.; Shewael, I.H.; Valiev, G.H.; Kianfar, E. Nanomaterial by Sol-Gel Method: Synthesis and Application. *Advances in Materials Science and Engineering* 2021, *2021*.
22. Feinle, A.; Hüsing, N. Mixed Metal Oxide Aerogels from Tailor-Made Precursors. *J Supercrit Fluids* 2015, *106*, 2–8, doi:10.1016/J.SUPFLU.2015.07.015.
23. Du, A.; Zhou, B.; Shen, J.; Gui, J.; Zhong, Y.; Liu, C.; Zhang, Z.; Wu, G. A Versatile Sol-Gel Route to Monolithic Oxidic Gels via Polyacrylic Acid Template. *New Journal of Chemistry* 2011, *35*, doi:10.1039/c0nj00909a.
24. Chemere, E.B.; Mhlabeni, T.L.; Mhike, W.; Mavhungu, M.L.; Shongwe, M.B. A Comprehensive Review of Types, Synthesis Strategies, Advanced Designing and Applications of Aerogels. *R Soc Open Sci* 2025, *12*, doi:10.1098/rsos.241975.
25. Gaponik, N.; Herrmann, A.K.; Eychmüller, A. Colloidal Nanocrystal-Based Gels and Aerogels: Material Aspects and Application Perspectives. *Journal of Physical Chemistry Letters* 2012, *3*.
26. Meti, P.; Wang, Q.; Mahadik, D.B.; Lee, K.Y.; Gong, Y.D.; Park, H.H. Evolutionary Progress of Silica Aerogels and Their Classification Based on Composition: An Overview. *Nanomaterials* 2023, *13*.
27. Ahmad, S.; Ahmad, S.; Sheikh, J.N. Silica Centered Aerogels as Advanced Functional Material and Their Applications: A Review. *J Non Cryst Solids* 2023, *611*, 122322, doi:10.1016/J.JNONCRYSOL.2023.122322.
28. Bag, S.; Arachchige, I.U.; Kanatzidis, M.G. Aerogels from Metal Chalcogenides and Their Emerging Unique Properties. *J Mater Chem* 2008, *18*, doi:10.1039/b804011g.
29. Bangi, U.K.H.; Lee, K.-Y.; Maldar, N.M.N.; Park, H.-H. Synthesis and Properties of Metal Oxide Aerogels via Ambient Pressure Drying. *J Nanosci Nanotechnol* 2018, *19*, doi:10.1166/jnn.2019.16240.
30. Qiu, J.; Cao, H.; Liao, J.; Du, R.; Dou, K.; Tsidaeva, N.; Wang, W. 3D Porous Coral-like Co1.29Ni1.71O4 Microspheres Embedded into Reduced Graphene Oxide Aerogels with Lightweight and Broadband Microwave Absorption. *J Colloid Interface Sci* 2022, *609*, 12–22, doi:10.1016/J.JCIS.2021.11.176.
31. Xiong, T.; Li, Q.; Li, K.; Zhang, Y.; Zhu, W. Construction of Novel Magnesium Oxide Aerogel for Highly Efficient Separation of Uranium(VI) from Wastewater. *Sep Purif Technol* 2022, *295*, 121296, doi:10.1016/J.SEPPUR.2022.121296.
32. Kistler, S.S. Coherent Expanded Aerogels and Jellies [5]. *Nature* 1931, *127*.
33. Lee, K.J.; Kang, Y.; Kim, Y.H.; Baek, S.W.; Hwang, H. Synthesis of Silicon Carbide Powders from Methyl-Modified Silica Aerogels. *Applied Sciences (Switzerland)* 2020, *10*, doi:10.3390/app10186161.
34. Oschatz, M.; Boukhalfa, S.; Nickel, W.; Hofmann, J.P.; Fischer, C.; Yushin, G.; Kaskel, S. Carbide-Derived Carbon Aerogels with Tunable Pore Structure as Versatile Electrode Material in High Power Supercapacitors. *Carbon N Y* 2017, *113*, 283–291, doi:10.1016/J.CARBON.2016.11.050.
35. Pu, Z.; Amiinu, I.S.; Kou, Z.; Li, W.; Mu, S. RuP2-Based Catalysts with Platinum-like Activity and Higher Durability for the Hydrogen Evolution Reaction at All PH Values. *Angewandte Chemie - International Edition* 2017, *56*, doi:10.1002/anie.201704911.
36. Jiang, W.; Ruan, Q.; Xie, J.; Chen, X.; Zhu, Y.; Tang, J. Oxygen-Doped Carbon Nitride Aerogel: A Self-Supported Photocatalyst for Solar-to-Chemical Energy Conversion. *Appl Catal B* 2018, *236*, 428–435, doi:10.1016/J.APCATB.2018.05.050.

 doi:10.20944/preprints202508.0009.v1

37. Tang, J.; Feng, Y.; Feng, W. Photothermal Storage and Controllable Release of a Phase-Change Azobenzene/Aluminum Nitride Aerogel Composite. *Composites Communications* 2021, *23*, 100575, doi:10.1016/J.COCO.2020.100575.
38. Wang, B.; Li, G.; Xu, L.; Liao, J.; Zhang, X. Nanoporous Boron Nitride Aerogel Film and Its Smart Composite with Phase Change Materials. *ACS Nano* 2020, *14*, doi:10.1021/acsnano.0c05931.
39. Krishna Kumar, A.S.; Warchol, J.; Matusik, J.; Tseng, W.L.; Rajesh, N.; Bajda, T. Heavy Metal and Organic Dye Removal via a Hybrid Porous Hexagonal Boron Nitride-Based Magnetic Aerogel. *NPJ Clean Water* 2022, *5*, doi:10.1038/s41545-022-00175-0.
40. Jiang, X.; Du, R.; Hübner, R.; Hu, Y.; Eychmüller, A. A Roadmap for 3D Metal Aerogels: Materials Design and Application Attempts. *Matter* 2021, *4*.
41. Nita, L.E.; Ghilan, A.; Rusu, A.G.; Neamtu, I.; Chiriac, A.P. New Trends in Bio-Based Aerogels. *Pharmaceutics* 2020, *12*.
42. Ganesan, K.; Budtova, T.; Ratke, L.; Gurikov, P.; Baudron, V.; Preibisch, I.; Niemeyer, P.; Smirnova, I.; Milow, B. Review on the Production of Polysaccharide Aerogel Particles. *Materials* 2018, *11*.
43. Wu, K.; Dong, W.; Pan, Y.; Cao, J.; Zhang, Y.; Long, D. Lightweight and Flexible Phenolic Aerogels with Three-Dimensional Foam Reinforcement for Acoustic and Thermal Insulation. *Ind Eng Chem Res* 2021, *60*, doi:10.1021/acs.iecr.0c05010.
44. Derflinger, C.; Kamm, B.; Paulik, C. Sustainable Aerogels Derived from Bio-Based 2,5-Diformylfuran and Depolymerization Products of Lignin. *International Journal of Biobased Plastics* 2021, *3*, doi:10.1080/24759651.2021.1877025.
45. PEKALA, R.W.; KONG, F.M. A SYNTHETIC ROUTE TO ORGANIC AEROGELS - MECHANISM, STRUCTURE, AND PROPERTIES. *Le Journal de Physique Colloques* 1989, *24*, doi:10.1051/jphyscol:1989406.
46. Leventis, N. Polyurea Aerogels: Synthesis, Material Properties, and Applications. *Polymers (Basel)* 2022, *14*.
47. Merillas, B.; Martín-De León, J.; Villafañe, F.; Rodríguez-Pérez, M.A. Transparent Polyisocyanurate-Polyurethane-Based Aerogels: Key Aspects on the Synthesis and Their Porous Structures. *ACS Appl Polym Mater* 2021, *3*, doi:10.1021/acsapm.1c00712.
48. Betz, M.; García-González, C.A.; Subrahmanyam, R.P.; Smirnova, I.; Kulozik, U. Preparation of Novel Whey Protein-Based Aerogels as Drug Carriers for Life Science Applications. *Journal of Supercritical Fluids* 2012, *72*, doi:10.1016/j.supflu.2012.08.019.
49. Selmer, I.; Kleemann, C.; Kulozik, U.; Heinrich, S.; Smirnova, I. Development of Egg White Protein Aerogels as New Matrix Material for Microencapsulation in Food. *Journal of Supercritical Fluids* 2015, *106*, doi:10.1016/j.supflu.2015.05.023.
50. Selvasekaran, P.; Chidambaram, R. Food-Grade Aerogels Obtained from Polysaccharides, Proteins, and Seed Mucilages: Role as a Carrier Matrix of Functional Food Ingredients. *Trends Food Sci Technol* 2021, *112*.
51. Kaushik, J.; Kumar, V.; Garg, A.K.; Dubey, P.; Tripathi, K.M.; Sonkar, S.K. Bio-Mass Derived Functionalized Graphene Aerogel: A Sustainable Approach for the Removal of Multiple Organic Dyes and Their Mixtures. *New Journal of Chemistry* 2021, *45*, doi:10.1039/d1nj00470k.
52. Zhang, T.; Yuan, D.; Guo, Q.; Qiu, F.; Yang, D.; Ou, Z. Preparation of a Renewable Biomass Carbon Aerogel Reinforced with Sisal for Oil Spillage Clean-up: Inspired by Green Leaves to Green Tofu. *Food and Bioproducts Processing* 2019, *114*, doi:10.1016/j.fbp.2018.12.007.
53. Zhu, W.; Li, Y.; Yu, Y.; Duan, T.; Zhou, D.; Wang, L.; Zhou, J.; Kuang, M. Environment-Friendly Bio-Materials Based on Cotton-Carbon Aerogel for Strontium Removal from Aqueous Solution. *J Radioanal Nucl Chem* 2018, *316*, doi:10.1007/s10967-018-5782-8.
54. Soleimani Dorcheh, A.; Abbasi, M.H. Silica Aerogel; Synthesis, Properties and Characterization. *J Mater Process Technol* 2008, *199*, 10–26, doi:10.1016/J.JMATPROTEC.2007.10.060.
55. Carlson, G.; Lewis, D.; McKinley, K.; Richardson, J.; Tillotson, T. Aerogel Commercialization: Technology, Markets and Costs. *J Non Cryst Solids* 1995, *186*, doi:10.1016/0022-3093(95)00069-0.
56. Bag, S.; Trikalitis, P.N.; Chupas, P.J.; Armatas, G.S.; Kanatzidis, M.G. Porous Semiconducting Gels and Aerogels from Chalcogenide Clusters. *Science (1979)* 2007, *317*, doi:10.1126/science.1142535.
57. Bag, S.; Gaudette, A.F.; Bussell, M.E.; Kanatzidis, M.G. Spongy Chalcogels of Non-Platinum Metals Act as Effective Hydrodesulfurization Catalysts. *Nat Chem* 2009, *1*, doi:10.1038/nchem.208.

 doi:10.20944/preprints202508.0009.v1

58. Polychronopoulou, K.; Malliakas, C.D.; He, J.; Kanatzidis, M.G. Selective Surfaces: Quaternary Co(Ni)MoS-Based Chalcogels with Divalent (Pb 2+, Cd 2+, Pd 2+) and Trivalent (Cr 3+, Bi 3+) Metals for Gas Separation. *Chemistry of Materials* 2012, *24*, doi:10.1021/cm301444p.
59. Oh, Y.; Bag, S.; Malliakas, C.D.; Kanatzidis, M.G. Selective Surfaces: High-Surface-Area Zinc Tin Sulfide Chalcogels. *Chemistry of Materials* 2011, *23*, doi:10.1021/cm2003462.
60. Riley, B.J.; Chun, J.; Ryan, J. V.; Matyáš, J.; Li, X.S.; Matson, D.W.; Sundaram, S.K.; Strachan, D.M.; Vienna, J.D. Chalcogen-Based Aerogels as a Multifunctional Platform for Remediation of Radioactive Iodine. *RSC Adv* 2011, *1*, doi:10.1039/c1ra00351h.
61. Ziegler, C.; Wolf, A.; Liu, W.; Herrmann, A.K.; Gaponik, N.; Eychmüller, A. Modern Inorganic Aerogels. *Angewandte Chemie - International Edition* 2017, *56*.
62. Choi, H.; Parale, V.G.; Kim, T.; Choi, Y.S.; Tae, J.; Park, H.H. Structural and Mechanical Properties of Hybrid Silica Aerogel Formed Using Triethoxy(1-Phenylethenyl)Silane. *Microporous and Mesoporous Materials* 2020, *298*, 110092, doi:10.1016/J.MICROMESO.2020.110092.
63. Rashid, A. Bin; Shishir, S.I.; Mahfuz, M.A.; Hossain, M.T.; Hoque, M.E. Silica Aerogel: Synthesis, Characterization, Applications, and Recent Advancements. *Particle and Particle Systems Characterization* 2023, *40*.
64. Niederberger, M.; Pinna, N. *Metal Oxide Nanoparticles in Organic Solvents*; Springer London: London, 2009; ISBN 978-1-84882-670-0.
65. Brinker, C.J.; Scherer, G.W. *Sol-Gel Science: The Physics and Chemistry of Sol-Gel Processing*; 2013;
66. Feinle, A.; Elsaesser, M.S.; Hüsing, N. Sol-Gel Synthesis of Monolithic Materials with Hierarchical Porosity. *Chem Soc Rev* 2016, *45*.
67. *Aerogels Handbook*; 2011;
68. Nakagawa, Y.; Kageyama, H.; Oaki, Y.; Imai, H. Direction Control of Oriented Self-Assembly for 1D, 2D, and 3D Microarrays of Anisotropic Rectangular Nanoblocks. *J Am Chem Soc* 2014, *136*, doi:10.1021/ja410183q.
69. Şahin, İ.; Özbakır, Y.; İnönü, Z.; Ulker, Z.; Erkey, C. Kinetics of Supercritical Drying of Gels. *Gels* 2018, *4*.
70. Estok, S.K.; Hughes, T.A.; Carroll, M.K.; Anderson, A.M. Fabrication and Characterization of TEOS-Based Silica Aerogels Prepared Using Rapid Supercritical Extraction. *J Solgel Sci Technol* 2014, *70*, doi:10.1007/s10971-014-3292-x.
71. Anderson, A.M.; Carroll, M.K.; Green, E.C.; Melville, J.T.; Bono, M.S. Hydrophobic Silica Aerogels Prepared via Rapid Supercritical Extraction. *J Solgel Sci Technol* 2010, *53*, doi:10.1007/s10971-009-2078-z.
72. Yoda, S.; Ohshima, S. Supercritical Drying Media Modification for Silica Aerogel Preparation. *J Non Cryst Solids* 1999, *248*, 224–234, doi:10.1016/S0022-3093(99)00250-1.
73. Quignard, F.; Valentin, R.; Di Renzo, F. Aerogel Materials from Marine Polysaccharides. *New Journal of Chemistry* 2008, *32*.
74. Brinker, C.J.; Keefer, K.D.; Schaefer, D.W.; Ashley, C.S. Sol-Gel Transition in Simple Silicates. *J Non Cryst Solids* 1982, *48*, 47–64, doi:10.1016/0022-3093(82)90245-9.
75. Cai, L.; Shan, G. Elastic Silica Aerogel Using Methyltrimethoxysilane Precusor via Ambient Pressure Drying. *Journal of Porous Materials* 2015, *22*, doi:10.1007/s10934-015-0026-6.
76. Feng, Q.; Chen, K.; Ma, D.; Lin, H.; Liu, Z.; Qin, S.; Luo, Y. Synthesis of High Specific Surface Area Silica Aerogel from Rice Husk Ash via Ambient Pressure Drying. *Colloids Surf A Physicochem Eng Asp* 2018, *539*, 399–406, doi:10.1016/J.COLSURFA.2017.12.025.
77. Yun, S.; Guo, T.; Zhang, J.; He, L.; Li, Y.; Li, H.; Zhu, X.; Gao, Y. Facile Synthesis of Large-Sized Monolithic Methyltrimethoxysilane-Based Silica Aerogel via Ambient Pressure Drying. *J Solgel Sci Technol* 2017, *83*, doi:10.1007/s10971-017-4377-0.
78. Zhao, C.; Li, Y.; Ye, W.; Shen, X.; Yuan, X.; Ma, C.; Cao, Y. Performance Regulation of Silica Aerogel Powder Synthesized by a Two-Step Sol-Gel Process with a Fast Ambient Pressure Drying Route. *J Non Cryst Solids* 2021, *567*, 120923, doi:10.1016/J.JNONCRYSOL.2021.120923.
79. Wu, X.; Fan, M.; Mclaughlin, J.F.; Shen, X.; Tan, G. A Novel Low-Cost Method of Silica Aerogel Fabrication Using Fly Ash and Trona Ore with Ambient Pressure Drying Technique. *Powder Technol* 2018, *323*, 310–322, doi:10.1016/J.POWTEC.2017.10.022.

 doi:10.20944/preprints202508.0009.v1

80. Pan, Y.; He, S.; Gong, L.; Cheng, X.; Li, C.; Li, Z.; Liu, Z.; Zhang, H. Low Thermal-Conductivity and High Thermal Stable Silica Aerogel Based on MTMS/Water-Glass Co-Precursor Prepared by Freeze Drying. *Mater Des* 2017, *113*, 246–253, doi:10.1016/J.MATDES.2016.09.083.
81. Zhou, T.; Cheng, X.; Pan, Y.; Li, C.; Gong, L.; Zhang, H. Mechanical Performance and Thermal Stability of Glass Fiber Reinforced Silica Aerogel Composites Based on Co-Precursor Method by Freeze Drying. *Appl Surf Sci* 2018, *437*, doi:10.1016/j.apsusc.2017.12.146.
82. Tillotson, T.M.; Sunderland, W.E.; Thomas, I.M.; Hrubesh, L.W. Synthesis of Lanthanide and Lanthanide-Silicate Aerogels. *J Solgel Sci Technol* 1994, *1*, doi:10.1007/BF00486167.
83. Gash, A.E.; Tillotson, T.M.; Satcher, J.H.; Poco, J.F.; Hrubesh, L.W.; Simpson, R.L. Use of Epoxides in the Sol-Gel Synthesis of Porous Iron(III) Oxide Monoliths from Fe(III) Salts. *Chemistry of Materials* 2001, *13*, doi:10.1021/cm0007611.
84. Gash, A.E.; Tillotson, T.M.; Satcher, J.H.; Hrubesh, L.W.; Simpson, R.L. New Sol–Gel Synthetic Route to Transition and Main-Group Metal Oxide Aerogels Using Inorganic Salt Precursors. *J Non Cryst Solids* 2001, *285*, 22–28, doi:10.1016/S0022-3093(01)00427-6.
85. Gash, A.E.; Satcher, J.H.; Simpson, R.L. Strong Akaganeite Aerogel Monoliths Using Epoxides: Synthesis and Characterization. *Chemistry of Materials* 2003, *15*, doi:10.1021/cm034211p.
86. Long, J.W.; Logan, M.S.; Rhodes, C.P.; Carpenter, E.E.; Stroud, R.M.; Rolison, D.R. Nanocrystalline Iron Oxide Aerogels as Mesoporous Magnetic Architectures. *J Am Chem Soc* 2004, *126*, doi:10.1021/ja046044f.
87. Zhang, Y.; Chai, C.P.; Luo, Y.J.; Wang, L.; Li, G.P. Synthesis, Structure and Electromagnetic Properties of Mesoporous Fe3O4 Aerogels by Sol–Gel Method. *Materials Science and Engineering: B* 2014, *188*, 13–19, doi:10.1016/J.MSEB.2014.06.002.
88. Kido, Y.; Nakanishi, K.; Miyasaka, A.; Kanamori, K. Synthesis of Monolithic Hierarchically Porous Iron-Based Xerogels from Iron(III) Salts via an Epoxide-Mediated Sol-Gel Process. *Chemistry of Materials* 2012, *24*, doi:10.1021/cm300495j.
89. Bali, S.; Huggins, F.E.; Huffman, G.P.; Ernst, R.D.; Pugmire, R.J.; Eyring, E.M. Iron Aerogel and Xerogel Catalysts for Fischer - Tropsch Synthesis of Diesel Fuel. *Energy and Fuels* 2009, *23*, doi:10.1021/ef8005367.
90. Bali, S.; Turpin, G.C.; Ernst, R.D.; Pugmire, R.J.; Singh, V.; Seehra, M.S.; Eyring, E.M. Water Gas Shift Catalysis Using Iron Aerogels Doped with Palladium by the Gas-Phase Incorporation Method. *Energy and Fuels* 2008, *22*, doi:10.1021/ef700691z.
91. Khaleel, A.; Al-Marzouqi, A. Alkoxide-Free Sol–Gel Synthesis of Aerogel Iron–Chromium Mixed Oxides with Unique Textural Properties. *Mater Lett* 2012, *68*, 385–387, doi:10.1016/J.MATLET.2011.11.002.
92. Wei, T.Y.; Chen, C.H.; Chien, H.C.; Lu, S.Y.; Hu, C.C. A Cost-Effective Supercapacitor Material of Ultrahigh Specific Capacitances: Spinel Nickel Cobaltite Aerogels from an Epoxide-Driven Sol-Gel Process. *Advanced Materials* 2010, *22*, doi:10.1002/adma.200902175.
93. Baumann, T.F.; Gash, A.E.; Chinn, S.C.; Sawvel, A.M.; Maxwell, R.S.; Satcher, J.H. Synthesis of High-Surface-Area Alumina Aerogels without the Use of Alkoxide Precursors. *Chemistry of Materials* 2005, *17*, doi:10.1021/cm048800m.
94. Gan, L.; Xu, Z.; Feng, Y.; Chen, L. Synthesis of Alumina Aerogels by Ambient Drying Method and Control of Their Structures. *Journal of Porous Materials* 2005, *12*, doi:10.1007/s10934-005-3130-1.
95. Tokudome, Y.; Nakanishi, K.; Kanamori, K.; Fujita, K.; Akamatsu, H.; Hanada, T. Structural Characterization of Hierarchically Porous Alumina Aerogel and Xerogel Monoliths. *J Colloid Interface Sci* 2009, *338*, 506–513, doi:10.1016/J.JCIS.2009.06.042.
96. Guo, Y.; Meyer-Zaika, W.; Muhler, M.; Vukojević, S.; Epple, M. Cu/Zn/Al Xerogels and Aerogels Prepared by a Sol-Gel Reaction as Catalysts for Methanol Synthesis. *Eur J Inorg Chem* 2006, doi:10.1002/ejic.200600550.
97. Gill, S.K.; Brown, P.; Ogundiya, M.T.; Hope-Weeks, L.J. High Surface Area Alumina-Supported Nickel (II) Oxide Aerogels Using Epoxide Addition Method. *J Solgel Sci Technol* 2010, *53*, doi:10.1007/s10971-009-2142-8.
98. Chervin, C.N.; Clapsaddle, B.J.; Chiu, H.W.; Gash, A.E.; Satcher, J.H.; Kauzlarich, S.M. Aerogel Synthesis of Yttria-Stabilized Zirconia by a Non-Alkoxide Sol-Gel Route. *Chemistry of Materials* 2005, *17*, doi:10.1021/cm0503679.

 doi:10.20944/preprints202508.0009.v1

99. Chervin, C.N.; Clapsaddle, B.J.; Chiu, H.W.; Gash, A.E.; Satcher, J.H.; Kauzlarich, S.M. Role of Cyclic Ether and Solvent in a Non-Alkoxide Sol-Gel Synthesis of Yttria-Stabilized Zirconia Nanoparticles. *Chemistry of Materials* 2006, *18*, doi:10.1021/cm061258c.
100. Li, X.; Jiao, Y.; Ji, H.; Sun, X. The Effect of Propylene Oxide on Microstructure of Zirconia Monolithic Aerogel. *Integrated Ferroelectrics* 2013, *146*, doi:10.1080/10584587.2013.789763.
101. Schäfer, H.; Brandt, S.; Milow, B.; Ichilmann, S.; Steinhart, M.; Ratke, L. Zirconia-Based Aerogels via Hydrolysis of Salts and Alkoxides: The Influence of the Synthesis Procedures on the Properties of the Aerogels. *Chem Asian J* 2013, *8*, doi:10.1002/asia.201300488.
102. Zhong, L.; Chen, X.; Song, H.; Guo, K.; Hu, Z. Synthesis of Monolithic Zirconia Aerogel via a Nitric Acid Assisted Epoxide Addition Method. *RSC Adv* 2014, *4*, doi:10.1039/c4ra04601c.
103. Baumann, T.F.; Kucheyev, S.O.; Gash, A.E.; Satcher, J.H. Facile Synthesis of a Crystalline, High-Surface-Area SnO2 Aerogel. *Advanced Materials* 2005, *17*, doi:10.1002/adma.200500074.
104. Gao, Y.P.; Sisk, C.N.; Hope-Weeks, L.J. A Sol-Gel Route to Synthesize Monolithic Zinc Oxide Aerogels. *Chemistry of Materials* 2007, *19*, doi:10.1021/cm0718419.
105. Chen, B.; Chen, G.; Zeng, T.; Liu, T.; Mei, Y.; Bi, Y.; Luo, X.; Zhang, L. Monolithic Zinc Oxide Aerogel with the Building Block of Nanoscale Crystalline Particle. *Journal of Porous Materials* 2013, *20*, doi:10.1007/s10934-013-9686-2.
106. Chen, B.; Wang, X.; Zhang, S.; Wei, C.; Zhang, L. Monolithic ZnO Aerogel Synthesized through Dispersed Inorganic Sol–Gel Method Using Citric Acid as Template. *Journal of Porous Materials* 2014, *21*, doi:10.1007/s10934-014-9853-0.
107. Davis, M.; Zhang, K.; Wang, S.; Hope-Weeks, L.J. Enhanced Electrical Conductivity in Mesoporous 3D Indium-Tin Oxide Materials. *J Mater Chem* 2012, *22*, doi:10.1039/c2jm34744j.
108. Vu, A.; Qian, Y.; Stein, A. Porous Electrode Materials for Lithium-Ion Batteries-How to Prepare Them and What Makes Them Special. *Adv Energy Mater* 2012, *2*.
109. Zhang, Z.; Liu, J.; Gu, J.; Su, L.; Cheng, L. An Overview of Metal Oxide Materials as Electrocatalysts and Supports for Polymer Electrolyte Fuel Cells. *Energy Environ Sci* 2014, *7*.
110. Ellmer, K. Past Achievements and Future Challenges in the Development of Optically Transparent Electrodes. *Nat Photonics* 2012, *6*.
111. Luo, L.; Bozyigit, D.; Wood, V.; Niederberger, M. High-Quality Transparent Electrodes Spin-Cast from Preformed Antimony-Doped Tin Oxide Nanocrystals for Thin Film Optoelectronics. *Chemistry of Materials* 2013, *25*, doi:10.1021/cm4030149.
112. Badawy, W.A. A Review on Solar Cells from Si-Single Crystals to Porous Materials and Quantum Dots. *J Adv Res* 2015, *6*, 123–132, doi:10.1016/J.JARE.2013.10.001.
113. Correa Baena, J.P.; Agrios, A.G. Antimony-Doped Tin Oxide Aerogels as Porous Electron Collectors for Dye-Sensitized Solar Cells. *Journal of Physical Chemistry C* 2014, *118*, doi:10.1021/jp500542v.
114. Correa Baena, J.P.; Agrios, A.G. Transparent Conducting Aerogels of Antimony-Doped Tin Oxide. *ACS Appl Mater Interfaces* 2014, *6*, doi:10.1021/am505115x.
115. Kucheyev, S.O.; Van Buuren, T.; Baumann, T.F.; Satcher, J.H.; Willey, T.M.; Meulenberg, R.W.; Felter, T.E.; Poco, J.F.; Gammon, S.A.; Terminello, L.J. Electronic Structure of Titania Aerogels from Soft X-Ray Absorption Spectroscopy. *Phys Rev B Condens Matter Mater Phys* 2004, *69*, doi:10.1103/PhysRevB.69.245102.
116. Choi, J.; Shin, C.B.; Suh, D.J. Polyvanadate Dominant Vanadia-Alumina Composite Aerogels Prepared by a Non-Alkoxide Sol-Gel Method. *J Mater Chem* 2009, *19*, doi:10.1039/b905435a.
117. Peterson, G.R.; Hung-Low, F.; Gumeci, C.; Bassett, W.P.; Korzeniewski, C.; Hope-Weeks, L.J. Preparation-Morphology-Performance Relationships in Cobalt Aerogels as Supercapacitors. *ACS Appl Mater Interfaces* 2014, *6*, doi:10.1021/am4047969.
118. Reibold, R.A.; Poco, J.F.; Baumann, T.F.; Simpson, R.L.; Satcher, J.H. Synthesis and Characterization of a Low-Density Urania (UO3) Aerogel. *J Non Cryst Solids* 2003, *319*, 241–246, doi:10.1016/S0022-3093(03)00012-7.
119. Zhang, H.D.; Li, B.; Zheng, Q.X.; Jiang, M.H.; Tao, X.T. Synthesis and Characterization of Monolithic Gd2O3 Aerogels. *J Non Cryst Solids* 2008, *354*, 4089–4093, doi:10.1016/J.JNONCRYSOL.2008.05.044.

 doi:10.20944/preprints202508.0009.v1

120. Clapsaddle, B.J.; Neumann, B.; Wittstock, A.; Sprehn, D.W.; Gash, A.E.; Satcher, J.H.; Simpson, R.L.; Bäumer, M. A Sol-Gel Methodology for the Preparation of Lanthanide-Oxide Aerogels: Preparation and Characterization. *J Solgel Sci Technol* 2012, *64*, doi:10.1007/s10971-012-2868-6.
121. Schäfer, H.; Milow, B.; Ratke, L. Synthesis of Inorganic Aerogels via Rapid Gelation Using Chloride Precursors. *RSC Adv* 2013, *3*, doi:10.1039/c3ra41688g.
122. Ren, H.; Zhang, L.; Shang, C.; Wang, X.; Bi, Y. Synthesis of a Low-Density Tantalum Oxide Tile-like Aerogel Monolithic. *J Solgel Sci Technol* 2010, *53*, doi:10.1007/s10971-009-2092-1.
123. Davis, M.; Gümeci, C.; Kiel, C.; Hope-Weeks, L.J. Preparation of Porous Manganese Oxide Nanomaterials by One-Pot Synthetic Sol-Gel Method. *J Solgel Sci Technol* 2011, *58*, doi:10.1007/s10971-011-2424-9.
124. Brown, P.D.; Gill, S.K.; Hope-Weeks, L.J. Influence of Solvent on Porosity and Microstructure of an Yttrium Based Aerogel. *J Mater Chem* 2011, *21*, doi:10.1039/c0jm03178j.
125. Eid, J.; Pierre, A.C.; Baret, G. Preparation and Characterization of Transparent Eu Doped Y2O3 Aerogel Monoliths, for Application in Luminescence. *J Non Cryst Solids* 2005, *351*, 218–227, doi:10.1016/J.JNONCRYSOL.2004.11.020.
126. Reibold, R.A.; Poco, J.F.; Baumann, T.F.; Simpson, R.L.; Satcher, J.H. Synthesis and Characterization of a Nanocrystalline Thoria Aerogel. *J Non Cryst Solids* 2004, *341*, 35–39, doi:10.1016/J.JNONCRYSOL.2004.05.008.
127. Yoo, J.; Bang, Y.; Han, S.J.; Park, S.; Song, J.H.; Song, I.K. Hydrogen Production by Tri-Reforming of Methane over Nickel–Alumina Aerogel Catalyst. *J Mol Catal A Chem* 2015, *410*, 74–80, doi:10.1016/J.MOLCATA.2015.09.008.
128. Brown, P.; Cearnaigh, D.U.; Fung, E.K.; Hope-Weeks, L.J. Controlling the Morphology of a Zinc Ferrite-Based Aerogel by Choice of Solvent. *J Solgel Sci Technol* 2012, *61*, doi:10.1007/s10971-011-2597-2.
129. Brown, P.; Hope-Weeks, L.J. The Synthesis and Characterization of Zinc Ferrite Aerogels Prepared by Epoxide Addition. *J Solgel Sci Technol* 2009, *51*, doi:10.1007/s10971-009-1985-3.
130. Chervin, C.N.; Ko, J.S.; Miller, B.W.; Dudek, L.; Mansour, A.N.; Donakowski, M.D.; Brintlinger, T.; Gogotsi, P.; Chattopadhyay, S.; Shibata, T.; et al. Defective by Design: Vanadium-Substituted Iron Oxide Nanoarchitectures as Cation-Insertion Hosts for Electrochemical Charge Storage. *J Mater Chem A Mater* 2015, *3*, doi:10.1039/c5ta01507c.
131. Chervin, C.N.; Clapsaddle, B.J.; Chiu, H.W.; Gash, A.E.; Satcher, J.H.; Kauzlarich, S.M. A Non-Alkoxide Sol-Gel Method for the Preparation of Homogeneous Nanocrystalline Powders of La 0.85Sr 0.15MnO 3. *Chemistry of Materials* 2006, *18*, doi:10.1021/cm052301j.
132. Long, J.W.; Logan, M.S.; Carpenter, E.E.; Rolison, D.R. Synthesis and Characterization of Mn–FeOx Aerogels with Magnetic Properties. *J Non Cryst Solids* 2004, *350*, 182–188, doi:10.1016/J.JNONCRYSOL.2004.06.036.
133. Pettigrew, K.A.; Long, J.W.; Carpenter, E.E.; Baker, C.C.; Lytle, J.C.; Chervin, C.N.; Logan, M.S.; Stroud, R.M.; Rolison, D.R. Nickel Ferrite Aerogels with Monodisperse Nanoscale Building Blocks - The Importance of Processing Temperature and Atmosphere. *ACS Nano* 2008, *2*, doi:10.1021/nn7002822.
134. Zhu, Y.; Zhang, X.; Lan, Z.; Li, H.; Zhang, X.; Li, Q. Hydrogen Bonding Directed Assembly of Simonkolleite Aerogel by a Sol–Gel Approach. *Mater Des* 2016, *93*, 503–508, doi:10.1016/J.MATDES.2016.01.002.
135. Gash, A.E.; Satcher, J.H.; Simpson, R.L. Monolithic Nickel(II)-Based Aerogels Using an Organic Epoxide: The Importance of the Counterion. *J Non Cryst Solids* 2004, *350*, 145–151, doi:10.1016/J.JNONCRYSOL.2004.06.030.
136. Du, A.; Zhou, B.; Shen, J.; Xiao, S.; Zhang, Z.; Liu, C.; Zhang, M. Monolithic Copper Oxide Aerogel via Dispersed Inorganic Sol–Gel Method. *J Non Cryst Solids* 2009, *355*, 175–181, doi:10.1016/J.JNONCRYSOL.2008.11.015.
137. Liu, W.; Herrmann, A.K.; Bigall, N.C.; Rodriguez, P.; Wen, D.; Oezaslan, M.; Schmidt, T.J.; Gaponik, N.; Eychmüller, A. Noble Metal Aerogels-Synthesis, Characterization, and Application as Electrocatalysts. *Acc Chem Res* 2015, *48*, doi:10.1021/ar500237c.
138. Wang, H.; Fang, Q.; Gu, W.; Du, D.; Lin, Y.; Zhu, C. Noble Metal Aerogels. *ACS Appl Mater Interfaces* 2020, *12*, 52234–52250, doi:10.1021/acsami.0c14007.
139. Burpo, F.J. Noble Metal Aerogels. In *Springer Handbooks*; 2023; Vol. Part F1485.

 doi:10.20944/preprints202508.0009.v1

140. Bigall, N.C.; Herrmann, A.K.; Vogel, M.; Rose, M.; Simon, P.; Carrillo-Cabrera, W.; Dorfs, D.; Kaskel, S.; Gaponik, N.; Eychmüller, A. Hydrogels and Aerogels from Noble Metal Nanoparticles. *Angewandte Chemie - International Edition* 2009, *48*, doi:10.1002/anie.200902543.
141. Herrmann, A.K.; Formanek, P.; Borchardt, L.; Klose, M.; Giebeler, L.; Eckert, J.; Kaskel, S.; Gaponik, N.; Eychmüller, A. Multimetallic Aerogels by Template-Free Self-Assembly of Au, Ag, Pt, and Pd Nanoparticles. *Chemistry of Materials* 2014, *26*, doi:10.1021/cm4033258.
142. Ranmohotti, K.G.S.; Gao, X.; Arachchige, I.U. Salt-Mediated Self-Assembly of Metal Nanoshells into Monolithic Aerogel Frameworks. *Chemistry of Materials* 2013, *25*, doi:10.1021/cm401968j.
143. Gao, X.; Esteves, R.J.; Luong, T.T.H.; Jaini, R.; Arachchige, I.U. Oxidation-Induced Self-Assembly of Ag Nanoshells into Transparent and Opaque Ag Hydrogels and Aerogels. *J Am Chem Soc* 2014, *136*, doi:10.1021/ja5020037.
144. Kühn, L.; Herrmann, A.K.; Rutkowski, B.; Oezaslan, M.; Nachtegaal, M.; Klose, M.; Giebeler, L.; Gaponik, N.; Eckert, J.; Schmidt, T.J.; et al. Alloying Behavior of Self-Assembled Noble Metal Nanoparticles. *Chemistry - A European Journal* 2016, *22*, doi:10.1002/chem.201602487.
145. Oezaslan, M.; Herrmann, A.K.; Werheid, M.; Frenkel, A.I.; Nachtegaal, M.; Dosche, C.; Laugier Bonnaud, C.; Yilmaz, H.C.; Kühn, L.; Rhiel, E.; et al. Structural Analysis and Electrochemical Properties of Bimetallic Palladium–Platinum Aerogels Prepared by a Two-Step Gelation Process. *ChemCatChem* 2017, *9*, doi:10.1002/cctc.201600667.
146. Cai, B.; Dianat, A.; Hübner, R.; Liu, W.; Wen, D.; Benad, A.; Sonntag, L.; Gemming, T.; Cuniberti, G.; Eychmüller, A. Multimetallic Hierarchical Aerogels: Shape Engineering of the Building Blocks for Efficient Electrocatalysis. *Advanced Materials* 2017, *29*, doi:10.1002/adma.201605254.
147. Cai, B.; Wen, D.; Liu, W.; Herrmann, A.K.; Benad, A.; Eychmüller, A. Function-Led Design of Aerogels: Self-Assembly of Alloyed PdNi Hollow Nanospheres for Efficient Electrocatalysis. *Angewandte Chemie - International Edition* 2015, *54*, doi:10.1002/anie.201505307.
148. Liu, W.; Herrmann, A.K.; Geiger, D.; Borchardt, L.; Simon, F.; Kaskel, S.; Gaponik, N.; Eychmüller, A. High-Performance Electrocatalysis on Palladium Aerogels. *Angewandte Chemie - International Edition* 2012, *51*, doi:10.1002/anie.201108575.
149. Liu, W.; Rodriguez, P.; Borchardt, L.; Foelske, A.; Yuan, J.; Herrmann, A.K.; Geiger, D.; Zheng, Z.; Kaskel, S.; Gaponik, N.; et al. Bimetallic Aerogels: High-Performance Electrocatalysts for the Oxygen Reduction Reaction. *Angewandte Chemie - International Edition* 2013, *52*, doi:10.1002/anie.201303109.
150. Zhu, C.; Shi, Q.; Fu, S.; Song, J.; Xia, H.; Du, D.; Lin, Y. Efficient Synthesis of MCu (M = Pd, Pt, and Au) Aerogels with Accelerated Gelation Kinetics and Their High Electrocatalytic Activity. *Advanced Materials* 2016, *28*, doi:10.1002/adma.201602546.
151. Shi, Q.; Zhu, C.; Du, D.; Bi, C.; Xia, H.; Feng, S.; Engelhard, M.H.; Lin, Y. Kinetically Controlled Synthesis of AuPt Bi-Metallic Aerogels and Their Enhanced Electrocatalytic Performances. *J Mater Chem A Mater* 2017, *5*, doi:10.1039/c7ta06375j.
152. Nyce, G.W.; Hayes, J.R.; Hamza, A. V.; Satcher, J.H. Synthesis and Characterization of Hierarchical Porous Gold Materials. *Chemistry of Materials* 2007, *19*, doi:10.1021/cm062569q.
153. Erlebacher, J.; Aziz, M.J.; Karma, A.; Dimitrov, N.; Sieradzki, K. Evolution of Nanoporosity in Dealloying. *Nature* 2001, *410*, doi:10.1038/35068529.
154. Zielasek, V.; Jürgens, B.; Schulz, C.; Biener, J.; Biener, M.M.; Hamza, A. V.; Bäumer, M. Gold Catalysts: Nanoporous Gold Foams. *Angewandte Chemie - International Edition* 2006, *45*, doi:10.1002/anie.200602484.
155. Hodge, A.M.; Hayes, J.R.; Caro, J.A.; Biener, J.; Hamza, A. V. Characterization and Mechanical Behavior of Nanoporous Gold. *Adv Eng Mater* 2006, *8*, doi:10.1002/adem.200600079.
156. Biener, J.; Wittstock, A.; Zepeda-Ruiz, L.A.; Biener, M.M.; Zielasek, V.; Kramer, D.; Viswanath, R.N.; Weissmüller, J.; Bäumer, M.; Hamza, A. V. Surface-Chemistry-Driven Actuation in Nanoporous Gold. *Nat Mater* 2009, *8*, doi:10.1038/nmat2335.
157. Nahar, L.; Farghaly, A.A.; Esteves, R.J.A.; Arachchige, I.U. Shape Controlled Synthesis of Au/Ag/Pd Nanoalloys and Their Oxidation-Induced Self-Assembly into Electrocatalytically Active Aerogel Monoliths. *Chemistry of Materials* 2017, *29*, doi:10.1021/acs.chemmater.7b01731.

 doi:10.20944/preprints202508.0009.v1

158. Bryce C, T.; Stephen A, S.; Luther, E.P. Nanoporous Metal Foams. *Angewandte Chemie - International Edition* 2010, *49*.
159. Tappan, B.C.; Huynh, M.H.; Hiskey, M.A.; Chavez, D.E.; Luther, E.P.; Mang, J.T.; Son, S.F. Ultralow-Density Nanostructured Metal Foams: Combustion Synthesis, Morphology, and Composition. *J Am Chem Soc* 2006, *128*, doi:10.1021/ja056550k.
160. Sotiropoulou, S.; Sierra-Sastre, Y.; Mark, S.S.; Batt, C.A. Biotemplated Nanostructured Materials. *Chemistry of Materials* 2008, *20*, doi:10.1021/cm702152a.
161. Fan, T.X.; Chow, S.K.; Zhang, D. Biomorphic Mineralization: From Biology to Materials. *Prog Mater Sci* 2009, *54*, 542–659, doi:10.1016/J.PMATSCI.2009.02.001.
162. Du, R.; Hu, Y.; Hübner, R.; Joswig, J.O.; Fan, X.; Schneider, K.; Eychmüller, A. Specific Ion Effects Directed Noble Metal Aerogels: Versatile Manipulation for Electrocatalysis and Beyond. *Sci Adv* 2019, *5*, doi:10.1126/sciadv.aaw4590.
163. Burpo, F.J.; Nagelli, E.A.; Losch, A.R.; Bui, J.K.; Forcherio, G.T.; Baker, D.R.; McClure, J.P.; Bartolucci, S.F.; Chu, D.D. Salt-Templated Platinum-Copper Porous Macrobeams for Ethanol Oxidation. *Catalysts* 2019, *9*, doi:10.3390/catal9080662.
164. Burpo, F.J.; Nagelli, E.A.; Mitropoulos, A.N.; Bartolucci, S.F.; McClure, J.P.; Baker, D.R.; Losch, A.R.; Chu, D.D. Saltlated Platinum-Palladium Porous Macrobeam Synthesis. *MRS Commun* 2019, *9*, doi:10.1557/mrc.2018.217.
165. Burpo, F.J.; Nagelli, E.A.; Morris, L.A.; Woronowicz, K.; Mitropoulos, A.N. Salt-Mediated Au-Cu Nanofoam and Au-Cu-Pd Porous Macrobeam Synthesis. *Molecules* 2018, *23*, doi:10.3390/molecules23071701.
166. Burpo, F.J.; Nagelli, E.A.; Winter, S.J.; McClure, J.P.; Bartolucci, S.F.; Burns, A.R.; O'Brien, S.F.; Chu, D.D. Salt-Templated Hierarchically Porous Platinum Macrotube Synthesis. *ChemistrySelect* 2018, *3*, doi:10.1002/slct.201800416.
167. Talapin, D. V. Lego Materials. *ACS Nano* 2008, *2*, doi:10.1021/nn8003179.
168. Heiligtag, F.J.; Airaghi Leccardi, M.J.I.; Erdem, D.; Süess, M.J.; Niederberger, M. Anisotropically Structured Magnetic Aerogel Monoliths. *Nanoscale* 2014, *6*, doi:10.1039/c4nr04694c.
169. Rechberger, F.; Heiligtag, F.J.; Süess, M.J.; Niederberger, M. Assembly of BaTiO3 Nanocrystals into Macroscopic Aerogel Monoliths with High Surface Area. *Angewandte Chemie - International Edition* 2014, *53*, doi:10.1002/anie.201402164.
170. Mohanan, J.L.; Arachchige, I.U.; Brock, S.L. Porous Semiconductor Chalcogenide Aerogels. *Science (1979)* 2005, *307*, doi:10.1126/science.1104226.
171. Pierre, A.C.; Pajonk, G.M. Chemistry of Aerogels and Their Applications. *Chem Rev* 2002, *102*, doi:10.1021/cr0101306.
172. Heiligtag, F.J.; Rossell, M.D.; Süess, M.J.; Niederberger, M. Template-Free Co-Assembly of Preformed Au and TiO2 Nanoparticles into Multicomponent 3D Aerogels. *J Mater Chem* 2011, *21*, doi:10.1039/c1jm11740h.
173. Rechberger, F.; Ilari, G.; Niederberger, M. Assembly of Antimony Doped Tin Oxide Nanocrystals into Conducting Macroscopic Aerogel Monoliths. *Chemical Communications* 2014, *50*, doi:10.1039/c4cc05648e.
174. Zeng, G.; Shi, N.; Hess, M.; Chen, X.; Cheng, W.; Fan, T.; Niederberger, M. A General Method of Fabricating Flexible Spinel-Type Oxide/Reduced Graphene Oxide Nanocomposite Aerogels as Advanced Anodes for Lithium-Ion Batteries. *ACS Nano* 2015, *9*, doi:10.1021/acsnano.5b00576.
175. Niederberger, M. Nonaqueous Sol-Gel Routes to Metal Oxide Nanoparticles. *Acc Chem Res* 2007, *40*.
176. Zhi, M.; Tang, H.; Wu, M.; Ouyang, C.; Hong, Z.; Wu, N. Synthesis and Photocatalysis of Metal Oxide Aerogels: A Review. *Energy and Fuels* 2022, *36*.
177. Danks, A.E.; Hall, S.R.; Schnepp, Z. The Evolution of "sol-Gel" Chemistry as a Technique for Materials Synthesis. *Mater Horiz* 2016, *3*, doi:10.1039/c5mh00260e.
178. Dong, H.; Chen, Y.C.; Feldmann, C. Polyol Synthesis of Nanoparticles: Status and Options Regarding Metals, Oxides, Chalcogenides, and Non-Metal Elements. *Green Chemistry* 2015, *17*, doi:10.1039/c5gc00943j.
179. De Mello Donegá, C.; Liljeroth, P.; Vanmaekelbergh, D. Physicochemical Evaluation of the Hot-Injection Method, a Synthesis Route for Monodisperse Nanocrystals. *Small* 2005, *1*.
180. Van Embden, J.; Chesman, A.S.R.; Jasieniak, J.J. The Heat-up Synthesis of Colloidal Nanocrystals. *Chemistry of Materials* 2015, *27*.

 doi:10.20944/preprints202508.0009.v1

181. Rajamathi, M.; Seshadri, R. Oxide and Chalcogenide Nanoparticles from Hydrothermal/Solvothermal Reactions. *Curr Opin Solid State Mater Sci* 2002, *6*, 337–345, doi:10.1016/S1359-0286(02)00029-3.
182. Hiemenz, P.C.; Rajagopalan, R. *Principles of Colloid and Surface Chemistry: Third Edition, Revised and Expanded*; 2016;
183. Whitesides, G.M.; Boncheva, M. Beyond Molecules: Self-Assembly of Mesoscopic and Macroscopic Components. *Proc Natl Acad Sci U S A* 2002, *99*, doi:10.1073/pnas.082065899.
184. Lee, Y.S. *Self-Assembly and Nanotechnology: A Force Balance Approach*; 2007;
185. Gaponik, N.; Wolf, A.; Marx, R.; Lesnyak, V.; Schilling, K.; Eychmüller, A. Three-Dimensional Self-Assembly of Thiol-Capped CdTe Nanocrystals: Gels and Aerogels as Building Blocks for Nanotechnology. *Advanced Materials* 2008, *20*, doi:10.1002/adma.200702986.
186. Hayase, G.; Nonomura, K.; Hasegawa, G.; Kanamori, K.; Nakanishi, K. Ultralow-Density, Transparent, Superamphiphobic Boehmite Nanofiber Aerogels and Their Alumina Derivatives. *Chemistry of Materials* 2015, *27*, doi:10.1021/cm503993n.
187. Mewis, J.; Wagner, N.J. *Colloidal Suspension Rheology*; 2011; Vol. 9780521515993;.
188. Dawson, K.A. The Glass Paradigm for Colloidal Glasses, Gels, and Other Arrested States Driven by Attractive Interactions. *Curr Opin Colloid Interface Sci* 2002, *7*, 218–227, doi:10.1016/S1359-0294(02)00052-3.
189. Dickinson, E. On Gelation Kinetics in a System of Particles with Both Weak and Strong Interactions. *Journal of the Chemical Society - Faraday Transactions* 1997, *93*, doi:10.1039/a605550h.
190. Lu, P.J.; Zaccarelli, E.; Ciulla, F.; Schofield, A.B.; Sciortino, F.; Weitz, D.A. Gelation of Particles with Short-Range Attraction. *Nature* 2008, *453*, doi:10.1038/nature06931.
191. Liu, P.; Gao, H.; Chen, X.; Chen, D.; Lv, J.; Han, M.; Cheng, P.; Wang, G. In Situ One-Step Construction of Monolithic Silica Aerogel-Based Composite Phase Change Materials for Thermal Protection. *Compos B Eng* 2020, *195*, doi:10.1016/j.compositesb.2020.108072.
192. Sharma, J.; Sheikh, J.; Behera, B.K. Aerogel Composites and Blankets with Embedded Fibrous Material by Ambient Drying: Reviewing Their Production, Characteristics, and Potential Applications. *Drying Technology* 2023, *41*, doi:10.1080/07373937.2022.2162918.
193. Liu, H.; Du, H.; Zheng, T.; Liu, K.; Ji, X.; Xu, T.; Zhang, X.; Si, C. Cellulose Based Composite Foams and Aerogels for Advanced Energy Storage Devices. *Chemical Engineering Journal* 2021, *426*, doi:10.1016/j.cej.2021.130817.
194. Handbook of Sol-Gel Science and Technology: Processing, Characterization and Applications, Volumes I–III Set Edited by Sumio Sakka (Professor Emeritus of Kyoto University). Kluwer Academic Publishers: Boston, Dordrecht, London. 2005. Lx + 1980 Pp. $1500.00. ISBN 1-4020-7969-9. *J Am Chem Soc* 2005, *127*, doi:10.1021/ja041056m.
195. Ahmad, S.; Ahmad, S.; Sheikh, J.N. Silica Centered Aerogels as Advanced Functional Material and Their Applications: A Review. *J Non Cryst Solids* 2023, *611*, 122322, doi:10.1016/J.JNONCRYSOL.2023.122322.
196. Maleki, H.; Durães, L.; García-González, C.A.; del Gaudio, P.; Portugal, A.; Mahmoudi, M. Synthesis and Biomedical Applications of Aerogels: Possibilities and Challenges. *Adv Colloid Interface Sci* 2016, *236*.
197. Hüsing, N.; Schubert, U. Aerogels—Airy Materials: Chemistry, Structure, and Properties. *Angewandte Chemie International Edition* 1998, *37*, 22–45, doi:10.1002/(SICI)1521-3773(19980202)37:1/2<22::AID-ANIE22>3.0.CO;2-I.
198. Salerno, A.; Diéguez, S.; Diaz-Gomez, L.; Gómez-Amoza, J.L.; Magariños, B.; Concheiro, A.; Domingo, C.; Alvarez-Lorenzo, C.; García-González, C.A. Synthetic Scaffolds with Full Pore Interconnectivity for Bone Regeneration Prepared by Supercritical Foaming Using Advanced Biofunctional Plasticizers. *Biofabrication* 2017, *9*, doi:10.1088/1758-5090/aa78c5.
199. Firoozi, A.A.; Firoozi, A.A.; El-Abbasy, A.A.; Aati, K. Enhanced Perspectives on Silica Aerogels: Novel Synthesis Methods and Emerging Engineering Applications. *Results in Engineering* 2025, *25*, 103615, doi:10.1016/j.rineng.2024.103615.
200. Shafi, S.; Navik, R.; Ding, X.; Zhao, Y. Improved Heat Insulation and Mechanical Properties of Silica Aerogel/Glass Fiber Composite by Impregnating Silica Gel. *J Non Cryst Solids* 2019, *503–504*, 78–83, doi:10.1016/J.JNONCRYSOL.2018.09.029.

 doi:10.20944/preprints202508.0009.v1

201. Li, X.; Wang, Q.; Li, H.; Ji, H.; Sun, X.; He, J. Effect of Sepiolite Fiber on the Structure and Properties of the Sepiolite/Silica Aerogel Composite. *J Solgel Sci Technol* 2013, *67*, doi:10.1007/s10971-013-3124-4.
202. Shi, D.; Sun, Y.; Feng, J.; Yang, X.; Han, S.; Mi, C.; Jiang, Y.; Qi, H. Experimental Investigation on High Temperature Anisotropic Compression Properties of Ceramic-Fiber-Reinforced SiO2 Aerogel. *Materials Science and Engineering: A* 2013, *585*, 25–31, doi:10.1016/J.MSEA.2013.07.029.
203. Li, S.; Ren, H.; Zhu, J.; Bi, Y.; Xu, Y.; Zhang, L. Facile Fabrication of Superhydrophobic, Mechanically Strong Multifunctional Silica-Based Aerogels at Benign Temperature. *J Non Cryst Solids* 2017, *473*, 59–63, doi:10.1016/J.JNONCRYSOL.2017.07.032.
204. Lamy-Mendes, A.; Malfait, W.J.; Sadeghpour, A.; Girão, A. V.; Silva, R.F.; Durães, L. Influence of 1D and 2D Carbon Nanostructures in Silica-Based Aerogels. *Carbon N Y* 2021, *180*, 146–162, doi:10.1016/J.CARBON.2021.05.004.
205. Di Luigi, M.; An, L.; Armstrong, J.N.; Ren, S. Scalable and Robust Silica Aerogel Materials from Ambient Pressure Drying. *Mater Adv* 2022, *3*, doi:10.1039/d1ma01086g.
206. Almeida, C.M.R.; Ghica, M.E.; Ramalho, A.L.; Durães, L. Silica-Based Aerogel Composites Reinforced with Different Aramid Fibres for Thermal Insulation in Space Environments. *J Mater Sci* 2021, *56*, doi:10.1007/s10853-021-06142-3.
207. Zou, W.; Wang, X.; Wu, Y.; Zou, L.; Zu, G.; Chen, D.; Shen, J. Opacifier Embedded and Fiber Reinforced Alumina-Based Aerogel Composites for Ultra-High Temperature Thermal Insulation. *Ceram Int* 2019, *45*, 644–650, doi:10.1016/J.CERAMINT.2018.09.223.
208. Demilecamps, A.; Beauger, C.; Hildenbrand, C.; Rigacci, A.; Budtova, T. Cellulose–Silica Aerogels. *Carbohydr Polym* 2015, *122*, 293–300, doi:10.1016/J.CARBPOL.2015.01.022.
209. Allahbakhsh, A.; Bahramian, A.R. Self-Assembled and Pyrolyzed Carbon Aerogels: An Overview of Their Preparation Mechanisms, Properties and Applications. *Nanoscale* 2015, *7*.
210. Maleki, H.; Durães, L.; Portugal, A. An Overview on Silica Aerogels Synthesis and Different Mechanical Reinforcing Strategies. *J Non Cryst Solids* 2014, *385*, doi:10.1016/j.jnoncrysol.2013.10.017.
211. Nardecchia, S.; Carriazo, D.; Ferrer, M.L.; Gutiérrez, M.C.; Monte, F. Del Three Dimensional Macroporous Architectures and Aerogels Built of Carbon Nanotubes and/or Graphene: Synthesis and Applications. *Chem Soc Rev* 2013, *42*, doi:10.1039/c2cs35353a.
212. Abdusalamov, R.; Scherdel, C.; Itskov, M.; Milow, B.; Reichenauer, G.; Rege, A. Modeling and Simulation of the Aggregation and the Structural and Mechanical Properties of Silica Aerogels. *Journal of Physical Chemistry B* 2021, *125*, doi:10.1021/acs.jpcb.0c10311.
213. Su, L.; Niu, M.; Li, M.; Lu, D.; Guo, P.; Zhuang, L.; Peng, K.; Wang, H. Engineering the Mechanical Properties of Resilient Ceramic Aerogels. *Journal of the American Ceramic Society* 2024, *107*, doi:10.1111/jace.19318.
214. Akhter, F.; Pinjaro, M.A.; Ahmed, J.; Ahmed, M.; Arain, H.J.; Ahsan, M.J.; Sanjrani, I.A. Recent Advances and Synthesis Approaches for Enhanced Heavy Metal Adsorption from Wastewater by Silica-Based and Nanocellulose-Based 3D Structured Aerogels: A State of the Art Review with Adsorption Mechanisms and Prospects. *Biomass Convers Biorefin* 2025, *15*.
215. Doke, S.D.; Patel, C.M.; Lad, V.N. Improving Physical Properties of Silica Aerogel Using Compatible Additives. *Chemical Papers* 2021, *75*, doi:10.1007/s11696-020-01281-4.
216. Valdez-Cano, R.; González-López, J.R.; Guerra-Cossío, M.A. Effects on the Mechanical and Thermal Behaviors of an Alternative Mortar When Adding Modified Silica Aerogel with Aminopropyl Triethoxysilane and PEG-PPG-PEG Triblock Copolymer Additives. *Silicon* 2023, *15*, doi:10.1007/s12633-023-02445-z.
217. Chen, Y.X.; Hendrix, Y.; Schollbach, K.; Brouwers, H.J.H. A Silica Aerogel Synthesized from Olivine and Its Application as a Photocatalytic Support. *Constr Build Mater* 2020, *248*, doi:10.1016/j.conbuildmat.2020.118709.
218. Sivaraman, D.; Zhao, S.; Iswar, S.; Lattuada, M.; Malfait, W.J. Aerogel Spring-Back Correlates with Strain Recovery: Effect of Silica Concentration and Aging. *Adv Eng Mater* 2021, *23*, doi:10.1002/adem.202100376.

 doi:10.20944/preprints202508.0009.v1

219. Li, Z.; Hu, M.; Shen, K.; Liu, Q.; Li, M.; Chen, Z.; Cheng, X.; Wu, X. Tuning Thermal Stability and Fire Hazards of Hydrophobic Silica Aerogels via Doping Reduced Graphene Oxide. *J Non Cryst Solids* 2024, *625*, doi:10.1016/j.jnoncrysol.2023.122747.
220. Lee, K.Y.; Mahadik, D.B.; Parale, V.G.; Park, H.H. Composites of Silica Aerogels with Organics: A Review of Synthesis and Mechanical Properties. *Journal of the Korean Ceramic Society* 2020, *57*.
221. Tabernero, A.; Baldino, L.; Misol, A.; Cardea, S.; del Valle, E.M.M. Role of Rheological Properties on Physical Chitosan Aerogels Obtained by Supercritical Drying. *Carbohydr Polym* 2020, *233*, doi:10.1016/j.carbpol.2020.115850.
222. Xue, J.; Han, R.; Li, Y.; Zhang, J.; Liu, J.; Yang, Y. Advances in Multiple Reinforcement Strategies and Applications for Silica Aerogel. *J Mater Sci* 2023, *58*.
223. Patil, S.P. Enhanced Mechanical Properties of Double-Walled Carbon Nanotubes Reinforced Silica Aerogels: An All-Atom Simulation Study. *Scr Mater* 2021, *196*, doi:10.1016/j.scriptamat.2021.113757.
224. Mahmoodi, N.M.; Mokhtari-Shourijeh, Z.; Langari, S.; Naeimi, A.; Hayati, B.; Jalili, M.; Seifpanahi-Shabani, K. Silica Aerogel/Polyacrylonitrile/Polyvinylidene Fluoride Nanofiber and Its Ability for Treatment of Colored Wastewater. *J Mol Struct* 2021, *1227*, doi:10.1016/j.molstruc.2020.129418.
225. Pettignano, A.; Aguilera, D.A.; Tanchoux, N.; Bernardi, L.; Quignard, F. Alginate: A Versatile Biopolymer for Functional Advanced Materials for Catalysis. In *Studies in Surface Science and Catalysis*; 2019; Vol. 178.
226. Cao, J.; Tao, J.; Yang, M.; Liu, C.; Yan, C.; Zhao, Y.; Yu, C.; Zhao, H.B.; Rao, W. A Novel Phosphorus-Modified Silica Aerogel for Simultaneously Improvement of Flame Retardancy, Mechanical and Thermal Insulation Properties in Rigid Polyurethane Foam. *Chemical Engineering Journal* 2024, *485*, doi:10.1016/j.cej.2024.149909.
227. Xue, T.; Yuan, S.; Yang, Y.; Wan, X.; Yang, Y.; Mu, X.; Zhang, L.; Zhang, C.; Fan, W.; Liu, T. Freezing-Assisted Direct Ink Writing of Customized Polyimide Aerogels with Controllable Micro- and Macro-Structures for Thermal Insulation. *Adv Funct Mater* 2025, *35*, doi:10.1002/adfm.202417734.
228. Du, Y.; Zhang, X.; Wang, J.; Liu, Z.; Zhang, K.; Ji, X.; You, Y.; Zhang, X. Reaction-Spun Transparent Silica Aerogel Fibers. *ACS Nano* 2020, *14*, doi:10.1021/acsnano.0c05016.
229. Yu, X.; Huang, M.; Wang, X.; Sun, Q.; Tang, G.H.; Du, M. Toward Optical Selectivity Aerogels by Plasmonic Nanoparticles Doping. *Renew Energy* 2022, *190*, doi:10.1016/j.renene.2022.03.102.
230. Wu, L.; Zhao, B.; Gao, D.; Jiao, D.; Hu, M.; Pei, G. Solar Transparent and Thermally Insulated Silica Aerogel for Efficiency Improvement of Photovoltaic/Thermal Collectors. *Carbon Neutrality* 2023, *2*, doi:10.1007/s43979-023-00046-8.
231. Sun, J.; Zhuo, S.; Zhang, R. Highly Transparent, Temperature-Resistant, and Flexible Polyimide Aerogels for Solar Energy Collection. *ACS Appl Mater Interfaces* 2023, *15*, doi:10.1021/acsami.3c07720.
232. Guo, J.F.; Tang, G.H.; Feng, J.; Jiang, Y.G.; Feng, J.Z. Non-Silica Fiber and Enabled Stratified Fiber Doping for High Temperature Aerogel Insulation. *Int J Heat Mass Transf* 2020, *160*, doi:10.1016/j.ijheatmasstransfer.2020.120194.
233. Gao, D.; Wu, L.; Hao, Y.; Pei, G. Ultrahigh-Efficiency Solar Energy Harvesting via a Non-Concentrating Evacuated Aerogel Flat-Plate Solar Collector. *Renew Energy* 2022, *196*, doi:10.1016/j.renene.2022.07.091.
234. Khaled Mohammad, A.; Ghosh, A. Exploring Energy Consumption for Less Energy-Hungry Building in UK Using Advanced Aerogel Window. *Solar Energy* 2023, *253*, doi:10.1016/j.solener.2023.02.049.
235. Walker, R.C.; Potochniak, A.E.; Hyer, A.P.; Ferri, J.K. Zirconia Aerogels for Thermal Management: Review of Synthesis, Processing, and Properties Information Architecture. *Adv Colloid Interface Sci* 2021, *295*.
236. Xu, X.; Huang, Q.; Chen, B.; Niu, B.; Zhang, Y.; Long, D. High-Precision 3D Reconstruction and Quantitative Structure Description: Linking Microstructure to Macroscopic Heat Transfer of Aerogels. *Chemical Engineering Journal* 2024, *488*, 150989, doi:10.1016/j.cej.2024.150989.
237. McNeil, S.J.; Gupta, H. Emerging Applications of Aerogels in Textiles. *Polym Test* 2022, *106*.
238. Hu, P.; Hu, X.; Liu, L.; Li, M.; Zhao, Z.; Zhang, P.; Wang, J.; Sun, Z. Dimensional Upgrading of 0D Silica Nanospheres to 3D Networking toward Robust Aerogels for Fire Resistance and Low-Carbon Applications. *Materials Science and Engineering: R: Reports* 2024, *161*, 100842, doi:10.1016/j.mser.2024.100842.

 doi:10.20944/preprints202508.0009.v1

239. Silviana, S.; Prastiti, E.C.; Hermawan, F.; Setyawan, A. Optimization of the Sound Absorption Coefficient (SAC) from Cellulose-Silica Aerogel Using the Box-Behnken Design. *ACS Omega* 2022, *7*, doi:10.1021/acsomega.2c03734.
240. Budtova, T.; Lokki, T.; Malakooti, S.; Rege, A.; Lu, H.; Milow, B.; Vapaavuori, J.; Vivod, S.L. Acoustic Properties of Aerogels: Current Status and Prospects. *Adv Eng Mater* 2023, *25*.
241. Aghababaei Tafreshi, O.; Saadatnia, Z.; Ghaffari-Mosanenzadeh, S.; Rastegardoost, M.M.; Zhang, C.; Park, C.B.; Naguib, H.E. Polyimide Aerogel Fiber Bundles for Extreme Thermal Management Systems in Aerospace Applications. *ACS Appl Mater Interfaces* 2024, *16*, 54597–54609, doi:10.1021/acsami.4c11236.
242. Zong, D.; Bai, W.; Geng, M.; Yin, X.; Yu, J.; Zhang, S.; Ding, B. Bubble Templated Flexible Ceramic Nanofiber Aerogels with Cascaded Resonant Cavities for High-Temperature Noise Absorption. *ACS Nano* 2022, *16*, doi:10.1021/acsnano.2c06011.
243. Hu, E.; Zhu, Y.; Cheng, X.; Liu, Q.; Zhu, M. Recent Progress on Organic Aerogels for Sound Absorption. *Mater Today Commun* 2024, *39*, 109243, doi:10.1016/j.mtcomm.2024.109243.
244. Yang, M.; Chen, Z.; Yang, L.; Ding, Y.; Chen, X.; Li, M.; Wu, Q.; Liu, T. Hierarchically Porous Networks Structure Based on Flexible SiO2 Nanofibrous Aerogel with Excellent Low Frequency Noise Absorption. *Ceram Int* 2023, *49*, doi:10.1016/j.ceramint.2022.08.344.
245. Umate, T.B.; Sawarkar, P.D. Thermal Performance Evaluation of Aerogel-Enhanced Polyurethane Insulation Panels for Refrigerated Vehicles: A Numerical and Experimental Study. *Thermal Science and Engineering Progress* 2024, *53*, 102752, doi:10.1016/j.tsep.2024.102752.
246. Merli, F.; Buratti, C. Properties and Energy Performance of Wood Waste Sustainable Panels Resulting from the Fabrication of Innovative Monolithic Aerogel Glazing Systems. *Constr Build Mater* 2024, *438*, 137310, doi:10.1016/j.conbuildmat.2024.137310.
247. Ba Thai, Q.; Ee Siang, T.; Khac Le, D.; Shah, W.A.; Phan-Thien, N.; Duong, H.M. Advanced Fabrication and Multi-Properties of Rubber Aerogels from Car Tire Waste. *Colloids Surf A Physicochem Eng Asp* 2019, *577*, doi:10.1016/j.colsurfa.2019.06.029.
248. Zhao, X.; Hu, Y.; Xu, X.; Li, M.; Han, Y.; Huang, S. Sound Absorption Polyimide Composite Aerogels for Ancient Architectures' Protection. *Adv Compos Hybrid Mater* 2023, *6*, doi:10.1007/s42114-023-00716-2.
249. Shen, S.; Zhang, Y.; Guo, W.; Gong, H.; Xu, Q.; Yan, M.; Li, H.; Zhang, D. Hierarchically Piezoelectric Aerogels for Efficient Sound Absorption and Machine-Learning-Assisted Sensing. *Adv Funct Mater* 2024, *34*, doi:10.1002/adfm.202406773.
250. Wang, G.; Yuan, P.; Ma, B.; Yuan, W.; Luo, J. Hierarchically Structured M13 Phage Aerogel for Enhanced Sound-Absorption. *Macromol Mater Eng* 2020, *305*, doi:10.1002/mame.202000452.
251. Hu, X.; Wang, Y.; Zhang, L.; Xu, M. Simple Ultrasonic-Assisted Approach to Prepare Polysaccharide-Based Aerogel for Cell Research and Histocompatibility Study. *Int J Biol Macromol* 2021, *188*, doi:10.1016/j.ijbiomac.2021.08.034.
252. Zhu, C.Y.; Li, Z.Y.; Pan, N. Design and Thermal Insulation Performance Analysis of Endothermic Opacifiers Doped Silica Aerogels. *International Journal of Thermal Sciences* 2019, *145*, doi:10.1016/j.ijthermalsci.2019.105995.
253. Fu, Z.; Corker, J.; Papathanasiou, T.; Wang, Y.; Zhou, Y.; Madyan, O.A.; Liao, F.; Fan, M. Critical Review on the Thermal Conductivity Modelling of Silica Aerogel Composites. *Journal of Building Engineering* 2022, *57*.
254. Krzemińska, S.; Greszta, A.; Różański, A.; Safandowska, M.; Okrasa, M. Effects of Heat Exposure on the Properties and Structure of Aerogels for Protective Clothing Applications. *Microporous and Mesoporous Materials* 2019, *285*, doi:10.1016/j.micromeso.2019.04.052.
255. Huang, M.; Tang, G.H.; Si, Q.; Pu, J.H.; Sun, Q.; Du, M. Plasmonic Aerogel Window with Structural Coloration for Energy-Efficient and Sustainable Building Envelopes. *Renew Energy* 2023, *216*, doi:10.1016/j.renene.2023.119006.
256. Luo, X.; Shen, J.; Ma, Y.; Liu, L.; Meng, R.; Yao, J. Robust, Sustainable Cellulose Composite Aerogels with Outstanding Flame Retardancy and Thermal Insulation. *Carbohydr Polym* 2020, *230*, doi:10.1016/j.carbpol.2019.115623.

 doi:10.20944/preprints202508.0009.v1

257. Yrieix, B. Architectured Materials in Building Energy Efficiency. In *Springer Series in Materials Science*; 2019; Vol. 282.
258. Zhang, Y.; Li, Y.; Lei, Q.; Fang, X.; Xie, H.; Yu, W. Tightly-Packed Fluorinated Graphene Aerogel/Polydimethylsiloxane Composite with Excellent Thermal Management Properties. *Compos Sci Technol* 2022, *220*, doi:10.1016/j.compscitech.2022.109302.
259. Wu, X.; Man, J.; Liu, S.; Huang, S.; Lu, J.; Tai, J.; Zhong, Y.; Shen, X.; Cui, S.; Chen, X. Isocyanate-Crosslinked Silica Aerogel Monolith with Low Thermal Conductivity and Much Enhanced Mechanical Properties: Fabrication and Analysis of Forming Mechanisms. *Ceram Int* 2021, *47*, doi:10.1016/j.ceramint.2021.06.074.
260. Walker, R.C.; Hyer, A.P.; Guo, H.; Ferri, J.K. Silica Aerogel Synthesis/Process-Property Predictions by Machine Learning. *Chemistry of Materials* 2023, *35*, doi:10.1021/acs.chemmater.2c03459.
261. He, S.; Huang, Y.; Chen, G.; Feng, M.; Dai, H.; Yuan, B.; Chen, X. Effect of Heat Treatment on Hydrophobic Silica Aerogel. *J Hazard Mater* 2019, *362*, doi:10.1016/j.jhazmat.2018.08.087.
262. Mandal, C.; Donthula, S.; Soni, R.; Bertino, M.; Sotiriou-Leventis, C.; Leventis, N. Light Scattering and Haze in TMOS-Co-APTES Silica Aerogels. *J Solgel Sci Technol* 2019, *90*, doi:10.1007/s10971-018-4801-0.
263. Zinzi, M.; Rossi, G.; Anderson, A.M.; Carroll, M.K.; Moretti, E.; Buratti, C. Optical and Visual Experimental Characterization of a Glazing System with Monolithic Silica Aerogel. *Solar Energy* 2019, *183*, doi:10.1016/j.solener.2019.03.013.
264. Lian, M.; Liu, S.; Ding, W.; Wang, Y.; Zhu, T.; Hu, N.; Fan, W.; Miao, Y.-E.; Zhang, C.; Liu, T. A Mechanically Robust and Optically Transparent Nanofiber-Aerogel-Reinforcing Polymeric Nanocomposite for Passive Cooling Window. *Chemical Engineering Journal* 2024, *498*, 154973, doi:10.1016/j.cej.2024.154973.
265. Bi, C.; Tang, G.H.; He, C.B.; Yang, X.; Lu, Y. Elastic Modulus Prediction Based on Thermal Conductivity for Silica Aerogels and Fiber Reinforced Composites. *Ceram Int* 2022, *48*, doi:10.1016/j.ceramint.2021.11.219.
266. Malfait, W.J.; Ebert, H.P.; Brunner, S.; Wernery, J.; Galmarini, S.; Zhao, S.; Reichenauer, G. The Poor Reliability of Thermal Conductivity Data in the Aerogel Literature: A Call to Action! *J Solgel Sci Technol* 2024, *109*, doi:10.1007/s10971-023-06282-9.
267. Gu, X.; Ling, Y. Research Progress of Aerogel Materials in the Field of Construction. *Alexandria Engineering Journal* 2024, *91*.
268. Cao, M.; Liu, B.W.; Zhang, L.; Peng, Z.C.; Zhang, Y.Y.; Wang, H.; Zhao, H.B.; Wang, Y.Z. Fully Biomass-Based Aerogels with Ultrahigh Mechanical Modulus, Enhanced Flame Retardancy, and Great Thermal Insulation Applications. *Compos B Eng* 2021, *225*, doi:10.1016/j.compositesb.2021.109309.
269. Chen, Y.; Dang, B.; Wang, C.; Wang, Y.; Yang, Y.; Liu, M.; Bi, H.; Sun, D.; Li, Y.; Li, J.; et al. Intelligent Designs from Nature: Biomimetic Applications in Wood Technology. *Prog Mater Sci* 2023, *139*.
270. Özbakır, Y.; Jonáš, A.; Kiraz, A.; Erkey, C. Application of Aerogels in Optical Devices. In *Springer Handbooks*; 2023; Vol. Part F1485.
271. Rocha, H.; Lafont, U.; Semprimoschnig, C. Environmental Testing and Characterization of Fibre Reinforced Silica Aerogel Materials for Mars Exploration. *Acta Astronaut* 2019, *165*, doi:10.1016/j.actaastro.2019.07.030.
272. Elshazli, M.T.; Mudaqiq, M.; Xing, T.; Ibrahim, A.; Johnson, B.; Yuan, J. Experimental Study of Using Aerogel Insulation for Residential Buildings. *Advances in Building Energy Research* 2022, *16*, doi:10.1080/17512549.2021.2001369.
273. Li, D.; Ma, Y.; Zhang, S.; Yang, R.; Zhang, C.; Liu, C. Photothermal and Energy Performance of an Innovative Roof Based on Silica Aerogel-PCM Glazing Systems. *Energy Convers Manag* 2022, *262*, doi:10.1016/j.enconman.2022.115567.
274. Liu, Y.; Chen, Y.; Lu, L.; Peng, J.; Zheng, D.; Lu, B. Optical Path Model and Energy Performance Optimization of Aerogel Glazing System Filled with Aerogel Granules. *Appl Energy* 2023, *334*, doi:10.1016/j.apenergy.2022.120623.
275. Liu, Y.; Lu, L.; Chen, Y.; Lu, B. Investigation on the Optical and Energy Performances of Different Kinds of Monolithic Aerogel Glazing Systems. *Appl Energy* 2020, *261*, 114487, doi:10.1016/J.APENERGY.2019.114487.
276. Belloni, E.; Buratti, C.; Merli, F.; Moretti, E.; Ihara, T. Thermal-Energy and Lighting Performance of Aerogel Glazings with Hollow Silica: Field Experimental Study and Dynamic Simulations. *Energy Build* 2021, *243*, doi:10.1016/j.enbuild.2021.110999.

 doi:10.20944/preprints202508.0009.v1

277. Jung, W.; Kim, D.; Ko, S.H. Recent Progress in High-Efficiency Transparent Vacuum Insulation Technologies for Carbon Neutrality. *International Journal of Precision Engineering and Manufacturing-Green Technology* 2024, *11*, 1681–1702, doi:10.1007/s40684-024-00623-x.
278. Revin, V. V.; Pestov, N.A.; Shchankin, M. V.; Mishkin, V.P.; Platonov, V.I.; Uglanov, D.A. A Study of the Physical and Mechanical Properties of Aerogels Obtained from Bacterial Cellulose. *Biomacromolecules* 2019, *20*, doi:10.1021/acs.biomac.8b01816.
279. Çok, S.S.; Gizli, N. Hydrophobic Silica Aerogels Synthesized in Ambient Conditions by Preserving the Pore Structure via Two-Step Silylation. *Ceram Int* 2020, *46*, 27789–27799, doi:10.1016/j.ceramint.2020.07.278.
280. Rezaei, S.; Zolali, A.M.; Jalali, A.; Park, C.B. Strong, Highly Hydrophobic, Transparent, and Super-Insulative Polyorganosiloxane-Based Aerogel. *Chemical Engineering Journal* 2021, *413*, 127488, doi:10.1016/j.cej.2020.127488.
281. Schultz, J.M.; Jensen, K.I. Evacuated Aerogel Glazings. *Vacuum* 2008, *82*, 723–729, doi:10.1016/J.VACUUM.2007.10.019.
282. Neugebauer, A.; Chen, K.; Tang, A.; Allgeier, A.; Glicksman, L.R.; Gibson, L.J. Thermal Conductivity and Characterization of Compacted, Granular Silica Aerogel. *Energy Build* 2014, *79*, 47–57, doi:10.1016/J.ENBUILD.2014.04.025.
283. Karim, A.N.; Johansson, P.; Sasic Kalagasidis, A. Knowledge Gaps Regarding the Hygrothermal and Long-Term Performance of Aerogel-Based Coating Mortars. *Constr Build Mater* 2022, *314*, 125602, doi:10.1016/j.conbuildmat.2021.125602.
284. Jia, G.; Guo, J.; Guo, Y.; Yang, F.; Ma, Z. CO2 Adsorption Properties of Aerogel and Application Prospects in Low-Carbon Building Materials: A Review. *Case Studies in Construction Materials* 2024, *20*, e03171, doi:10.1016/j.cscm.2024.e03171.
285. Fantucci, S.; Fenoglio, E.; Grosso, G.; Serra, V.; Perino, M.; Marino, V.; Dutto, M. Development of an Aerogel-Based Thermal Coating for the Energy Retrofit and the Prevention of Condensation Risk in Existing Buildings. *Sci Technol Built Environ* 2019, *25*, doi:10.1080/23744731.2019.1634931.
286. Han, F.; Lv, Y.; Liang, T.; Kong, X.; Mei, H.; Wang, S. Improvement of Aerogel-Incorporated Concrete by Incorporating Polyvinyl Alcohol Fiber: Mechanical Strength and Thermal Insulation. *Constr Build Mater* 2024, *449*, 138422, doi:10.1016/j.conbuildmat.2024.138422.
287. Kan, A.; Zheng, N.; Zhu, W.; Cao, D.; Wang, W. Innovation and Development of Vacuum Insulation Panels in China: A State-of-the-Art Review. *Journal of Building Engineering* 2022, *48*.
288. Talebi, Z.; Soltani, P.; Habibi, N.; Latifi, F. Silica Aerogel/Polyester Blankets for Efficient Sound Absorption in Buildings. *Constr Build Mater* 2019, *220*, doi:10.1016/j.conbuildmat.2019.06.031.
289. Pedroso, M.; Flores-Colen, I.; Silvestre, J.D.; Gomes, M.G.; Hawreen, A.; Ball, R.J. Synergistic Effect of Fibres on the Physical, Mechanical, and Microstructural Properties of Aerogel-Based Thermal Insulating Renders. *Cem Concr Compos* 2023, *139*, doi:10.1016/j.cemconcomp.2023.105045.
290. Li, P.; Wu, H.; Liu, Y.; Yang, J.; Fang, Z.; Lin, B. Preparation and Optimization of Ultra-Light and Thermal Insulative Aerogel Foam Concrete. *Constr Build Mater* 2019, *205*, doi:10.1016/j.conbuildmat.2019.01.212.
291. Song, Y.; Xue, C.; Guo, W.; Bai, Y.; Shi, Y.; Zhao, Q. Foamed Geopolymer Insulation Materials: Research Progress on Insulation Performance and Durability. *J Clean Prod* 2024, *444*.
292. Fantucci, S.; Fenoglio, E.; Serra, V.; Perino, M.; Dutto, M.; Marino, V. Hygrothermal Characterization of High-Performance Aerogel-Based Internal Plaster. In Proceedings of the Smart Innovation, Systems and Technologies; 2020; Vol. 163.
293. Zhu, P.; Brunner, S.; Zhao, S.; Griffa, M.; Leemann, A.; Toropovs, N.; Malekos, A.; Koebel, M.M.; Lura, P. Study of Physical Properties and Microstructure of Aerogel-Cement Mortars for Improving the Fire Safety of High-Performance Concrete Linings in Tunnels. *Cem Concr Compos* 2019, *104*, doi:10.1016/j.cemconcomp.2019.103414.
294. Wang, J.; Zhou, Y.; Wang, Z.; He, C.; Zhao, Y.; Huang, X.; Richard, Y.K.K. Fire-Resistant and Mechanically-Robust Phosphorus-Doped MoS2/Epoxy Composite as Barrier of the Thermal Runaway Propagation of Lithium-Ion Batteries. *Chemical Engineering Journal* 2024, *497*, 154866, doi:10.1016/j.cej.2024.154866.
295. Ganobjak, M.; Brunner, S.; Wernery, J. Aerogel Materials for Heritage Buildings: Materials, Properties and Case Studies. *J Cult Herit* 2020, *42*, doi:10.1016/j.culher.2019.09.007.

296. Rostami, J.; Khandel, O.; Sedighardekani, R.; Sahneh, A.R.; Ghahari, S.A. Enhanced Workability, Durability, and Thermal Properties of Cement-Based Composites with Aerogel and Paraffin Coated Recycled Aggregates. *J Clean Prod* 2021, *297*, doi:10.1016/j.jclepro.2021.126518.
297. Zhang, H.; Yang, J.; Wu, H.; Fu, P.; Liu, Y.; Yang, W. Dynamic Thermal Performance of Ultra-Light and Thermal-Insulative Aerogel Foamed Concrete for Building Energy Efficiency. *Solar Energy* 2020, *204*, doi:10.1016/j.solener.2020.04.092.
298. Jatoi, A.S.; Hashmi, Z.; Mazari, S.A.; Abro, R.; Sabzoi, N. Recent Developments and Progress of Aerogel Assisted Environmental Remediation: A Review. *Journal of Porous Materials* 2021, *28*, doi:10.1007/s10934-021-01136-7.
299. Yao, C.; Dong, X.; Gao, G.; Sha, F.; Xu, D. Microstructure and Adsorption Properties of MTMS / TEOS Co-Precursor Silica Aerogels Dried at Ambient Pressure. *J Non Cryst Solids* 2021, *562*, doi:10.1016/j.jnoncrysol.2021.120778.
300. Zhang, X.; Zhou, J.; Zheng, Y.; Wei, H.; Su, Z. Graphene-Based Hybrid Aerogels for Energy and Environmental Applications. *Chemical Engineering Journal* 2021, *420*.
301. Barnyakov, A.Y.; Barnyakov, M.Y.; Bobrovnikov, V.S.; Buzykaev, A.R.; Danilyuk, A.F.; Katcin, A.A.; Kononov, S.A.; Kirilenko, P.S.; Kravchenko, E.A.; Kuyanov, I.A.; et al. Impact of Polishing on the Light Scattering at Aerogel Surface. *Nucl Instrum Methods Phys Res A* 2016, *824*, 123–124, doi:10.1016/J.NIMA.2015.11.096.
302. Renjith, P.K.; Sarathchandran, C.; Chandramohanakumar, N.; Sekkar, V. Silica Aerogel Composite with Inherent Superparamagnetic Property: A Pragmatic and Ecofriendly Approach for Oil Spill Clean-up under Harsh Conditions. *Materials Today Sustainability* 2023, *24*, 100498, doi:10.1016/J.MTSUST.2023.100498.
303. Muhammad, S.; Albadn, Y.M.; Yahya, E.B.; Nasr, S.; Khalil, H.P.S.A.; Ahmad, M.I.; Kamaruddin, M.A. Trends in Enhancing the Efficiency of Biomass-Based Aerogels for Oil Spill Clean-Up. *Giant* 2024, *18*, 100249, doi:10.1016/J.GIANT.2024.100249.
304. Saharan, Y.; Singh, J.; Goyat, R.; Umar, A.; Algadi, H.; Ibrahim, A.A.; Kumar, R.; Baskoutas, S. Nanoporous and Hydrophobic New Chitosan-Silica Blend Aerogels for Enhanced Oil Adsorption Capacity. *J Clean Prod* 2022, *351*, 131247, doi:10.1016/J.JCLEPRO.2022.131247.
305. Keshavarz, L.; Ghaani, M.R.; MacElroy, J.M.D.; English, N.J. A Comprehensive Review on the Application of Aerogels in CO2-Adsorption: Materials and Characterisation. *Chemical Engineering Journal* 2021, *412*.
306. Yan, Y.; Zhang, M.; Sheng, L.; Zhang, T.; Yin, H.; Weng, X.; Li, Y.; Sun, W.; Hu, G.; Hu, H. Analysis and Measurement of Optical Properties and Time Characterization of Silica Aerogel Used as a Cherenkov Radiator. *Radiat Meas* 2024, *177*, 107259, doi:10.1016/J.RADMEAS.2024.107259.
307. Kharzheev, Y.N. Use of Silica Aerogels in Cherenkov Counters. *Physics of Particles and Nuclei* 2008, *39*, doi:10.1134/s1063779608010085.
308. Tabata, M. Transparent Silica Aerogel Blocks for High-Energy Physics Research. In *Springer Handbooks*; 2023; Vol. Part F1485.
309. Tabata, M.; Adachi, I.; Hatakeyama, Y.; Kawai, H.; Morita, T.; Sumiyoshi, T. Large-Area Silica Aerogel for Use as Cherenkov Radiators with High Refractive Index, Developed by Supercritical Carbon Dioxide Drying. *J Supercrit Fluids* 2016, *110*, 183–192, doi:10.1016/J.SUPFLU.2015.11.022.
310. Tabata, M.; Allison, P.; Beatty, J.J.; Coutu, S.; Gebhard, M.; Green, N.; Hanna, D.; Kunkler, B.; Lang, M.; McBride, K.; et al. Developing a Silica Aerogel Radiator for the HELIX Ring-Imaging Cherenkov System. *Nucl Instrum Methods Phys Res A* 2020, *952*, 161879, doi:10.1016/J.NIMA.2019.02.006.
311. García-González, C.A.; Sosnik, A.; Kalmár, J.; De Marco, I.; Erkey, C.; Concheiro, A.; Alvarez-Lorenzo, C. Aerogels in Drug Delivery: From Design to Application. *Journal of Controlled Release* 2021, *332*, 40–63, doi:10.1016/J.JCONREL.2021.02.012.
312. Esquivel-Castro, T.A.; Ibarra-Alonso, M.C.; Oliva, J.; Martínez-Luévanos, A. Porous Aerogel and Core/Shell Nanoparticles for Controlled Drug Delivery: A Review. *Materials Science and Engineering C* 2019, *96*.
313. Yang, J.; Wu, H.; Xu, X.; Huang, G.; Xu, T.; Guo, S.; Liang, Y. Numerical and Experimental Study on the Thermal Performance of Aerogel Insulating Panels for Building Energy Efficiency. *Renew Energy* 2019, *138*, doi:10.1016/j.renene.2019.01.120.

 doi:10.20944/preprints202508.0009.v1

314. Pierre, A.C. Applications of Sol-Gel Processing. In *Introduction to Sol-Gel Processing*; Springer International Publishing: Cham, 2020; pp. 597–685.
315. López-Iglesias, C.; Barros, J.; Ardao, I.; Monteiro, F.J.; Alvarez-Lorenzo, C.; Gómez-Amoza, J.L.; García-González, C.A. Vancomycin-Loaded Chitosan Aerogel Particles for Chronic Wound Applications. *Carbohydr Polym* 2019, *204*, 223–231, doi:10.1016/J.CARBPOL.2018.10.012.
316. Chen, Y.; Xiang, Y.; Zhang, H.; Zhu, T.; Chen, S.; Li, J.; Du, J.; Yan, X. A Multifunctional Chitosan Composite Aerogel Based on High Density Amidation for Chronic Wound Healing. *Carbohydr Polym* 2023, *321*, doi:10.1016/j.carbpol.2023.121248.
317. Afrashi, M.; Semnani, D.; Talebi, Z.; Dehghan, P.; Maherolnaghsh, M. Comparing the Drug Loading and Release of Silica Aerogel and PVA Nano Fibers. *J Non Cryst Solids* 2019, *503–504*, doi:10.1016/j.jnoncrysol.2018.09.045.
318. Batista, M.P.; Gonçalves, V.S.S.; Gaspar, F.B.; Nogueira, I.D.; Matias, A.A.; Gurikov, P. Novel Alginate-Chitosan Aerogel Fibres for Potential Wound Healing Applications. *Int J Biol Macromol* 2020, *156*, doi:10.1016/j.ijbiomac.2020.04.089.
319. Takeshita, S.; Zhao, S.; Malfait, W.J.; Koebel, M.M. Chemistry of Chitosan Aerogels: Three-Dimensional Pore Control for Tailored Applications. *Angewandte Chemie - International Edition* 2021, *60*.
320. Phaechamud, T.; Charoenteeraboon, J. Antibacterial Activity and Drug Release of Chitosan Sponge Containing Doxycycline Hyclate. *AAPS PharmSciTech* 2008, *9*, 829–835, doi:10.1208/s12249-008-9117-x.
321. Patel, V.R.; Amiji, M.M. Preparation and Characterization of Freeze-Dried Chitosan-Poly(Ethylene Oxide) Hydrogels for Site-Specific Antibiotic Delivery in the Stomach. *Pharm Res* 1996, *13*, doi:10.1023/A:1016054306763.
322. Stoyneva, V.; Momekova, D.; Kostova, B.; Petrov, P. Stimuli Sensitive Super-Macroporous Cryogels Based on Photo-Crosslinked 2-Hydroxyethylcellulose and Chitosan. *Carbohydr Polym* 2014, *99*, 825–830, doi:10.1016/J.CARBPOL.2013.08.095.
323. Ji, C.; Barrett, A.; Poole-Warren, L.A.; Foster, N.R.; Dehghani, F. The Development of a Dense Gas Solvent Exchange Process for the Impregnation of Pharmaceuticals into Porous Chitosan. *Int J Pharm* 2010, *391*, 187–196, doi:10.1016/J.IJPHARM.2010.03.006.
324. Mi, F.L.; Shyu, S.S.; Chen, C.T.; Lai, J.Y. Adsorption of Indomethacin onto Chemically Modified Chitosan Beads. *Polymer (Guildf)* 2002, *43*, 757–765, doi:10.1016/S0032-3861(01)00580-8.
325. Cabral, R.P.; Sousa, A.M.L.; Silva, A.S.; Paninho, A.I.; Temtem, M.; Costa, E.; Casimiro, T.; Aguiar-Ricardo, A. Design of Experiments Approach on the Preparation of Dry Inhaler Chitosan Composite Formulations by Supercritical CO2-Assisted Spray-Drying. *J Supercrit Fluids* 2016, *116*, 26–35, doi:10.1016/J.SUPFLU.2016.04.001.
326. Said-Galiev, E.E.; Rubina, M.S.; Naumkin, A. V.; Ikonnikov, N.S.; Vasil'kov, A.Y. Production of a Novel Material Based on a Collagen–Chitosan Composite and Ibuprofen in a Supercritical Medium. *Doklady Physical Chemistry* 2018, *482*, doi:10.1134/S0012501618090038.
327. Dinu, M.V.; Cocarta, A.I.; Dragan, E.S. Synthesis, Characterization and Drug Release Properties of 3D Chitosan/Clinoptilolite Biocomposite Cryogels. *Carbohydr Polym* 2016, *153*, 203–211, doi:10.1016/J.CARBPOL.2016.07.111.
328. Radwan-Pragłowska, J.; Piątkowski, M.; Janus, Ł.; Bogdał, D.; Matysek, D. Biodegradable, PH-Responsive Chitosan Aerogels for Biomedical Applications. *RSC Adv* 2017, *7*, 32960–32965, doi:10.1039/C6RA27474A.
329. Wang, R.; Shou, D.; Lv, O.; Kong, Y.; Deng, L.; Shen, J. PH-Controlled Drug Delivery with Hybrid Aerogel of Chitosan, Carboxymethyl Cellulose and Graphene Oxide as the Carrier. *Int J Biol Macromol* 2017, *103*, 248–253, doi:10.1016/J.IJBIOMAC.2017.05.064.
330. Duarte, A.R.C.; Mano, J.F.; Reis, R.L. Preparation of Chitosan Scaffolds Loaded with Dexamethasone for Tissue Engineering Applications Using Supercritical Fluid Technology. *Eur Polym J* 2009, *45*, 141–148, doi:10.1016/J.EURPOLYMJ.2008.10.004.
331. Diop, M.; Auberval, N.; Viciglio, A.; Langlois, A.; Bietiger, W.; Mura, C.; Peronet, C.; Bekel, A.; Julien David, D.; Zhao, M.; et al. Design, Characterisation, and Bioefficiency of Insulin–Chitosan Nanoparticles after Stabilisation by Freeze-Drying or Cross-Linking. *Int J Pharm* 2015, *491*, 402–408, doi:10.1016/j.ijpharm.2015.05.065.

 doi:10.20944/preprints202508.0009.v1

332. Portero, A.; Teijeiro-Osorio, D.; Alonso, M.J.; Remuñán-López, C. Development of Chitosan Sponges for Buccal Administration of Insulin. *Carbohydr Polym* 2007, *68*, 617–625, doi:10.1016/J.CARBPOL.2006.07.028.
333. Sonaje, K.; Chen, Y.J.; Chen, H.L.; Wey, S.P.; Juang, J.H.; Nguyen, H.N.; Hsu, C.W.; Lin, K.J.; Sung, H.W. Enteric-Coated Capsules Filled with Freeze-Dried Chitosan/Poly(γ-Glutamic Acid) Nanoparticles for Oral Insulin Delivery. *Biomaterials* 2010, *31*, 3384–3394, doi:10.1016/J.BIOMATERIALS.2010.01.042.
334. Dragan, E.S.; Cocarta, A.I.; Gierszewska, M. Designing Novel Macroporous Composite Hydrogels Based on Methacrylic Acid Copolymers and Chitosan and in Vitro Assessment of Lysozyme Controlled Delivery. *Colloids Surf B Biointerfaces* 2016, *139*, 33–41, doi:10.1016/J.COLSURFB.2015.12.011.
335. Caro-León, F.J.; Argüelles-Monal, W.; Carvajal-Millán, E.; López-Franco, Y.L.; Goycoolea-Valencia, F.M.; San Román del Barrio, J.; Lizardi-Mendoza, J. Production and Characterization of Supercritical CO2 Dried Chitosan Nanoparticles as Novel Carrier Device. *Carbohydr Polym* 2018, *198*, 556–562, doi:10.1016/j.carbpol.2018.06.102.
336. Ayensu, I.; Mitchell, J.C.; Boateng, J.S. In Vitro Characterisation of Chitosan Based Xerogels for Potential Buccal Delivery of Proteins. *Carbohydr Polym* 2012, *89*, 935–941, doi:10.1016/J.CARBPOL.2012.04.039.
337. Ihara, D.; Hattori, N.; Horimasu, Y.; Masuda, T.; Nakashima, T.; Senoo, T.; Iwamoto, H.; Fujitaka, K.; Okamoto, H.; Kohno, N. Histological Quantification of Gene Silencing by Intratracheal Administration of Dry Powdered Small-Interfering RNA/Chitosan Complexes in the Murine Lung. *Pharm Res* 2015, *32*, doi:10.1007/s11095-015-1747-6.
338. Reverchon, E.; Antonacci, A. Chitosan Microparticles Production by Supercritical Fluid Processing. *Ind Eng Chem Res* 2006, *45*, doi:10.1021/ie060233k.
339. Kim, S.E.; Suh, D.H.; Yun, Y.P.; Lee, J.Y.; Park, K.; Chung, J.Y.; Lee, D.W. Local Delivery of Alendronate Eluting Chitosan Scaffold Can Effectively Increase Osteoblast Functions and Inhibit Osteoclast Differentiation. *J Mater Sci Mater Med* 2012, *23*, doi:10.1007/s10856-012-4729-9.
340. Sirviö, J.A.; Kantola, A.M.; Komulainen, S.; Filonenko, S. Aqueous Modification of Chitosan with Itaconic Acid to Produce Strong Oxygen Barrier Film. *Biomacromolecules* 2021, *22*, doi:10.1021/acs.biomac.1c00216.
341. Ghoreishi, S.M.; Hedayati, A.; Kordnejad, M. Micronization of Chitosan via Rapid Expansion of Supercritical Solution. *J Supercrit Fluids* 2016, *111*, 162–170, doi:10.1016/J.SUPFLU.2016.01.005.
342. Yu, H.; Tran, T.T.; Teo, J.; Hadinoto, K. Dry Powder Aerosols of Curcumin-Chitosan Nanoparticle Complex Prepared by Spray Freeze Drying and Their Antimicrobial Efficacy against Common Respiratory Bacterial Pathogens. *Colloids Surf A Physicochem Eng Asp* 2016, *504*, 34–42, doi:10.1016/J.COLSURFA.2016.05.053.
343. Rawal, T.; Parmar, R.; Tyagi, R.K.; Butani, S. Rifampicin Loaded Chitosan Nanoparticle Dry Powder Presents an Improved Therapeutic Approach for Alveolar Tuberculosis. *Colloids Surf B Biointerfaces* 2017, *154*, 321–330, doi:10.1016/J.COLSURFB.2017.03.044.
344. Obaidat, R.M.; Tashtoush, B.M.; Bayan, M.F.; T. Al Bustami, R.; Alnaief, M. Drying Using Supercritical Fluid Technology as a Potential Method for Preparation of Chitosan Aerogel Microparticles. *AAPS PharmSciTech* 2015, *16*, doi:10.1208/s12249-015-0312-2.
345. Nakagawa, K.; Sowasod, N.; Tanthapanichakoon, W.; Charinpanitkul, T. Hydrogel Based Oil Encapsulation for Controlled Release of Curcumin Byusing a Ternary System of Chitosan, Kappa-Carrageenan, and Carboxymethylcellulose Sodium Salt. *LWT* 2013, *54*, doi:10.1016/j.lwt.2013.06.011.
346. Hnátová, M.; Bakoš, D.; Černáková, L.; Michliková, M. Chitosan Sponge Matrices with β-Cyclodextrin for Berberine Loadinging. In Proceedings of the Chemical Papers; 2016; Vol. 70.
347. Peniche, H.; Reyes-Ortega, F.; Aguilar, M.R.; Rodríguez, G.; Abradelo, C.; García-Fernández, L.; Peniche, C.; Román, J.S. Thermosensitive Macroporous Cryogels Functionalized with Bioactive Chitosan/Bemiparin Nanoparticles. *Macromol Biosci* 2013, *13*, doi:10.1002/mabi.201300184.
348. Wang, Y.; Wang, X.; Li, L.; Gu, Z.; Yu, X. Controlled Drug Release from a Novel Drug Carrier of Calcium Polyphosphate/Chitosan/Aldehyde Alginate Scaffolds Containing Chitosan Microspheres. *RSC Adv* 2014, *4*, doi:10.1039/c4ra03566f.
349. George, D.; Maheswari, P.U.; Sheriffa Begum, K.M.M.; Arthanareeswaran, G. Biomass-Derived Dialdehyde Cellulose Cross-Linked Chitosan-Based Nanocomposite Hydrogel with Phytosynthesized Zinc Oxide Nanoparticles for Enhanced Curcumin Delivery and Bioactivity. *J Agric Food Chem* 2019, *67*, doi:10.1021/acs.jafc.9b01933.

 doi:10.20944/preprints202508.0009.v1

350. Athamneh, T.; Amin, A.; Benke, E.; Ambrus, R.; Leopold, C.S.; Gurikov, P.; Smirnova, I. Alginate and Hybrid Alginate-Hyaluronic Acid Aerogel Microspheres as Potential Carrier for Pulmonary Drug Delivery. *J Supercrit Fluids* 2019, *150*, 49–55, doi:10.1016/J.SUPFLU.2019.04.013.
351. Athamneh, T.; Amin, A.; Benke, E.; Ambrus, R.; Gurikov, P.; Smirnova, I.; Leopold, C.S. Pulmonary Drug Delivery with Aerogels: Engineering of Alginate and Alginate–Hyaluronic Acid Microspheres. *Pharm Dev Technol* 2021, *26*, doi:10.1080/10837450.2021.1888979.
352. Du, A.; Zhou, B.; Zhang, Z.; Shen, J. A Special Material or a New State of Matter: A Review and Reconsideration of the Aerogel. *Materials* 2013, *6*, doi:10.3390/ma6030941.
353. Wu, Y.; Wang, X.; Shen, J. Metal Oxide Aerogels for High-Temperature Applications. *J Solgel Sci Technol* 2023, *106*.
354. Kurajica, S. A Brief Review on the Use of Chelation Agents in Sol-Gel Synthesis with Emphasis on β-Diketones and β-Ketoesters. *Chem Biochem Eng Q* 2019, *33*, doi:10.15255/CABEQ.2018.1566.
355. Yoldas, B.E. Alumina Gels That Form Porous Transparent Al2O3. *J Mater Sci* 1975, *10*, doi:10.1007/BF00754473.
356. Yoldas, B.E. Thermal Stabilization of an Active Alumina and Effect of Dopants on the Surface Area. *J Mater Sci* 1976, *11*, doi:10.1007/BF00540927.
357. Janosovits, U.; Ziegler, G.; Scharf, U.; Wokaun, A. Structural Characterization of Intermediate Species during Synthesis of Al2O3-Aerogels. *J Non Cryst Solids* 1997, *210*, 1–13, doi:10.1016/S0022-3093(96)00573-X.
358. Poco, J.F.; Satcher, J.H.; Hrubesh, L.W. Synthesis of High Porosity, Monolithic Alumina Aerogels. *J Non Cryst Solids* 2001, *285*, 57–63, doi:10.1016/S0022-3093(01)00432-X.
359. Ponthieu, E.; Grimblot, J.; Elaloui, E.; Pajonk, G.M. Synthesis and Characterization of Pure and Yttrium-Containing Alumina Aerogels. *J Mater Chem* 1993, *3*, doi:10.1039/jm9930300287.
360. Raschko, J.S.; Willey, R.J.; Peri, J.B. Infrared Investigation of Ni0-Al203 Aerogel Catalysts for the Nitroxidation of Propene to Nitriles. *Chem Eng Commun* 1991, *104*, doi:10.1080/00986449108910882.
361. Osaki, T.; Horiuchi, T.; Sugiyama, T.; Suzuki, K.; Mori, T. NiO–Al2O3 Aerogel from (CH2O)2Ni and AlOOH Sol. *J Non Cryst Solids* 1998, *225*, 111–114, doi:10.1016/S0022-3093(98)00015-5.
362. Horiuchi, T.; Chen, L.; Osaki, T.; Mori, T. Thermally Stable Alumina-Gallia Aerogel as a Catalyst for NO Reduction with C3H6 in the Presence of Excess Oxygen. *Catal Letters* 2001, *72*, doi:10.1023/A:1009009832490.
363. Courthéoux, L.; Popa, F.; Gautron, E.; Rossignol, S.; Kappenstein, C. Platinum Supported on Doped Alumina Catalysts for Propulsion Applications. Xerogels versus Aerogels. *J Non Cryst Solids* 2004, *350*, 113–119, doi:10.1016/J.JNONCRYSOL.2004.06.051.
364. Jones, S.M. Non-Silica Aerogels as Hypervelocity Particle Capture Materials. *Meteorit Planet Sci* 2010, *45*, doi:10.1111/j.1945-5100.2009.01007.x.
365. Horiuchi, T.; Osaki, T.; Sugiyama, T.; Masuda, H.; Horio, M.; Suzuki, K.; Mori, T.; Sago, T. High Surface Area Alumina Aerogel at Elevated Temperatures. *Journal of the Chemical Society, Faraday Transactions* 1994, *90*, doi:10.1039/FT9949002573.
366. Pierre, A.; Begag, R.; Pajonk, G. Structure and Texture of Alumina Aerogel Monoliths Made by Complexation with Ethyl Acetoacetate. *J Mater Sci* 1999, *34*, doi:10.1023/A:1004703504103.
367. Kim, S.W.; Iwamoto, S.; Inoue, M. Surface and Pore Structure of Alumina Derived from Xerogel/Aerogel. *Journal of Porous Materials* 2010, *17*, doi:10.1007/s10934-009-9302-7.
368. Tokudome, Y.; Nakanishi, K.; Kanamori, K.; Fujita, K.; Akamatsu, H.; Hanada, T. Structural Characterization of Hierarchically Porous Alumina Aerogel and Xerogel Monoliths. *J Colloid Interface Sci* 2009, *338*, 506–513, doi:10.1016/J.JCIS.2009.06.042.
369. Bao, W.; Guo, F.; Zou, H.; Gan, S.; Xu, X.; Zheng, K. Synthesis of Hydrophobic Alumina Aerogel with Surface Modification from Oil Shale Ash. *Powder Technol* 2013, *249*, 220–224, doi:10.1016/J.POWTEC.2013.08.001.
370. Yang, X.; Wei, J.; Shi, D.; Sun, Y.; Lv, S.; Feng, J.; Jiang, Y. Comparative Investigation of Creep Behavior of Ceramic Fiber-Reinforced Alumina and Silica Aerogel. *Materials Science and Engineering: A* 2014, *609*, 125–130, doi:10.1016/J.MSEA.2014.04.099.

 doi:10.20944/preprints202508.0009.v1

371. Wu, L.A.; Qiao, X.; Cui, S.; Hong, Z.; Fan, X. Synthesis of Monolithic Aerogel-like Alumina via the Accumulation of Mesoporous Hollow Microspheres. *Microporous and Mesoporous Materials* 2015, *202*, 234–240, doi:10.1016/J.MICROMESO.2014.10.015.
372. Gutierrez-Sanchez, C.D.; Téllez-Jurado, L.; Dorantes-Rosales, H.J. Synthesis of Zirconia Nanoparticles by Sol-Gel. Influence of Acidity-Basicity on the Stability Transformation, Particle, and Crystallite Size. *Ceram Int* 2024, *50*, 20547–20560, doi:10.1016/J.CERAMINT.2024.03.177.
373. Torres-Rodríguez, J.; Kalmár, J.; Menelaou, M.; Čelko, L.; Dvořak, K.; Cihlář, J.; Cihlař, J.; Kaiser, J.; Győri, E.; Veres, P.; et al. Heat Treatment Induced Phase Transformations in Zirconia and Yttria-Stabilized Zirconia Monolithic Aerogels. *J Supercrit Fluids* 2019, *149*, 54–63, doi:10.1016/J.SUPFLU.2019.02.011.
374. Teichner, S.J.; Nicolaon, G.A.; Vicarini, M.A.; Gardes, G.E.E. Inorganic Oxide Aerogels. *Adv Colloid Interface Sci* 1976, *5*, 245–273, doi:10.1016/0001-8686(76)80004-8.
375. Ward, D.A.; Ko, E.I. Synthesis and Structural Transformation of Zirconia Aerogels. *Chemistry of Materials* 1993, *5*, doi:10.1021/cm00031a014.
376. Suh, D.J.; Park, T.J. Sol-Gel Strategies for Pore Size Control of High-Surface-Area Transition-Metal Oxide Aerogels. *Chemistry of Materials* 1996, *8*, doi:10.1021/cm950407g.
377. Hudson, M.J.; Knowles, J.A. Preparation and Characterisation of Mesoporous, High-Surface-Area Zirconium (IV) Oxide. *J Mater Chem* 1996, *6*, doi:10.1039/jm9960600089.
378. Bedilo, A.F.; Klabunde, K.J. Synthesis of High Surface Area Zirconia Aerogels Using High Temperature Supercritical Drying. *Nanostructured Materials* 1997, *8*, 119–135, doi:10.1016/S0965-9773(97)00011-1.
379. Cao, Y.; Hu, J.C.; Hong, Z.S.; Deng, J.F.; Fan, K.N. Characterization of High-Surface-Area Zirconia Aerogel Synthesized from Combined Alcohothermal and Supercritical Fluid Drying Techniques. *Catal Letters* 2002, *81*, doi:10.1023/A:1016024509710.
380. Sui, R.; Rizkalla, A.S.; Charpentier, P.A. Direct Synthesis of Zirconia Aerogel Nanoarchitecture in Supercritical CO2. *Langmuir* 2006, *22*, doi:10.1021/la053513y.
381. Stöcker, C.; Baiker, A. Zirconia Aerogels: Effect of the Use of Mono- And Dicarboxylic Acids in the Sol-Gel Process on Structural Properties. *J Solgel Sci Technol* 1997, *10*, doi:10.1023/A:1018321317121.
382. Stöcker, C.; Baiker, A. Zirconia Aerogels: Effect of Acid-to-Alkoxide Ratio, Alcoholic Solvent and Supercritical Drying Method on Structural Properties. *J Non Cryst Solids* 1998, *223*, 165–178, doi:10.1016/S0022-3093(97)00340-2.
383. Zeng, Y.W.; Fagherazzi, G.; Pinna, F.; Polizzi, S.; Riello, P.; Signoretto, M. Short-Range Structure of Zirconia Xerogel and Aerogel, Determined by Wide Angle X-Ray Scattering. *J Non Cryst Solids* 1993, *155*, 259–266, doi:10.1016/0022-3093(93)91260-A.
384. Benedetti, A.; Fagherazzi, G.; Riello, P.; Zeng, Y.W.; Pinna, F.; Signoretto, M. Fractal Properties of a Partially Crystalline Zirconium Oxide Aerogel. *J Appl Crystallogr* 1993, *26*, doi:10.1107/S002188989300442X.
385. Pajonk, G.M.; Tanany, A. El Isomerization and Hydrogenation of Butene-1 on a Zirconia Aerogel Catalyst. *Reaction Kinetics & Catalysis Letters* 1992, *47*, doi:10.1007/BF02137646.
386. Huang, Y.Y.; Zhao, B.Y.; Xie, Y.C. Preparation of Zirconia-Based Acid Catalysts from Zirconia Aerogel of Tetragonal Phase. *Appl Catal A Gen* 1998, *172*, 327–331, doi:10.1016/S0926-860X(98)00138-0.
387. Lee, Y.; Choi, J.W.; Suh, D.J.; Ha, J.M.; Lee, C.H. Ketonization of Hexanoic Acid to Diesel-Blendable 6-Undecanone on the Stable Zirconia Aerogel Catalyst. *Appl Catal A Gen* 2015, *506*, 288–293, doi:10.1016/J.APCATA.2015.09.008.
388. Boyse, R.A.; Ko, E.I. Study of Tungsten Oxide and Sulfate Interactions on Doubly-Doped Zirconia Aerogels. *Catal Letters* 1997, *49*, doi:10.1023/a:1019016229415.
389. Huang, Y.Y.; Zhao, B.Y.; Xie, Y.C. Preparation of Zirconia-Based Acid Catalysts from Zirconia Aerogel of Tetragonal Phase. *Appl Catal A Gen* 1998, *172*, 327–331, doi:10.1016/S0926-860X(98)00138-0.
390. Bedilo, A.F.; Klabunde, K.J. Synthesis of Catalytically Active Sulfated Zirconia Aerogels. *J Catal* 1998, *176*, 448–458, doi:10.1006/JCAT.1998.2052.
391. Signoretto, M.; Oliva, L.; Pinna, F.; Strukul, G. Synthesis of Sulfated-Zirconia Aerogel: Effect of the Chemical Modification of Precursor on Catalyst Porosity. *J Non Cryst Solids* 2001, *290*, 145–152, doi:10.1016/S0022-3093(01)00734-7.

 doi:10.20944/preprints202508.0009.v1

392. Kamoun, N.; Younes, M.K.; Ghorbel, A.; Mamede, A.S.; Rives, A. Comparative Study of the Texture and Structure of Aerogel and Xerogel Sulphated Zirconia Doped with Nickel. *Journal of Porous Materials* 2012, *19*, doi:10.1007/s10934-011-9484-7.
393. Raissi, S.; Younes, M.K. Improved Stabilization of Sulfated Zirconia by Molybdenum: Synergy of Metal Sites and Acid Sites in the n-Hexane Hydro-Isomerization. *Arab J Sci Eng* 2023, *48*, doi:10.1007/s13369-022-07504-y.
394. Kamoun, N.; Younes, M.K.; Ghorbel, A.; Mamede, A.S.; Rives, A. Comparative Study of Aerogels Nanostructured Catalysts: Ni/ZrO2-SO42- and Ni/ZrO2-Al2O3-SO42-. *Ionics (Kiel)* 2015, *21*, doi:10.1007/s11581-014-1168-2.
395. Saravanan, K.; Tyagi, B.; Bajaj, H.C. Nano-Crystalline, Mesoporous Aerogel Sulfated Zirconia as an Efficient Catalyst for Esterification of Stearic Acid with Methanol. *Appl Catal B* 2016, *192*, 161–170, doi:10.1016/J.APCATB.2016.03.037.
396. Zhang, L.; Zhang, L.; Xu, J.; Sun, L.; Ma, J.; Yang, K.; Liang, Z.; Zhang, Y. Zirconium Oxide Aerogel for Effective Enrichment of Phosphopeptides with High Binding Capacity. *Anal Bioanal Chem* 2011, *399*, doi:10.1007/s00216-011-4657-4.
397. Hrubesh, L.W.; Pekala, R.W. Thermal Properties of Organic and Inorganic Aerogels. *J Mater Res* 1994, *9*, doi:10.1557/jmr.1994.0731.
398. Sermon, P.A.; Self, V.A.; Sun, Y. Doped-ZrO2 Aerogels: Catalysts of Controlled Structure and Properties. *J Solgel Sci Technol* 1997, *8*, doi:10.1007/BF02436950.
399. Zhao, Z.; Chen, D.; Jiao, X. Zirconia Aerogels with High Surface Area Derived from Sols Prepared by Electrolyzing Zirconium Oxychloride Solution: Comparison of Aerogels Prepared by Freeze-Drying and Supercritical CO2(l) Extraction. *Journal of Physical Chemistry C* 2007, *111*, doi:10.1021/jp075150b.
400. Chen, L.; Hu, J.; Richards, R.M. Catalytic Properties of Nanoscale Iron-Doped Zirconia Solid-Solution Aerogels. *ChemPhysChem* 2008, *9*, doi:10.1002/cphc.200800041.
401. Sun, Y.; Sermon, P.A. Cu-Doped ZrO2 Aerogel: A Novel Catalyst for CO Hydrogenation to CH3OH. *Top Catal* 1994, *1*, doi:10.1007/BF01379584.
402. Kohama, K.; Imai, H.; Hirashima, H.; Hamada, H.; Inaba, M. Application of ZrO2-Al2O3 Aerogels to Catalysts. *J Solgel Sci Technol* 1998, *13*, doi:10.1023/a:1008620617595.
403. Weissman, J.G.; Ko, E.I.; Kaytal, S. Titania-Zirconia Mixed Oxide Aerogels as Supports for Hydrotreating Catalysts. *Appl Catal A Gen* 1993, *94*, 45–59, doi:10.1016/0926-860X(93)80044-Q.
404. Jung, H.N.R.; Han, W.; Cho, H.H.; Park, H.H. Effect of Cationic and Non-Ionic Surfactants on the Microstructure of Ambient Pressure Dried Zirconia Aerogel. *Materials Express* 2017, *7*, doi:10.1166/mex.2017.1371.
405. Bangi, U.K.H.; Park, H.-H. Evolution of Textural Characteristics of Surfactant-Mediated Mesoporous Zirconia Aerogel Powders Prepared via Ambient Pressure Drying Route. *Int Nano Lett* 2018, *8*, doi:10.1007/s40089-018-0241-7.
406. Wang, X.; Li, C.; Shi, Z.; Zhi, M.; Hong, Z. The Investigation of an Organic Acid Assisted Sol-Gel Method for Preparing Monolithic Zirconia Aerogels. *RSC Adv* 2018, *8*, doi:10.1039/c7ra13041d.
407. Long, J.W.; Chervin, C.N.; Balow, R.B.; Jeon, S.; Miller, J.B.; Helms, M.E.; Owrutsky, J.C.; Rolison, D.R.; Fears, K.P. Zirconia-Based Aerogels for Sorption and Degradation of Dimethyl Methylphosphonate. *Ind Eng Chem Res* 2020, *59*, doi:10.1021/acs.iecr.0c02983.
408. Lermontov, S.A.; Straumal, E.A.; Mazilkin, A.A.; Baranchikov, A.E.; Straumal, B.B.; Ivanov, V.K. An Approach for Highly Transparent Titania Aerogels Preparation. *Mater Lett* 2018, *215*, 19–22, doi:10.1016/J.MATLET.2017.12.031.
409. Schneider, M.; Baiker, A. Titania-Based Aerogels. *Catal Today* 1997, *35*, 339–365, doi:10.1016/S0920-5861(96)00164-2.
410. Schneider, M.; Baiker, A. High-Surface-Area Titania Aerogels: Preparation and Structural Properties. *J Mater Chem* 1992, *2*, doi:10.1039/jm9920200587.
411. Masson, O.; Rieux, V.; Guinebretière, R.; Dauger, A. Size and Shape Characterization of TiO2 Aerogel Nanocrystals. *Nanostructured Materials* 1996, *7*, 725–731, doi:10.1016/S0965-9773(96)00049-9.

 doi:10.20944/preprints202508.0009.v1

412. Malinowska, B.; Walendziewski, J.; Robert, D.; Weber, J. V.; Stolarski, M. Titania Aerogels: Preparation and Photocatalytic Tests. *International Journal of Photoenergy* 2003, *5*, doi:10.1155/S1110662X03000266.
413. Sui, R.; Liu, S.; Lajoie, G.A.; Charpentier, P.A. Preparing Titania Aerogel Monolithic Chromatography Columns Using Supercritical Carbon Dioxide. *J Sep Sci* 2010, *33*, doi:10.1002/jssc.201000032.
414. DeSario, P.A.; Pietron, J.J.; Taffa, D.H.; Compton, R.; Schünemann, S.; Marschall, R.; Brintlinger, T.H.; Stroud, R.M.; Wark, M.; Owrutsky, J.C.; et al. Correlating Changes in Electron Lifetime and Mobility on Photocatalytic Activity at Network-Modified TiO2 Aerogels. *Journal of Physical Chemistry C* 2015, *119*, doi:10.1021/acs.jpcc.5b04013.
415. Nisticò, R.; Magnacca, G. The Hypersaline Synthesis of Titania: From Powders to Aerogels. *RSC Adv* 2015, *5*, doi:10.1039/c4ra13573c.
416. Kim, C.Y.; Park, Y.S. Nanostructure Developments of TiO2 Nanocrystals and Aerogels and Their Dye-Sensitized Solar Cell Application. *J Nanosci Nanotechnol* 2015, *15*, doi:10.1166/jnn.2015.10412.
417. Zhao, Z.; Jiao, X.; Chen, D. Preparation of TiO2 Aerogels by a Sol-Gel Combined Solvothermal Route. *J Mater Chem* 2009, *19*, doi:10.1039/b819849g.
418. Yang, H.; Zhu, W.; Sun, S.; Guo, X. Preparation of Monolithic Titania Aerogels with High Surface Area by a Sol-Gel Process Combined Surface Modification. *RSC Adv* 2014, *4*, doi:10.1039/c4ra03812f.
419. Miller, J.B.; Mathers, L.J.; Ko, E.I. Preparation of Titania-Silica Aerogels with a Double Metal Alkoxide Precursor. *J Mater Chem* 1995, *5*, doi:10.1039/JM9950501759.
420. Pietron, J.J.; Rolison, D.R. Improving the Efficiency of Titania Aerogel-Based Photovoltaic Electrodes by Electrochemically Grafting Isopropyl Moieties on the Titania Surface. *J Non Cryst Solids* 2004, *350*, 107–112, doi:10.1016/J.JNONCRYSOL.2004.06.035.
421. Brodzik, K.; Walendziewski, J.; Stolarski, M.; Van Ginneken, L.; Elst, K.; Meynen, V. The Influence of Preparation Method on the Physicochemical Properties of Titania-Silica Aerogels: Part Two. *Journal of Porous Materials* 2008, *15*, doi:10.1007/s10934-007-9130-6.
422. Yao, N.; Cao, S.; Yeung, K.L. Mesoporous TiO2–SiO2 Aerogels with Hierarchal Pore Structures. *Microporous and Mesoporous Materials* 2009, *117*, 570–579, doi:10.1016/J.MICROMESO.2008.08.020.
423. Zhao, Y.; Ren, W.; Cui, H. Surfactant-Free Synthesis of Water-Soluble Anatase Nanoparticles and Their Application in Preparation of High Optic Performance Monoliths. *J Colloid Interface Sci* 2013, *398*, 7–12, doi:10.1016/J.JCIS.2013.02.025.
424. Kibombo, H.S.; Weber, A.S.; Wu, C.M.; Raghupathi, K.R.; Koodali, R.T. Effectively Dispersed Europium Oxide Dopants in TiO2 Aerogel Supports for Enhanced Photocatalytic Pollutant Degradation. *J Photochem Photobiol A Chem* 2013, *269*, 49–58, doi:10.1016/J.JPHOTOCHEM.2013.07.006.
425. Wang, C.T.; Ro, S.H. Nanoparticle Iron–Titanium Oxide Aerogels. *Mater Chem Phys* 2007, *101*, 41–48, doi:10.1016/J.MATCHEMPHYS.2006.02.010.
426. Puskelova, J.; Baia, L.; Vulpoi, A.; Baia, M.; Antoniadou, M.; Dracopoulos, V.; Stathatos, E.; Gabor, K.; Pap, Z.; Danciu, V.; et al. Photocatalytic Hydrogen Production Using TiO2–Pt Aerogels. *Chemical Engineering Journal* 2014, *242*, 96–101, doi:10.1016/J.CEJ.2013.12.018.
427. Pietron, J.J.; Stroud, R.M.; Rolison, D.R. Using Three Dimensions in Catalytic Mesoporous Nanoarchitectures. *Nano Lett* 2002, *2*, doi:10.1021/nl025536s.
428. Hammedi, T.; Triki, M.; Ksibi, Z.; Ghorbel, A.; Medina, F. Comparative Study of Textural, Structural and Catalytic Properties of Xerogels and Aerogels CeO2–TiO2 Mixed Oxides. *Journal of Porous Materials* 2015, *22*, doi:10.1007/s10934-015-9967-z.
429. Swider, K.E.; Merzbacher, C.I.; Hagans, P.L.; Rolison, D.R. Synthesis of Ruthenium Dioxide-Titanium Dioxide Aerogels: Redistribution of Electrical Properties on the Nanoscale. *Chemistry of Materials* 1997, *9*, doi:10.1021/cm960622c.
430. Choi, J.; Suh, D.J. Complete Oxidation of 1,2-Dichlorobenzene over V2O5-TiO2 and MnOx-TiO2 Aerogels. *Korean Journal of Chemical Engineering* 2014, *31*, doi:10.1007/s11814-014-0128-x.
431. Wan, Y.; Ma, J.; Zhou, W.; Zhu, Y.; Song, X.; Li, H. Preparation of Titania–Zirconia Composite Aerogel Material by Sol–Gel Combined with Supercritical Fluid Drying. *Appl Catal A Gen* 2004, *277*, 55–59, doi:10.1016/J.APCATA.2004.08.022.

 doi:10.20944/preprints202508.0009.v1

432. Sadrieyeh, S.; Malekfar, R. The Effects of Hydrolysis Level on Structural Properties of Titania Aerogels. *J Non Cryst Solids* 2017, *457*, 175–179, doi:10.1016/J.JNONCRYSOL.2016.11.031.
433. Zhang, B. xing; Yu, H.; Zhang, Y.; Luo, Z.; Han, W.; Qiu, W.; Zhao, T. Bacterial Cellulose Derived Monolithic Titania Aerogel Consisting of 3D Reticulate Titania Nanofibers. *Cellulose* 2018, *25*, doi:10.1007/s10570-018-2073-z.
434. Wang, C.T.; Ro, S.H. Nanocluster Iron Oxide-Silica Aerogel Catalysts for Methanol Partial Oxidation. *Appl Catal A Gen* 2005, *285*, 196–204, doi:10.1016/J.APCATA.2005.02.029.
435. Casula, M.F.; Corrias, A.; Paschina, G. Iron Oxide–Silica Aerogel and Xerogel Nanocomposite Materials. *J Non Cryst Solids* 2001, *293–295*, 25–31, doi:10.1016/S0022-3093(01)00641-X.
436. Fernández van Raap, M.B.; Sanchez, F.H.; Leyva, A.G.; Japas, M.L.; Cabanillas, E.; Troiani, H. Synthesis and Magnetic Properties of Iron Oxide–Silica Aerogel Nanocomposites. *Physica B Condens Matter* 2007, *398*, 229–234, doi:10.1016/J.PHYSB.2007.04.021.
437. Maamur, K.N.; Jais, U.S.; Yahya, S.Y.S. Magnetic Phase Development of Iron Oxide-SiO2 Aerogel and Xerogel Prepared Using Rice Husk Ash as Precursor. In Proceedings of the AIP Conference Proceedings; 2010; Vol. 1217.
438. Yoo, J.K.; Kong, H.J.; Wagle, R.; Shon, B.H.; Kim, I.K.; Kim, T.H. A Study on the Methods for Making Iron Oxide Aerogel. *Journal of Industrial and Engineering Chemistry* 2019, *72*, 332–337, doi:10.1016/J.JIEC.2018.12.033.
439. Mohanan, J.L.; Brock, S.L. Influence of Synthetic and Processing Parameters on the Surface Area, Speciation, and Particle Formation in Copper Oxide/Silica Aerogel Composites. *Chemistry of Materials* 2003, *15*, doi:10.1021/cm021741x.
440. Bi, Y.; Ren, H.; Zhang, L. Synthesis of a Low-Density Copper Oxide Monolithic Aerogel Using Inorganic Salt Precursor. In Proceedings of the Advanced Materials Research; 2011; Vol. 217–218.
441. Song, Z.; Liu, W.; Sun, N.; Wei, W.; Zhang, Z.; Liu, H.; Liu, G.; Zhao, Z. One-Step Self-Assembly Fabrication of Three-Dimensional Copper Oxide/Graphene Oxide Aerogel Composite Material for Supercapacitors. *Solid State Commun* 2019, *287*, doi:10.1016/j.ssc.2018.10.007.
442. El Ghoul, J.; Barthou, C.; El Mir, L. Synthesis, Structural and Optical Properties of Nanocrystalline Vanadium Doped Zinc Oxide Aerogel. *Physica E Low Dimens Syst Nanostruct* 2012, *44*, doi:10.1016/j.physe.2012.05.020.
443. Dong, W.; Sakamoto, J.; Dunn, B. Electrochemical Properties of Vanadium Oxide Aerogels and Aerogel Nanocomposites. In Proceedings of the Journal of Sol-Gel Science and Technology; 2003; Vol. 26.
444. Khaddar-Zine, S.; Ghorbel, A.; Naccache, C. Characterization and Catalytic Properties of Aerogel Chromium Oxide Supported by Alumina or Silica. *J Solgel Sci Technol* 2000, *19*, doi:10.1023/A:1008729815266.
445. Hasanpour, M.; Motahari, S.; Jing, D.; Hatami, M. Investigation of the Different Morphologies of Zinc Oxide (ZnO) in Cellulose/ZnO Hybrid Aerogel on the Photocatalytic Degradation Efficiency of Methyl Orange. *Top Catal* 2024, *67*, doi:10.1007/s11244-021-01476-3.
446. Hammiche, L.; Slimi, O.; Djouadi, D.; Chelouche, A.; Touam, T. Effect of Supercritical Organic Solvent on Structural and Optical Properties of Cerium Doped Zinc Oxide Aerogel Nanoparticles. *Optik (Stuttg)* 2017, *145*, doi:10.1016/j.ijleo.2017.08.029.
447. Qiu, X.; Xu, D.; Ma, L.; Wang, Y. Preparation of Manganese Oxide/Graphene Aerogel and Its Application as an Advanced Supercapacitor Electrode Material. *Int J Electrochem Sci* 2017, *12*, doi:10.20964/2017.03.07.
448. Wang, C.C.; Chen, H.C.; Lu, S.Y. Manganese Oxide/Graphene Aerogel Composites as an Outstanding Supercapacitor Electrode Material. *Chemistry - A European Journal* 2014, *20*, doi:10.1002/chem.201303483.
449. Elmanovich, I. V.; Stakhanov, A.I.; Zefirov, V. V.; Pavlov, A.A.; Lokshin, B. V.; Gallyamov, M.O. Thermal Oxidation of Polypropylene Catalyzed by Manganese Oxide Aerogel in Oxygen-Enriched Supercritical Carbon Dioxide. *Journal of Supercritical Fluids* 2020, *158*, doi:10.1016/j.supflu.2019.104744.
450. Slama, R.; Ghribi, F.; Houas, A.; Barthou, C.; El Mir, L. Visible Photocatalytic Properties of Vanadium Doped Zinc Oxide Aerogel Nanopowder. *Thin Solid Films* 2011, *519*, 5792–5795, doi:10.1016/J.TSF.2010.12.197.
451. Chaput, F.; Dunn, B.; Fuqua, P.; Salloux, K. Synthesis and Characterization of Vanadium Oxide Aerogels. *J Non Cryst Solids* 1995, *188*, doi:10.1016/0022-3093(95)00026-7.

 doi:10.20944/preprints202508.0009.v1

452. Le, D.B.; Passerini, S.; Guo, J.; Ressler, J.; Owens, B.B.; Smyrl, W.H. High Surface Area V 2 O 5 Aerogel Intercalation Electrodes. *J Electrochem Soc* 1996, *143*, doi:10.1149/1.1836965.
453. Passerini, S.; Le, D.B.; Smyrl, W.H.; Berrettoni, M.; Tossici, R.; Marassi, R.; Giorgetti, M. XAS and Electrochemical Characterization of Lithiated High Surface Area V2O5 Aerogels. *Solid State Ion* 1997, *104*, doi:10.1016/s0167-2738(97)00438-4.
454. Harreld, J.H.; Dong, W.; Dunn, B. Ambient Pressure Synthesis of Aerogel-Like Vanadium Oxide and Molybdenum Oxide. *Mater Res Bull* 1998, *33*, 561–567, doi:10.1016/S0025-5408(98)00022-1.
455. Li, H.; He, P.; Wang, Y.; Hosono, E.; Zhou, H. High-Surface Vanadium Oxides with Large Capacities for Lithium-Ion Batteries: From Hydrated Aerogel to Nanocrystalline VO2(B), V6O13 and V2O5. *J Mater Chem* 2011, *21*, doi:10.1039/c1jm11523e.
456. Mansour, A.N.; Smith, P.H.; Baker, W.M.; Balasubramanian, M.; McBreen, J. In Situ XAS Investigation of the Oxidation State and Local Structure of Vanadium in Discharged and Charged V2O5 Aerogel Cathodes. *Electrochim Acta* 2002, *47*, 3151–3161, doi:10.1016/S0013-4686(02)00234-7.
457. Mansour, A.N.; Smith, P.H.; Baker, W.M.; Balasubramanian, M.; McBreen, J. A Comparative In Situ X-Ray Absorption Spectroscopy Study of Nanophase V[Sub 2]O[Sub 5] Aerogel and Ambigel Cathodes. *J Electrochem Soc* 2003, *150*, doi:10.1149/1.1554911.
458. Sudant, G.; Baudrin, E.; Dunn, B.; Tarascon, J.-M. Synthesis and Electrochemical Properties of Vanadium Oxide Aerogels Prepared by a Freeze-Drying Process. *J Electrochem Soc* 2004, *151*, doi:10.1149/1.1687427.
459. Xiao, K.; Wu, G.; Shen, J.; Xie, D.; Zhou, B. Preparation and Electrochemical Properties of Vanadium Pentoxide Aerogel Film Derived at the Ambient Pressure. *Mater Chem Phys* 2006, *100*, doi:10.1016/j.matchemphys.2005.11.037.
460. Augustyn, V.; Dunn, B. Vanadium Oxide Aerogels: Nanostructured Materials for Enhanced Energy Storage. *Comptes Rendus Chimie* 2010, *13*.
461. Zhang, L.; Wu, G.; Gao, G.; Yang, H. Electrochemical Performance of V2O5 Nano-Porous Aerogel Film. In Proceedings of the Key Engineering Materials; 2013; Vol. 537.
462. Moretti, A.; Maroni, F.; Osada, I.; Nobili, F.; Passerini, S. V2O5 Aerogel as a Versatile Cathode Material for Lithium and Sodium Batteries. *ChemElectroChem* 2015, *2*, doi:10.1002/celc.201402394.
463. Balakhonov, S. V.; Vatsadze, S.Z.; Churagulov, B.R. Effect of Supercritical Drying Parameters on the Phase Composition and Morphology of Aerogels Based on Vanadium Oxide. *Russian Journal of Inorganic Chemistry* 2015, *60*, doi:10.1134/S0036023615010027.
464. Le, D.B.; Passerini, S.; Coustier, F.; Guo, J.; Soderstrom, T.; Owens, B.B.; Smyrl, W.H. Intercalation of Polyvalent Cations into V2O5 Aerogels. *Chemistry of Materials* 1998, *10*, doi:10.1021/cm9705101.
465. Tang, P.E.; Sakamoto, J.S.; Baudrin, E.; Dunn, B. V2O5 Aerogel as a Versatile Host for Metal Ions. In Proceedings of the Journal of Non-Crystalline Solids; 2004; Vol. 350.
466. Frabetti, E.; Deluga, G.A.; Smyrl, W.H.; Giorgetti, M.; Berrettoni, M. X-Ray Absorption Spectroscopy Study of Cu0.25V2O 5 and Zn0.25V2O5 Aerogel-Like Cathodes for Lithium Batteries. *Journal of Physical Chemistry B* 2004, *108*, doi:10.1021/jp037656+.
467. Zhang, F.; Passerini, S.; Owens, B.B.; Smyrl, W.H. Nanocomposites of V2O5 Aerogel and RuO2 as Cathode Materials for Lithium Intercalation. *Electrochemical and Solid-State Letters* 2001, *4*, doi:10.1149/1.1416128.
468. Harreld, J.; Wong, H.P.; Dave, B.C.; Dunn, B.; Nazar, L.F. Synthesis and Properties of Polypyrrole-Vanadium Oxide Hybrid Aerogels. *J Non Cryst Solids* 1998, *225*, doi:10.1016/S0022-3093(98)00321-4.
469. Balakhonov, S. V.; Astafyeva, K.I.; Efremova, M. V.; Kulova, T.L.; Skundin, A.M.; Churagulov, B.R.; Tretyakov, Y.D. Completely Functional Composite Cathode Material Based on an Aerogel of Vanadium Oxides. *Mendeleev Communications* 2011, *21*, doi:10.1016/j.mencom.2011.11.007.
470. Merdrignac-Conanec, O.; El Badraoui, K.; L'Haridon, P. Nitridation under Ammonia of High Surface Area Vanadium Aerogels. *J Solid State Chem* 2005, *178*, 218–223, doi:10.1016/J.JSSC.2004.11.010.
471. Schneider, H.; Tschudin, S.; Schneider, M.; Wokaun, A.; Baiker, A. In Situ Diffuse Reflectance FTIR Study of the Selective Catalytic Reduction of No by NH3 over Vanadia-Titania Aerogels. *J Catal* 1994, *147*, doi:10.1006/jcat.1994.1109.
472. Scharf, U.; Schneider, M.; Baiker, A.; Wokaun, A. Vanadia-Titania Aerogels: II. Spectroscopic Investigation of the Structural Properties. *J Catal* 1994, *149*, 344–355, doi:10.1006/JCAT.1994.1302.

 doi:10.20944/preprints202508.0009.v1

473. Willey, R.J.; Wang, C.T.; Peri, J.B. Vanadium-Titanium Oxide Aerogel Catalysts. *J Non Cryst Solids* 1995, *186*, 408–414, doi:10.1016/0022-3093(95)00063-1.
474. Zegaoui, O.; Hoang-Van, C.; Karroua, M. Selective Catalytic Reduction of Nitric Oxide by Propane over Vanadia-Titania Aerogels. *Appl Catal B* 1996, *9*, 211–227, doi:10.1016/0926-3373(96)90082-X.
475. Willi, R.; Köppel, R.A.; Baiker, A. High-Performance Aerogel DeNOx Catalyst: Catalytic Behavior and Kinetic Modeling. *Ind Eng Chem Res* 1997, *36*, doi:10.1021/ie960379r.
476. Hoang-Van, C.; Zegaoui, O.; Pichat, P. Vanadia–Titania Aerogel DeNOx Catalysts. *J Non Cryst Solids* 1998, *225*, 157–162, doi:10.1016/S0022-3093(98)00036-2.
477. Kim, M.I.; Park, D.W.; Park, S.W.; Yang, X.; Choi, J.S.; Suh, D.J. Selective Oxidation of Hydrogen Sulfide Containing Excess Water and Ammonia over Vanadia-Titania Aerogel Catalysts. In Proceedings of the Catalysis Today; 2006; Vol. 111.
478. Kang, M.; Choi, J.; Kim, Y.T.; Park, E.D.; Shin, C.B.; Suh, D.J.; Yie, J.E. Effects of Preparation Methods for V2O5-TiO 2 Aerogel Catalysts on the Selective Catalytic Reduction of NO with NH3. *Korean Journal of Chemical Engineering* 2009, *26*, doi:10.1007/s11814-009-0148-0.
479. Du, A.; Zhou, B.; Shen, J.; Xiao, S.; Zhang, Z.; Liu, C.; Zhang, M. Monolithic Copper Oxide Aerogel via Dispersed Inorganic Sol–Gel Method. *J Non Cryst Solids* 2009, *355*, 175–181, doi:10.1016/J.JNONCRYSOL.2008.11.015.
480. Harreld, J.H.; Dong, W.; Dunn, B. Ambient Pressure Synthesis of Aerogel-Like Vanadium Oxide and Molybdenum Oxide. *Mater Res Bull* 1998, *33*, 561–567, doi:10.1016/S0025-5408(98)00022-1.
481. Khaleel, A.; Al-Marzouqi, A. Alkoxide-Free Sol–Gel Synthesis of Aerogel Iron–Chromium Mixed Oxides with Unique Textural Properties. *Mater Lett* 2012, *68*, 385–387, doi:10.1016/J.MATLET.2011.11.002.
482. Utamapanya, S.; Klabunde, K.J.; Schlup, J.R. Nanoscale Metal Oxide Particles/Clusters as Chemical Reagents. Synthesis and Properties of Ultrahigh Surface Area Magnesium Hydroxide and Magnesium Oxide. *Chemistry of Materials* 1991, *3*, doi:10.1021/cm00013a036.
483. Itoh, H.; Utamapanya, S.; Stark, J. V.; Klabunde, K.J.; Schlup, J.R. Nanoscale Metal Oxide Particles as Chemical Reagents. Intrinsic Effects of Particle Size on Hydroxyl Content and on Reactivity and Acid/Base Properties of Ultrafine Magnesium Oxide. *Chemistry of Materials* 1993, *5*, doi:10.1021/cm00025a015.
484. Jeevanandam, P.; Klabunde, K.J. A Study on Adsorption of Surfactant Molecules on Magnesium Oxide Nanocrystals Prepared by an Aerogel Route. *Langmuir* 2002, *18*, doi:10.1021/la0200921.
485. Richards, R.M.; Volodin, A.M.; Bedilo, A.F.; Klabunde, K.J. ESR Study of Nanocrystalline Aerogel-Prepared Magnesium Oxide. *Physical Chemistry Chemical Physics* 2003, *5*, doi:10.1039/b309059k.
486. Dong, W.; Yen, S.P.; Paik, J.A.; Sakamoto, J. The Role of Acetic Acid and Glycerol in the Synthesis of Amorphous MgO Aerogels. *Journal of the American Ceramic Society* 2009, *92*, doi:10.1111/j.1551-2916.2009.02997.x.
487. Feinle, A.; Heugenhauser, A.; Hüsing, N. Impact of Surfactants and Acids on the Sol-Gel Synthesis of MgO Aerogels. *Journal of Supercritical Fluids* 2015, *106*, doi:10.1016/j.supflu.2015.06.019.
488. Štengl, V.; Bakardjieva, S.; Maříková, M.; Šubrt, J.; Opluštil, F.; Olšanská, M. Aerogel Nanoscale Magnesium Oxides as a Destructive Sorbent for Toxic Chemical Agents. *Central European Journal of Chemistry* 2004, *2*, doi:10.2478/BF02476182.
489. Nur, H.; Misnon, I.I.; Hamdan, H. Alkylsilylated Gold Loaded Magnesium Oxide Aerogel Catalyst in the Oxidation of Styrene. *Catal Letters* 2009, *130*, doi:10.1007/s10562-009-9843-z.
490. Mishakov, I. V.; Ilyina, E. V.; Bedilo, A.F.; Vedyagin, A.A. Nanocrystalline Aerogel VOx/MgO as a Catalyst for Oxidative Dehydrogenation of Propane. *Reaction Kinetics and Catalysis Letters* 2009, *97*, doi:10.1007/s11144-009-0041-1.
491. Ilyina, E. V.; Mishakov, I. V.; Vedyagin, A.A.; Cherepanova, S. V.; Nadeev, A.N.; Bedilo, A.F.; Klabunde, K.J. Synthesis and Characterization of Mesoporous VOx/MgO Aerogels with High Surface Area. *Microporous and Mesoporous Materials* 2012, *160*, 32–40, doi:10.1016/J.MICROMESO.2012.04.016.
492. Sádaba, I.; Ojeda, M.; Mariscal, R.; Richards, R.; López Granados, M. Preparation and Characterization of Mg-Zr Mixed Oxide Aerogels and Their Application as Aldol Condensation Catalysts. *ChemPhysChem* 2012, *13*, doi:10.1002/cphc.201200440.

493. Skapin, T. Influence of the Organic Phase on the Properties of CrO3-Derived Chromia Aerogels. *J Non Cryst Solids* 2001, *285*, 128–134, doi:10.1016/S0022-3093(01)00443-4.
494. Skapin, T.; Kemnitz, E. Fluorination Effects in Chromia Aerogels and Xerogels. *J Non Cryst Solids* 1998, *225*, 163–167, doi:10.1016/S0022-3093(98)00037-4.
495. Skapin, T. Preparation and Properties of Highly Fluorinated Alumina Prepared from Boehmite Aerogels or Commercial γ-Al 2 O 3. *J. Mater. Chem.* 1995, *5*, 1215–1222, doi:10.1039/JM9950501215.
496. Skapin, T.; Kemnitz, E. Fluorinated ?-Alumina Aerogels and Xerogels: Characterisation and Catalytic Behaviour. *Catal Letters* 1996, *40*, 241–247, doi:10.1007/BF00815289.
497. Bozorgzadeh, H.; Kemnitz, E.; Nickkho-Amiry, M.; Skapin, T.; Winfield, J.M. Catalytic Reactions of Chlorofluoroethanes at Fluorinated Alumina and Chromia Aerogels and Xerogels: A Comparison of Reaction Pathways in Alumina- and Chromia-Based Catalysts. *J Fluor Chem* 2001, *110*, 181–189, doi:10.1016/S0022-1139(01)00427-4.
498. Bozorgzadeh, H.; Kemnitz, E.; Nickkho-Amiry, M.; Skapin, T.; Winfield, J.M. Dynamic Behaviour of Chlorofluoroethanes at Fluorinated Chromia Aerogels and Fluorinated Zinc(II) or Magnesium(II) Doped Chromia Aerogels. *J Fluor Chem* 2003, *121*, 83–92, doi:10.1016/S0022-1139(02)00340-8.
499. Abecassis-Wolfovich, M.; Rotter, H.; Landau, M. V.; Korin, E.; Erenburg, A.I.; Mogilyansky, D.; Gartstein, E. Texture and Nanostructure of Chromia Aerogels Prepared by Urea-Assisted Homogeneous Precipitation and Low-Temperature Supercritical Drying. *J Non Cryst Solids* 2003, *318*, 95–111, doi:10.1016/S0022-3093(02)01881-1.
500. Rotter, H.; Landau, M. V.; Carrera, M.; Goldfarb, D.; Herskowitz, M. High Surface Area Chromia Aerogel Efficient Catalyst and Catalyst Support for Ethylacetate Combustion. *Appl Catal B* 2004, *47*, 111–126, doi:10.1016/J.APCATB.2003.08.006.
501. Rotter, H.; Landau, M. V.; Herskowitz, M. Combustion of Chlorinated VOC on Nanostructured Chromia Aerogel as Catalyst and Catalyst Support. *Environ Sci Technol* 2005, *39*, 6845–6850, doi:10.1021/es0500052.
502. Younes, M.K.; Ghorbel, A. Catalytic Nitroxidation of Toluene into Benzonitrile on Chromia–Alumina Aerogel Catalyst. *Appl Catal A Gen* 2000, *197*, 269–277, doi:10.1016/S0926-860X(99)00494-9.
503. Willey, R.J.; Lai, H.; Peri, J.B. Investigation of Iron Oxide-Chromia-Alumina Aerogels for the Selective Catalytic Reduction of Nitric Oxide by Ammonia. *J Catal* 1991, *130*, 319–331, doi:10.1016/0021-9517(91)90116-L.
504. Ping Chen, J.; Willey, R.J.; Teichner, S.J. Porosity of Mixed Iron Oxide-Chromia Alumina Aerogels. *Journal of Porous Materials* 1997, *4*, 113–119, doi:10.1023/A:1009680701009.
505. Wang, C.T. Photocatalytic Activity of Nanoparticle Gold/Iron Oxide Aerogels for Azo Dye Degradation. *J Non Cryst Solids* 2007, *353*, 1126–1133, doi:10.1016/J.JNONCRYSOL.2006.12.028.
506. Dong, W.; Dunn, B. Sol–Gel Synthesis and Characterization of Molybdenum Oxide Gels. *J Non Cryst Solids* 1998, *225*, 135–140, doi:10.1016/S0022-3093(98)00018-0.
507. Dong, W.; Mansour, A.N.; Dunn, B. Structural and Electrochemical Properties of Amorphous and Crystalline Molybdenum Oxide Aerogels. *Solid State Ion* 2001, *144*, 31–40, doi:10.1016/S0167-2738(01)00901-8.
508. Dong, W.; Mansour, A.N.; Dunn, B. Structural and Electrochemical Properties of Amorphous and Crystalline Molybdenum Oxide Aerogels. *Solid State Ion* 2001, *144*, 31–40, doi:10.1016/S0167-2738(01)00901-8.
509. Novak, Z.; Kotnik, P.; Knez, Ž. Preparation of WO3 Aerogel Catalysts Using Supercritical CO2 Drying. *J Non Cryst Solids* 2004, *350*, 308–313, doi:10.1016/J.JNONCRYSOL.2004.06.045.
510. Sun, Q.-Q.; Xu, M.; Bao, S.-J.; Ming Li, C. PH-Controllable Synthesis of Unique Nanostructured Tungsten Oxide Aerogel and Its Sensitive Glucose Biosensor. *Nanotechnology* 2015, *26*, 115602, doi:10.1088/0957-4484/26/11/115602.
511. Brinker, C.J.; Ward, K.J.; Keefer, K.D.; Holupka, E.; Bray, P.J.; Pearson, R.K. Synthesis and Structure of Borate Based Aerogels. In; 1986; pp. 57–67.
512. Zhang, L.; Chen, G.; Chen, B.; Liu, T.; Mei, Y.; Luo, X. Monolithic Germanium Oxide Aerogel with the Building Block of Nano-Crystals. *Mater Lett* 2013, *104*, 41–43, doi:10.1016/J.MATLET.2013.04.012.

 doi:10.20944/preprints202508.0009.v1

513. Krumm, M.; Pueyo, C.L.; Polarz, S. Monolithic Zinc Oxide Aerogels from Organometallic Sol–Gel Precursors. *Chemistry of Materials* 2010, *22*, 5129–5136, doi:10.1021/cm1006907.
514. El Mir, L.; El Ghoul, J.; Alaya, S.; Ben Salem, M.; Barthou, C.; von Bardeleben, H.J. Synthesis and Luminescence Properties of Vanadium-Doped Nanosized Zinc Oxide Aerogel. *Physica B Condens Matter* 2008, *403*, 1770–1774, doi:10.1016/J.PHYSB.2007.10.069.
515. Ghoul, J. El; Alaya, A.; Mir, L. El; Barthou, C.; Saadoun, M.; Alaya, S. Elaboration and Characterisation of (Al, V) Co-Doped Nanosized Zinc Oxide Aerogel. *International Journal of Nano and Biomaterials* 2009, *2*, 273, doi:10.1504/IJNBM.2009.027722.
516. Slama, R.; Ghribi, F.; Houas, A.; Barthou, C.; El Mir, L. Visible Photocatalytic Properties of Vanadium Doped Zinc Oxide Aerogel Nanopowder. *Thin Solid Films* 2011, *519*, 5792–5795, doi:10.1016/J.TSF.2010.12.197.
517. Harrison, P.G.; Guest, A. Tin Oxide Surfaces. Part 17.—An Infrared and Thermogravimetric Analysis of the Thermal Dehydration of Tin(IV) Oxide Gel. *Journal of the Chemical Society, Faraday Transactions 1: Physical Chemistry in Condensed Phases* 1987, *83*, 3383, doi:10.1039/f19878303383.
518. Wu, N.-L.; Wu, L.-F.; Yang, Y.-C.; Huang, S.-J. Spontaneous Solution-Sol-Gel Process for Preparing Tin Oxide Monolith. *J Mater Res* 1996, *11*, 813–820, doi:10.1557/JMR.1996.0098.
519. Huang, R.; Hou, L.; Zhou, B.; Zhao, Q.; Ren, S. Formation and Characterization of Tin Oxide Aerogel Derived from Sol–Gel Process Based on Tetra(n-Butoxy)Tin(IV). *J Non Cryst Solids* 2005, *351*, 23–28, doi:10.1016/J.JNONCRYSOL.2004.09.023.
520. Harreld, J.H.; Sakamoto, J.; Dunn, B. Non-Hydrolytic Sol–Gel Synthesis and Electrochemical Characterization of Tin-Based Oxide Aerogels. *J Power Sources* 2003, *115*, 19–26, doi:10.1016/S0378-7753(02)00626-2.
521. Maurer, S.M.; Ko, E.I. Structural and Acidic Characterization of Niobia Aerogels. *J Catal* 1992, *135*, 125–134, doi:10.1016/0021-9517(92)90274-L.
522. Gasser-Ramirez, J.L.; Dunn, B.C.; Ramirez, D.W.; Fillerup, E.P.; Turpin, G.C.; Shi, Y.; Ernst, R.D.; Pugmire, R.J.; Eyring, E.M.; Pettigrew, K.A.; et al. A Simple Synthesis of Catalytically Active, High Surface Area Ceria Aerogels. *J Non Cryst Solids* 2008, *354*, 5509–5514, doi:10.1016/J.JNONCRYSOL.2008.09.011.
523. Long, J.W. Design of Pore and Matter Architectures in Manganese Oxide Charge-Storage Materials. *Electrochemical and Solid-State Letters* 1999, *3*, 453, doi:10.1149/1.1391177.
524. Tang, H.; Sui, Y.; Zhu, X.; Bao, Z. Synthesis of Mn3O4-Based Aerogels and Their Lithium-Storage Abilities. *Nanoscale Res Lett* 2015, *10*, 260, doi:10.1186/s11671-015-0960-x.
525. Frederick, C.A.; Forsman, A.C.; Hund, J.F.; Eddinger, S.A. Fabrication of Ta 2 O 5 Aerogel Targets for Radiation Transport Experiments Using Thin Film Fabrication and Laser Processing. *Fusion Science and Technology* 2009, *55*, 499–504, doi:10.13182/FST55-4-499.
526. Willey, R.J.; Oliver, S.A.; Oliveri, G.; Busca, G. Chemistry and Structure of Mixed Magnesium Ferric Oxide Aerogels. *J Mater Res* 1993, *8*, 1418–1427, doi:10.1557/JMR.1993.1418.
527. Shimooka, H.; Yamada, K.-I.; Takahashi, S.; Kuwabara, M. Preparation of Transparent, Partially-Crystallized BaTiO3 Monolithic Xerogels by Sol-Gel Processing. *J Solgel Sci Technol* 1998, *13*, 873–876, doi:10.1023/A:1008662904874.
528. Shimooka, H.; Kuwabara, M. Crystallinity and Stoichiometry of Nano-Structured Sol-Gel-Derived BaTiO 3 Monolithic Gels. *Journal of the American Ceramic Society* 1996, *79*, 2983–2985, doi:10.1111/j.1151-2916.1996.tb08739.x.
529. Demydov, D.; Klabunde, K.J. Characterization of Mixed Metal Oxides (SrTiO3 and BaTiO3) Synthesized by a Modified Aerogel Procedure. *J Non Cryst Solids* 2004, *350*, 165–172, doi:10.1016/J.JNONCRYSOL.2004.06.022.
530. Löbmann, P.; Glaubitt, W.; Gross, J.; Fricke, J. Preparation and Characterization of Lead Titanate Aerogels. *J Non Cryst Solids* 1995, *186*, 59–63, doi:10.1016/0022-3093(95)00081-X.
531. Maloney, R.P.; Kim, H.J.; Sakamoto, J.S. Lithium Titanate Aerogel for Advanced Lithium-Ion Batteries. *ACS Appl Mater Interfaces* 2012, *4*, doi:10.1021/am3002742.

 doi:10.20944/preprints202508.0009.v1

532. Sydorchuk, V.; Zazhigalov, V.; Khalameida, S.; Diyuk, E.; Skubiszewska-Ziba, J.; Leboda, R.; Kuznetsova, L. Solvothermal Synthesis of Vanadium Phosphates in the Form of Xerogels, Aerogels and Mesostructures. *Mater Res Bull* 2010, *45*, 1096–1105, doi:10.1016/J.MATERRESBULL.2010.06.010.
533. Kersen, U.; Keiski, R. Characterization of La 2Mo 2O 9 Aerogels Synthesized by the Sol-Gel Chemistry and High-Temperature Supercritical Drying. *J Nanosci Nanotechnol* 2005, *5*, doi:10.1166/jnn.2005.163.
534. Hu, C.; Zhu, Q.; Jiang, Z. Nanosized CuO-ZrxCe1 - XOy Aerogel Catalysts Prepared by Ethanol Supercritical Drying for Catalytic Deep Oxidation of Benzene. *Powder Technol* 2009, *194*, doi:10.1016/j.powtec.2009.03.035.
535. Du, A.; Zhou, B.; Zhong, Y.; Zhu, X.; Gao, G.; Wu, G.; Zhang, Z.; Shen, J. Hierarchical Microstructure and Formative Mechanism of Low-Density Molybdena-Based Aerogel Derived from MoCl5. *J Solgel Sci Technol* 2011, *58*, doi:10.1007/s10971-010-2381-8.
536. Abu-Jdayil, B.; Mourad, A.H.; Hittini, W.; Hassan, M.; Hameedi, S. Traditional, State-of-the-Art and Renewable Thermal Building Insulation Materials: An Overview. *Constr Build Mater* 2019, *214*.
537. Lamy-Mendes, A.; Pontinha, A.D.R.; Alves, P.; Santos, P.; Durães, L. Progress in Silica Aerogel-Containing Materials for Buildings' Thermal Insulation. *Constr Build Mater* 2021, *286*, doi:10.1016/j.conbuildmat.2021.122815.
538. Zhu, C.Y.; Xu, H.B.; Zhao, X.P.; Gong, L.; Li, Z.Y. A Review on Heat Transfer in Nanoporous Silica Aerogel Insulation Materials and Its Modeling. *Energy Storage and Saving* 2022, *1*.
539. Xiao, K.; Zhang, W.; Zhu, M.; Yin, Q.; Fortunelli, A.; Goddard, W.A.; Wu, X. Dynamical Performance of Graphene Aerogel with Ductile and Brittle Characteristics. *Adv Funct Mater* 2024, *34*, doi:10.1002/adfm.202401473.
540. Ansari, M.O.; Kumar, R.; Pervez Ansari, S.; Abdel-Wahab Hassan, M.S.; Alshahrie, A.; Barakat, M.A.E.F. Nanocarbon Aerogel Composites. In *Nanocarbon and its Composites: Preparation, Properties and Applications*; 2018.
541. Borzova, M.; Lenigk, V.; Gauvin, F.; Schollbach, K. Life Cycle Assessment of Silica Aerogel Produced from Waste Glass via Ambient Pressure Drying Method. *J Clean Prod* 2024, *477*, 143839, doi:10.1016/j.jclepro.2024.143839.
542. Guo, P.; Su, L.; Peng, K.; Lu, D.; Xu, L.; Li, M.; Wang, H. Additive Manufacturing of Resilient SiC Nanowire Aerogels. *ACS Nano* 2022, *16*, doi:10.1021/acsnano.2c01039.
543. Djati Utomo, H.; Li, X.; Ng, E.T.J. Sustainable Production in Circular Economy: Aerogel Upscaling Production. *Environmental Science and Pollution Research* 2022, *29*.
544. Do, N.H.N.; Can, N.N.T.; Le, P.K. Thermal Insulation of Flame Retardant Silica Aerogel Composites from Rice Husk Ash and Plastic Waste Fibers. *J Inorg Organomet Polym Mater* 2024, *34*, doi:10.1007/s10904-023-02805-7.
545. Cheng, M.; Hu, J.; Xia, J.; Liu, Q.; Wei, T.; Ling, Y.; Li, W.; Liu, B. One-Step in-Situ Green Synthesis of Cellulose Nanocrystal Aerogel Based Shape Stable Phase Change Material. *Chemical Engineering Journal* 2022, *431*, doi:10.1016/j.cej.2021.133935.
546. Sun, J.; Wu, T.; Wu, H.; Li, W.; Li, L.; Liu, S.; Wang, J.; Malfait, W.J.; Zhao, S. Aerogel-Based Solar-Powered Water Production from Atmosphere and Ocean: A Review. *Materials Science and Engineering R: Reports* 2023, *154*.
547. Zhou, X.; Fu, Q.; Liu, H.; Gu, H.; Guo, Z. Solvent-Free Nanoalumina Loaded Nanocellulose Aerogel for Efficient Oil and Organic Solvent Adsorption. *J Colloid Interface Sci* 2021, *581*, doi:10.1016/j.jcis.2020.07.099.
548. Nassar, G.; Daou, E.; Najjar, R.; Bassil, M.; Habchi, R. A Review on the Current Research on Graphene-Based Aerogels and Their Applications. *Carbon Trends* 2021, *4*.
549. Nguyen, P.T.T.; Do, N.H.N.; Goh, X.Y.; Goh, C.J.; Ong, R.H.; Le, P.K.; Phan-Thien, N.; Duong, H.M. Recent Progresses in Eco-Friendly Fabrication and Applications of Sustainable Aerogels from Various Waste Materials. *Waste Biomass Valorization* 2022, *13*.
550. Sheng, Z.; Liu, Z.; Hou, Y.; Jiang, H.; Li, Y.; Li, G.; Zhang, X. The Rising Aerogel Fibers: Status, Challenges, and Opportunities. *Advanced Science* 2023, *10*.
551. Zheng, L.; Zhang, S.; Ying, Z.; Liu, J.; Zhou, Y.; Chen, F. Engineering of Aerogel-Based Biomaterials for Biomedical Applications. *Int J Nanomedicine* 2020, *15*.

 doi:10.20944/preprints202508.0009.v1

552. Awang, N.; Nasir, A.M.; Yajid, M.A.M.; Jaafar, J. A Review on Advancement and Future Perspective of 3D Hierarchical Porous Aerogels Based on Electrospun Polymer Nanofibers for Electrochemical Energy Storage Application. *J Environ Chem Eng* 2021, *9*, doi:10.1016/j.jece.2021.105437.
553. Orsini, F.; Marrone, P.; Asdrubali, F.; Roncone, M.; Grazieschi, G. Aerogel Insulation in Building Energy Retrofit. Performance Testing and Cost Analysis on a Case Study in Rome. *Energy Reports* 2020, *6*, doi:10.1016/j.egyr.2020.10.045.
554. Tafreshi, O.A.; Mosanenzadeh, S.G.; Karamikamkar, S.; Saadatnia, Z.; Park, C.B.; Naguib, H.E. A Review on Multifunctional Aerogel Fibers: Processing, Fabrication, Functionalization, and Applications. *Mater Today Chem* 2022, *23*.
555. Song, Z.; Su, L.; Yuan, M.; Shang, S.; Cui, S. Self-Cleaning, Energy-Saving Aerogel Composites Possessed Sandwich Structure: Improving Indoor Comfort with Excellent Thermal Insulation and Acoustic Performance. *Energy Build* 2024, *310*, doi:10.1016/j.enbuild.2024.114098.
556. Shah, S.N.; Mo, K.H.; Yap, S.P.; Radwan, M.K.H. Towards an Energy Efficient Cement Composite Incorporating Silica Aerogel: A State of the Art Review. *Journal of Building Engineering* 2021, *44*.